UNIVERSITY OF
LIVERPOOL

IMPROVEMENT OF ENERGY EFFICIENCY OF PNEUMATIC CYLINDER ACTUATOR SYSTEMS

Thesis submitted in accordance with the requirements of the University of Liverpool for the degree of Doctor in Philosophy

by

Jia Ke

May 2007

Department of Electrical Engineering and Electronics

The University of Liverpool

Dedicated to
my parents

Acknowledgements

I would like to give my greatest gratitude to my supervisor, Dr. Jihong Wang for her invaluable support and intellectual guidance during my PhD study. The great knowledge and experience she imparted to me is not restricted to the field of study but her amazing skills of presentation and management have had a profoundly positive impact on my development as a person.

My heartfelt thanks also go to Prof. Qinghua Wu for his valuable supporting, advice and encouragement.

I also wish to thank Prof. Alan Zinober from the University of Sheffield for his great knowledge and generous help in mathematics.

Finally, I would like to thank my family and my fiancé Nan Jia, for their love, support and understanding during my PhD study.

Abstract

Improvement of Energy Efficiency of Pneumatic Cylinder Actuator Systems

Jia Ke

Pneumatic actuators provide solutions through motion technology in a wide range of applications. In production plants, considerable amount of electricity is consumed for generating compressed air for pneumatic actuators. However, the energy efficiency of pneumatic actuators remains low, only 23%-30% can be achieved. This thesis aims to describe the research work on improvement of the energy efficiency of one typical type of pneumatic actuator systems, *i.e.* pneumatic cylinder systems by using optimal trajectories obtained from optimal control method and innovation of the mechanical structure of cylinders.

To find the optimal energy efficient profiles, the optimal control theory has been applied to servo-controlled pneumatic cylinder systems. To avoid the difficulties of solving complicated nonlinear differential equations which generated from Pontryagin's principle, the pneumatic cylinder system is linearised by input/output state feedback. Then the optimal control theory is applied to the linearised system model. A group of optimal energy efficient profiles are derived. The work has been extended to tracking control, and a feedback tracking control has been developed for the linearised model. Some simplification work has been done for easier implementation in practice.

Furthermore, a novel mechanical structure of the pneumatic cylinder is proposed in the thesis. Its geometrical structure and the mathematical model are described. Simulation study has been conducted and the results show the new cylinder can improve energy efficiency dramatically compared to conventional cylinders.

Contents

List of Figures

List of Tables

Nomenclature

a, b Subscripts for inlet and outlet chambers respectively

A Ram area (m^2)

C_d Discharge coefficient

Δ The generalized residual chamber volume

K_f Viscous frictional coefficient

k Specific heat constant

l Stroke length (m) and $\tilde{x} \in (-l/2,\ l/2)$

M Mass flow rate (kg/s)

m Payload (kg)

P_d Down stream pressure (N/m^2)

P_e Exhaust pressure (N/m^2)

P_s Supply pressure (N/m^2)

P_u Up stream pressure (N/m^2)

R Universal gas constant (J/kg/K)

T_s Supply temperature (K)

w Port width (m)

$\tilde{x}$ Load position (m)

$X_{1,2}$ Spool displacement of Valve 1 or Valve 2 (m)

Chapter 1

Introduction

1.1 Background and Objectives

Actuators are the devices which convert energy to motion: linear motion, rotary motion or a combination of the two. They can be powered by electricity, compressed air or fluid. Pneumatic actuator systems convert the energy of compressed air into movements and forces for machine drive mechanisms by means of cylinders and motors, which are controlled by valves. P neumatic actuators are widely used in manufacturing industries, agriculture and even our daily life. From food processing to vehicle assembly, from medical instrument to facilities in amusement park, the actuation of cams, detents, and levers in machines, pneumatic actuators play very important roles. Especially in automated manufacturing processes, which involve a great deal of clamping, holding and transportation tasks, pneumatics represent a solution, which offers advantages in terms of speed, simplicity and cost-effectiveness. Over 60 percent of all machine movements are linear, which are much simpler to realize by pneumatic cylinders than by electric motors (BOSCH, 1998). Some typical linear pneumatic actuators are shown in Figure 1.1.

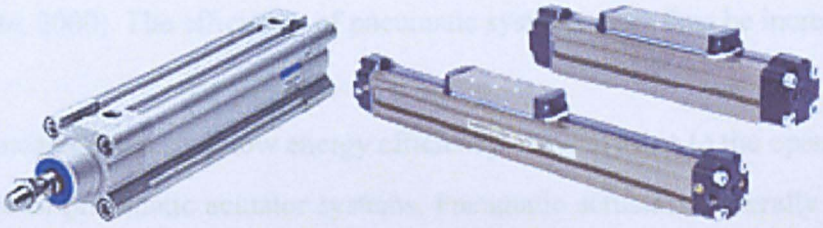

Figure 1.1 Typical pneumatic linear actuators (Pictures courtesy of Festo and Norgren)

A wide range of industries rely on pneumatics since pneumatic actuators have distinct advantages: environmentally clean, rapid point-to-point positioning, high load-carrying capacity relative to their size, mechanical simplicity, low cost, ease in maintenance, *etc.* In the UK, a massive energy consumer, over 10% of the National Grid output is used to generate compressed air (Horne, 1998; Drives and Control, 1999). Pneumatic actuators have many positive attributes. However, their lack of energy efficiency is costly for individual companies, for the nation in terms of electricity generation, and for the environment. Energy consumption issues have long been neglected in the sector of pneumatic systems. However, these topics have begun to attract increasing interest recently, partly as a result of changes on the international scene. Of particular importance in this context was the 1997 Tokyo conference, which called for a 7% cut in CO_2 emissions from levels in 1995 (Belforte, 2000). This cut impacts a number of general aspects of pneumatic systems, from the generation of compressed air to its distribution and end users. As regards the efficiency of end use circuits, the efficiency of pneumatic actuator systems is rather low. A recent report by British Fluid Power Association indicates that, in the UK and other European countries, an energy efficiency of between 23%-30% is achieved in working systems, as against 80% for electrical systems and 40% for hydraulic systems

(Belforte, 2000). The efficiency of pneumatic systems must thus be increased.

It is considered that such low energy efficiency is mainly due to the open-circuit structure of pneumatic actuator systems. Pneumatic actuators generally operate at air supply pressures around 6 bars. The air released into the atmosphere at the exhaust still has a relatively high pressure. The costs associated with this are far from negligible: it has been estimated that in the UK around 20 percent of the electricity supplied to manufacturers is used to generate compressed air (Pearce, 2005). Attempts have been made to improve the energy efficiency, with varying results. It was reported that an additional air tank is connected to the downstream of a pneumatic system, to close the circuit of compressed air (Quaglia *et al.*, 1995). An energy-efficient pneumatic control valve system was proposed to save energy by minimizing the compressed air pressure needed during certain parts of the operation and to compensate for air leakage (Horstmann *et al.*, 1993). A by-pass valve was adopted to work with the main control valve in order to recycle a part of the downstream compressed air (Pu *et al.*, 1997). Energy efficiency of pneumatic cylinder actuating systems was analysed using air exergy, which denotes the air possible to be transformed to work on the surrounding of the atmosphere (Kagawa, *et al.* 2000; Cai, *et al.* 2002). Norgren, one of the leading American companies in manufacturing pneumatic components, has taken the initiative in helping compressed air users to increase energy efficiency (Norgren, 2003). Engineeringtalk reported that Boge Compressors used screw compressors to cut the energy costs by half (Engineeringtalk, 2006). Active and passive controllers using sliding mode control has been used to improve energy efficiency (Al-Dakkan, 2003 and 2006). Although much effort has been made, there is still extensive space for

improvement of energy efficiency in pneumatic actuator systems. Therefore, there is considerable scope for research in this subject.

Energy saving and the efficient use of energy is one of the most important issues which worldwide industries have to confront. The proposed research is therefore concerned with the investigation of methods to improve energy efficiency of pneumatic cylinder actuator systems. Firstly, the challenge and excitement of the work is to improve energy efficiency through optimal design of motion and gas flow time profiles without putting extra costs on hardware. Secondly, possible innovation on the mechanical or geometrical structure of the pneumatic cylinder will be investigated. To achieve the objectives, the project will focus on the following tasks:

a) Study of the pneumatic cylinder actuating system model and its dynamic characteristics;
b) Problem formulation of the energy efficient optimal control on pneumatic cylinders and acquisition its solutions using optimal control theory;
c) Derivation of optimal energy efficient profiles of general servo-controlled pneumatic systems;
d) Investigation on possible innovation of the mechanical or geometrical structure of pneumatic cylinders.

1.2 Introduction to Pneumatic Actuator Systems

Products or objects are required to be moved from one location to another in most industry processes, or they are required to be held, shaped or compressed.

These can be accomplished by electrical drives, or via devices driven by high pressure air (pneumatics) or fluids (hydraulics) (Andrew 1998). For pneumatic systems, the most common working gas used in industry is simply compressed air, occasionally nitrogen is used. A pneumatic system generally consists of compressed air suppliers, control valves, pneumatic actuators and miscellaneous parts, such as pipes and lubricators. A typical example is shown in Figure 1.2, which includes an air compressor, air filter, a compressed air container, a five port directional control valve, and an asymmetric cylinder *etc.*

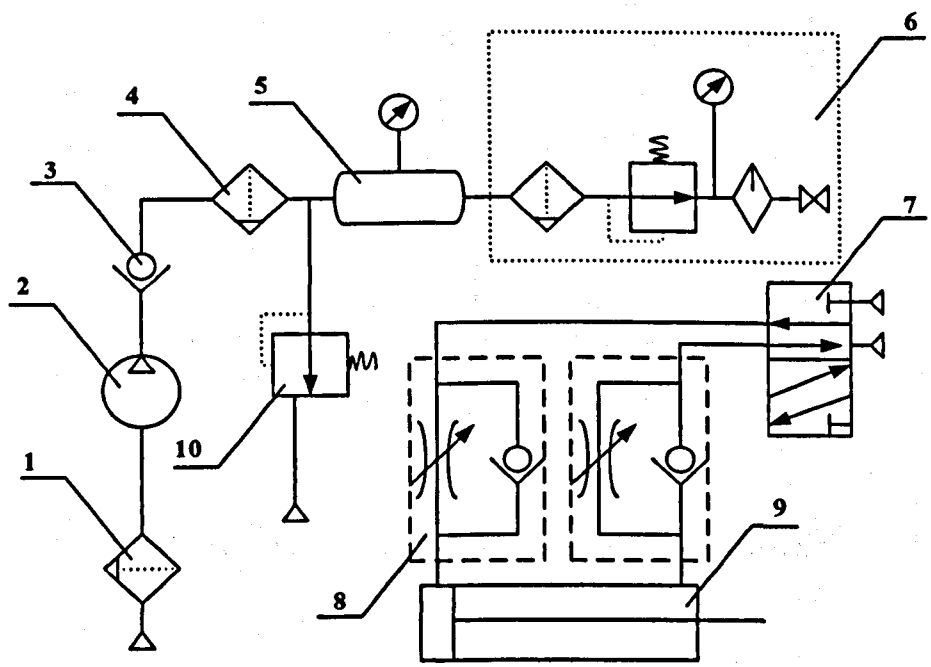

1. Filter; 2. Air compressor; 3. Non-return valve; 4. Filter; 5. Pressure accumulator; 6. Air service units; 7. Control valve; 8. Flow control regulator; 9. Double acting cylinder; 10. Pressure relief valve

Figure 1.2 General pneumatic system setup schematic (Figure courtesy of Lin-Chen, 2001)

The components of a pneumatic system can be classified into four groups. They are air preparation equipments, control valves, pneumatic actuators, and miscellaneous parts.

(1) Air preparation equipments

The vast majority of pneumatic systems use compressed atmospheric air as the operating medium. Compressed air is generally generated by air compressors that are shown in Figure 1.3. A good quality compressed air supply is very important for the system. There are many types of air compressors, for example, piston compressors, screw compressors, rotary compressors and dynamic compressors. Air receiver is used to store high-pressure air generated by the compressor, to provide constant supplies. In order to provide reliable and effective operation of pneumatic components, additional units are used to guarantee the quality of air supply, which include filters, regulators, lubricators, *etc.*

Figure 1.3 Typical industry air compressors (Pictures courtesy of Aircompressors.co.uk)

(2) Control valves

The primary functions of control valves are to alert, generate or cancel signals for purpose of sensing, processing and controlling. Additionally, the valve is used as a power component for the supply of working fluid to the actuator. Some typical control valves used in industry are shown in Figure 1.4. According to the valves' position placement, control valves can be classified into two main categories. The first type is the infinite position valve, which can take any

position between fully open and fully closed. It can be used to freely modulate air flow or pressure. A servo valve is one of examples in this category. The other type of control valve has finite positions, which are only used to allow or block the flow of fluid. These valves are called finite position valves or on/off valves, which are conventional valves. Typically, conventional valves only have two operating positions, on and off. They change from one to the other alternative dependent on the control signals. For some applications, a three-position control valve with a central neutral position is used.

Figure 1.4 Typical control valves (Pictures courtesy of Festo)

(3) Pneumatic actuators:

Pneumatic actuators come in a variety of forms. But one common ground can be found, that is, actuators convert energy to motion: linear motion, rotary motion or a combination of the two. Thus, pneumatic actuators can also be divided into two types, linear and rotary actuators. The symbols of actuators in fluid circuit are shown in Figure 1.5.

Linear actuators are used to move objects or apply forces linearly. It is the most important type of actuators used in industry. It can be divided into two groups: single-acting cylinders and double-acting cylinders. A single-acting cylinder is only powered for one direction. The fluid is only applied on one side of the piston to move it in one direction. The other side of the piston is open to the

atmosphere. The piston returns backward by the force of an internal spring or other external force. Double-acting cylinders have the similar construction as single-acting cylinders. However, there is no return spring. Two ports are used alternative as supply and exhaust port. It has advantages because the cylinder can work in both directions. The double-acting cylinder is also under control of the supply fluid in both directions. There are two kinds of typical double acting cylinders: rodded and rodless cylinders as shown in Figure 1.5.

Rotary actuators are used to move objects in circular path. Rotary actuators are the fluid power equivalent to an electric motor. It makes the design of flexible transfer and handling system possible and optimizes effective space utilization.

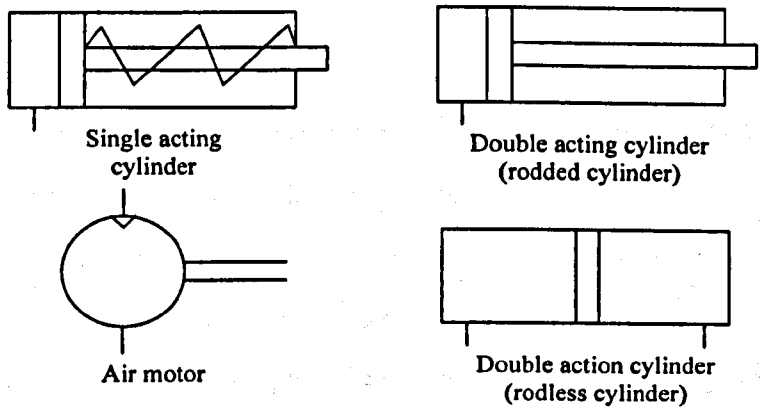

Figure 1.5 Symbols of actuators in fluid circuit

(4) Miscellaneous parts include pneumatic system connectors, pipes and dampers *etc.*

Compared to hydraulic and electrical drive systems, pneumatic systems have significant advantages, which are as follows (Johnson, 1975; Andrew, 1998; Weston *et al.*, 1984; Backe, 1986 and 1993; Liu and Bobrow, 1988; Pu and

Weston, 1988, 1989 and 1990; Moore *et al.*, 1993; Fok *et al.*, 1995; Turner, 1996; Uebing and Vaughan, 1997):

- Safety: There is no high-pressure leakage problem; no spark generation; no requirement for high current supply; little risk for explosion, fire or overload.
- Cost: For low and medium power, a pneumatic system has excellent cost/performance ratio. Its components are relatively simple and inexpensive, thus pneumatic system is generally economical, convenient and relatively efficient. The selection of appropriate size of actuators can be made to optimize the cost and size of the unit.
- Load characteristics: Insensitive to load changes over relatively wide ranges and high stall torque. Pneumatic system can operate consistently at full load. It can also stall indefinitely at full load without overheating.
- Cleanliness: Unlubricated exhaust air is clean. And possible leakage is less of a concern than that of hydraulic systems.
- Storage and distribution: Energy can easily be stored as compressed air, which can be treated as a plant-wide service.
- Maintenance: Pneumatic system is reliable and easy to maintain and design with compact size, less complex and high life expectancy and it can resist physical damage from load vibration and shock.
- Environment: Pneumatic system can be operated in high temperature environments with high duty cycles. It is also well suited to potentially flammable or explosive environments.
- Speed: Higher speed compared to hydraulic actuator system.

However, there are also limitations in the application of pneumatic systems. The

main disadvantages of pneumatic systems are:

- Compressibility of air results in poor dynamic performance, which will give rise to time delay when a signal passes down a long pipe.
- Pneumatic systems use mainly air as a means of actuation, but compressed air almost invariably contains water vapour, which can result in oxidation. Hence, working gas should be free from vapour.
- Compressing air is noisy even after the dampers are applied.
- Servo-controlled pneumatic systems are difficult to regulate.
- Low stiffness and slow response are problems. However, the advantages of energy storage and small size have outweighed the disadvantages of compressibility and non-linearity.
- The energy efficiency is rather low, which is mainly caused by open-circuit of the pneumatic system structure.

In many cases, pneumatic drives are the better choice, especially in the cases where the environmental constraints, such as harsh or corrosive atmospheric conditions and high levels of dust and dirt, great fluctuations of temperature, and safety considerations, high duty cycle or relatively low precision profile following tasks are involved, such as food processing, agriculture, woodwork and textile industries (Pu *et al.*, 1995a; Turner, 1996; Belforte, 2000).

1.3 Historical Overview of Development in Pneumatic Actuator Systems

The components of pneumatic actuator systems and control technology were greatly advanced in the last century. Early pneumatic control circuits were used

on three-way or four-way power valves. These power valves were designed to extend and retract air cylinders or operate air motors. The installation of the circuit was a problem when it involved large and rather awkward valves connected together by hose or steel tubing (McCord, 1983). In the late 1940s and early 1950s, two things happened which made the application of pneumatic control somewhat more attractive. The first was the availability of small-diameter plastic tubing and fittings. The second was the miniaturisation of air cylinders and valves (Lin-Chen, 2001). These small, manual, mechanical, and pilot-operated valves, although still designed as power valves for small cylinders, greatly reduced the space, cost and workforce required to install a system. Air control systems then became practical in an increasing number of applications. The electrical operated valves allowed machines to be connected to the electrical switch cabinet easily.

In the mid 1960s, fluid power engineering emerged with a new generation of pneumatic control engineering. Although the air valves were still three-way spool or poppet valves, the considerations given to various aspects of their design were quite different from those of a power valve. However, the low-powered signal and information processing method did not gain general acceptance and then has been overtaken by the speedy development of electronics (BOSCH, 1998).

The foundation of research on control and modelling of servo pneumatic actuator with high pressure and high temperature originated in the 1950s (Shearer, 1954; Blackburn *et al.* 1960) and 1960s (Vaughan, 1965; Burrows, 1969) for military purposes. In the 1950s, Shearer started his work on an

open-loop system. By analysing the behaviour of the pneumatic servo-motor, he gave a series of fundamental equations to describe the pneumatic system. Subsequently, he studied a closed loop pneumatic system with mechanical position feedback between the load and the valve (Shearer, 1957). The results of Shearer's work were also successfully applied in spacecraft and missile engine controls (Blackburn *et al.* 1960; Vaughan, 1965; Botting *et al.* 1970).

During the 1960s, Burrows and Webb (1966, 1967-1968 and 1969-1970) revealed some specific dynamics of pneumatic systems when they studied low pressure pneumatic servomechanisms. They used the root-locus technique to provide a simple design procedure. The effects of parameter changes on system performance, such as viscous and Coulomb friction, have been studied. They simulated pneumatic servo system by using on/off valves rather than servo valves due to the availability and manufacturing cost of servo valves at that time. However, there was no significant progress in research of pneumatic actuator systems in the 1970s.

Early pneumatic components, such as valves and actuators, have many similarities with their hydraulic counterparts. Some hydraulic components are directly used in pneumatics. However, they are too expensive because they are developed for high pressures and high forces (Backe, 1986). For safety reasons, the working pressure of industrial pneumatic system is normally limited within 10 bars (Burrows and Webb, 1969-1970; Mannetje, 1981), which is much lower than that of hydraulic systems. The lack of true control hardware limited the application of pneumatic control to only the extreme cases, such as explosive environments (McCord, 1983). Pneumatic control system was much more easily

accomplished by electrical relays at a much lower cost at that time. Nevertheless, electro-pneumatic servo valves were on the market in the late 1980s.

Since the early 1980s, the main activities have focused on the technical development aspects, namely designing and producing analogue and digital controlled servo-pneumatic actuator systems. For example, state feedback or minor-loop compensation, *i.e.* velocity and acceleration feedback, is to date the most widely used technique for controlling servo-pneumatic systems (Weston *et al.* 1984; Pu, *et al.* 1995a).

With the increasing mechanisation and automation of production processes, control technology in particular has gained considerably in importance. In the research area, Mannetje introduced the feedback loop by using high gain differential pressure. His work showed that keeping the pressure of the supply stable would improve the system bandwidth (Mannetje, 1981). Weston developed a fourth-order linearised model of pneumatic systems, when he studied microprocessor-based low cost pneumatic servo drives (Weston *et al.* 1984). His work was based on Burrows' linearised analysis of pneumatic drives (Burrows, 1969) and the assumption of negligible friction. This approximate model was very helpful to develop a suitable control strategy. By feedback of position, velocity and acceleration, Backe developed a three-loop controller for the high performance pneumatic servo valve (Backe, 1986 and 1993). His study also indicated that it was difficult to build models of pneumatic systems due to the non-linearities. He also indicated that the positioning performance of servo pneumatic system is strongly affected by the quality and the time response of

the servo valve. Kawakami investigated the effects of heat transfer and linearisation on the dynamics of pneumatic systems (Kawakami *et al.*, 1988 and 1993). His results show that, there was little difference between considering and neglecting the heat transfer effect in the dynamic model under normal cylinder usage conditions.

Pneumatic devices are one of the most widely used means of actuation in industry, alongside electric, electromechanical and hydraulic drives. Traditionally they have been widely used in applications for simple speed control. In recent years, the ready availability of low cost microprocessors and mechatronic components allow industrial users to consider adopting servo-controlled pneumatic actuators at an acceptable cost (Pu *et al.*, 1993; Wang *et al.*, 1999a; Belforte, 2000; Kagawa, 2002). Pneumatic actuators have been employing to accomplish more sophisticated motion control tasks. Servo-pneumatic systems can address a diverse range of applications (Weston *et al.*, 1984; Moore *et al.*, 1985 and 1992; Morgan, 1985; Pu *et al.*, 1993; Mannetje, 1981; Klein and Backe, 1992; Zhou, 1995; Belforte, 2000; Al-Dakkan *et al.*, 2003 and 2006), including robotics, vehicles (motor vehicles, trains, ships), agriculture, textiles, bioengineering, pneumatic handling, hazardous environments, *etc.*

Renewed interests in the last twenty years in the development of pneumatic servo systems mean that they can be considered as an alternative to electric and hydraulic servos in industrial applications (Pu, *et al.*, 1995b). High positioning accuracy and high speed of positioning are required to achieve acceptable cycle times (Morgan 1985). In addition, digital signal processors allow servo

controllers to be compensated for the complex behaviour of pneumatic circuits, such as nonlinear flow and actuator frictions. Compensating for static frictions (Pu *et al.*, 1995b; Wang *et al.*, 2007) is especially important and has actually made precise velocity and acceleration control possible, even at low speed. Therefore, opportunities now exist to significantly extend the capabilities and application boundary of pneumatic drives for more sophisticated applications.

However, electric devices also have made significant progress in terms of increased performance, particularly in the field of linear motors, and cost reduction, making them increasingly competitive with other technologies. Pneumatics is thus called upon to make further advances in order to stay competitive and move into new applications (Belforte, 2000). The development of pneumatics is to be seen as an evolution of mechatronic systems, integrated with mechanical and electrical technologies and featuring connections with control units via both electronic and optical fibre bus. Pneumatics continue to have an essential role in industrial applications, where it is ever more closely associated with electromechanical and electronic devices in manufacturing systems and automated production lines (Belforte, 2000).

Current trends in pneumatics can be broken down into the following areas: (1) Increasing components' performance and reliability, with particular attention to miniaturising valves and cylinders, reducing friction, *etc*; (2) Development of innovative actuators, particularly, frictionless and flexible units; (3) Increasing attention to energy issues; and (4) Integration with sensors and control electronics to implement intelligent servo systems. In this thesis, it will discuss mainly the energy issue and in the last chapter it proposes an innovative

actuator.

1.4 Thesis Outline

There are 7 chapters in the thesis, which are organized as follows:

Chapter 1. In this chapter, project background and objectives are presented. The pneumatic actuator system is introduced, which includes a brief description of the components and their functions in a pneumatic actuator system. A brief history review of development in pneumatic actuator systems has been given.

Chapter 2. The mathematical model of the pneumatic cylinder system is described by integration of mathematical models of each component in the system. Friction characteristics in the cylinder are also studied. And open-loop simulation studies show the dynamic responses of the pneumatic cylinder actuating system with step input signals.

Chapter 3. Optimal control theory is briefly summarised in this chapter. In order to find the optimal profiles to improve energy efficiency, optimal control theory has been applied to a typical pneumatic cylinder system. A group of co-state equations are generated by using Pontryagin's principle.

Chapter 4. To avoid the difficulties of solving complicated nonlinear differential equations which generated in Chapter 3, the pneumatic cylinder system is linearised by input/output state feedback. Then the optimal control theory is applied to the linearised system model. A group of optimal energy

efficient profiles are derived through simulation work.

Chapter 5. Based on the same idea presented in Chapter 4, the pneumatic cylinder model is linearised via input/output state feedback initially, and then a feedback tracking control is developed for the linearised model. Since the nonlinear feedback controller is too complicated to use in practice, some simplification work has been done. Static and Coulomb frictions are included in the system model. And then corresponding changes have been made to the tracking controller.

Chapter 6. To improve the energy efficiency further, the mechanical structure of a pneumatic cylinder has been innovated. The structure of the new cylinder and its mathematical model are illustrated. To understand the dynamic response of this new design, the open-loop simulation results and analysis are also presented. Simulation results prove the new cylinder can improve the energy efficiency dramatically compared to conventional cylinders.

Chapter 7. Major achievements and findings are summarised, conclusions are drawn, and recommended future work is presented.

1.5 Publications

Part of the contents of this thesis has been published. The publications are listed below:

1. Ke, J., Thanapalan, K., Wang, J. and Wu, Q.H., 2004, Development of energy efficient optimal control of servo pneumatic systems, *The*

Proceedings of IEE Control Conference 2004, September 6-9, Bath, UK.

2. Ke, J., Wang, J., Jia, N., Yang, L. and Wu, Q.H., 2005, Energy efficiency analysis and optimal control of servo pneumatic cylinders, *The Proceedings of IEEE Conference on Control Applications 2005*, August 29-31, Toronto, Canada.
3. Ke, J. and Wang. J., 2006, Improvement of energy efficiency of servo pneumatic cylinders by optimising velocity profiles, *International Journal of Modelling, Identification and Control*, 6(1), pp. 301-307.
4. Wang, J., Ke, J. and Wei, J.L., A high speed energy efficient pneumatic cylinder, *Mechatronics 2006, The 10th Mechatronics Forum Biennial International Conference*, June 19-21, Penn State, USA.
5. Ke, J., Wang, J. and Yang, L., 2006, A fast response energy efficient pneumatic cylinder, *CACSK06, Proceedings of the 12th Chinese Automation & Computing Society Conference in the UK*, September 16, Loughborough, UK.
6. Wang, J., Kotta, U. and Ke, J., 2007, Tracking control of nonlinear pneumatic actuator systems using static state feedback linearization of the input-output map, *Proceedings of the Estonian Academy of Sciences (Physics Mathematics)*, 56(1), pp. 47-66.

Chapter 2

Mathematical Model of Pneumatic Actuator Systems

2.1 Modelling for Pneumatic Actuator Systems

To facilitate accurate position control and high speed driving of pneumatic actuator systems, a dynamic model which describes the system accurately must be employed. From the analysis of the dynamics of individual pneumatic system components and the standard orifice theory, mathematical models for individual components are derived in this section, and a complete model of a pneumatic actuator system is integrated from the interconnection of the components' models.

Some basic assumptions are made to analyse the mathematical models of pneumatic systems. Firstly, supply pressure P_s and supply temperature T_s are assumed constant. Secondly, heat transfer between air and its environment can be negligible (Kawakami, *et al.* 1988). The temperature of the working gas flowing between the valve and the actuator is equal to the supply temperature T_s at any time. Thirdly, the working gas is assumed to be an ideal gas, so that the general gas laws can be applied (*e.g.* $PV = mRT$). Finally, each port of the control valve is assumed to act like a standard orifice, so that standard orifice

theory can be applied.

2.1.1 Mathematical Model of Compressible Flow

The equations and principles used to calculate mass flow rate are presented and examined in this section. It is important to note that the study of compressible gas flow involves temperature, pressure and density changes.

For steady flow of compressible gas passing through a tube, suppose this kind of flow process does not involve work transfer or heat transfer. The steady flow energy equation is (Andersen, 1976):

$$h_0 = h_2 + \frac{U_2^2}{2} \tag{2-1}$$

where h_2 is the enthalpy, $\frac{U_2^2}{2}$ is the kinetic energy, h_0 is the stagnation enthalpy (Kane and Sternheim, 1980) and subscript "0" represents total condition, "2" represents static condition. For an ideal gas, $dh = c_p dT$ (Winnick, 1997). Equation (2-1) can be rewritten as:

$$c_p T_0 = c_p T_2 + \frac{U_2^2}{2} \tag{2-2}$$

Because $c_p = c_v + R$ and $c_p / c_v = k$, it follows that $c_p = \frac{kR}{k-1}$, where c_p is specific heat at constant pressure, c_v is specific heat at constant volume, k is the ratio of specific heat and R is gas constant. So Equation (2-2) can be written as

$$\frac{kR}{k-1}T_0 = \frac{kR}{k-1}T_2 + \frac{U_2^2}{2} \tag{2-3}$$

In the isentropic process, because there is no change in entropy (no heat is gained or lost during an isentropic process) (Kane and Sternheim, 1980),

$$\frac{\rho_2}{\rho_0} = \left(\frac{P_2}{P_0}\right)^{1/k} \tag{2-4}$$

$$\frac{T_2}{T_0} = \left(\frac{P_2}{P_0}\right)^{(k-1)/k} \tag{2-5}$$

and $$P_0 = \rho_0 RT, \quad P_2 = \rho_2 RT \tag{2-6}$$

From Equation (2-3), the following equation can be derived:

$$U_2 = \sqrt{2c_p(T_0 - T_2)} = \sqrt{2\frac{kR}{k-1}T_0\left(1-\frac{T_2}{T_0}\right)} = \sqrt{\frac{2k}{k-1}RT_0\left[1-\left(\frac{P_2}{P_0}\right)^{\frac{k-1}{k}}\right]} \tag{2-7}$$

If the velocity is assumed to be uniform across the section, and the section area is A_2, then the mass flow rate is given by:

$$M = \rho_2 U_2 A_2 = \rho_2 A_2 \sqrt{\frac{2k}{k-1}RT_0\left[1-\left(\frac{P_2}{P_0}\right)^{\frac{k-1}{k}}\right]} \tag{2-8}$$

From Equation (2-4) and (2-6), the relation between static density, pressure ratio and total pressure becomes:

$$\rho_2 = \frac{\rho_2}{\rho_0}\rho_0 = \rho_0\left(\frac{P_2}{P_0}\right)^{1/k} = \frac{P_0}{RT_0}\left(\frac{P_2}{P_0}\right)^{1/k} \tag{2-9}$$

Substituting Equation (2-9) into Equation (2-8) leads to the expression for mass flow rate:

$$M = P_0 A_2 \sqrt{\frac{2kRT_0}{R^2 T_0^2 (k-1)} \left[\left(\frac{P_2}{P_0}\right)^{\frac{2}{k}} - \left(\frac{P_2}{P_0}\right)^{\frac{2}{k}} \left(\frac{P_2}{P_0}\right)^{\frac{k-1}{k}} \right]}$$
$$= \frac{P_0 A_2}{\sqrt{T_0}} \sqrt{\frac{2k}{R(k-1)} \left[\left(\frac{P_2}{P_0}\right)^{\frac{2}{k}} - \left(\frac{P_2}{P_0}\right)^{\frac{k+1}{k}} \right]} \qquad (2\text{-}10)$$

The characteristics of Equation (2-10) can be examined now. To obtain the pressure ratio corresponding to the maximum mass flow rate, Equation (2-10) can be differentiated with respect to P_2 / P_0 and the derivative set to zero. This gives the critical pressure ratio C_r:

$$C_r = \left(\frac{P_2}{P_0}\right)_{cr} = \left(\frac{2}{k+1}\right)^{\frac{k}{k-1}} \qquad (2\text{-}11)$$

Substituting this value into Equation (2-7) gives the critical velocity

$$U_{2cr} = \sqrt{kRT_2} \qquad (2\text{-}12)$$

This is the equation for the speed of sound at temperature T_2. It indicates that, for a given value of total pressure and temperature, the maximum mass flow that can be passed through any area occurs at the local speed of sound. Substituting Equation (2-12) into (2-10) gives the critical mass flow:

$$M_{cr} = \frac{P_0 A_2}{\sqrt{T_0}} \sqrt{\frac{k}{R} \left(\frac{2}{k+1}\right)^{\frac{k+1}{k-1}}} = c_0 \frac{P_0 A_2}{\sqrt{T_0}} \qquad (2\text{-}13)$$

here $$c_0 = \sqrt{\frac{k}{R} \left(\frac{2}{k+1}\right)^{\frac{k+1}{k-1}}} \qquad (2\text{-}14)$$

If both sides of Equation (2-10) are divided by the sides of Equation (2-13) respectively, the following can be derived:

$$\frac{M}{M_{cr}}=\left[\frac{2}{k-1}\left(\frac{k+1}{2}\right)^{\frac{k+1}{k-1}}\right]^{\frac{1}{2}}\left[\left(\frac{P_2}{P_0}\right)^{\frac{2}{k}}-\left(\frac{P_2}{P_0}\right)^{\frac{k+1}{k}}\right]^{\frac{1}{2}}=c_k\left[\left(\frac{P_2}{P_0}\right)^{\frac{2}{k}}-\left(\frac{P_2}{P_0}\right)^{\frac{k+1}{k}}\right]^{\frac{1}{2}}$$

Then $$M=c_0c_k\frac{P_0A_2}{\sqrt{T_0}}\left[\left(\frac{P_2}{P_0}\right)^{\frac{2}{k}}-\left(\frac{P_2}{P_0}\right)^{\frac{k+1}{k}}\right]^{\frac{1}{2}} \tag{2-15}$$

where $$c_k=\left[\frac{2}{k-1}\left(\frac{k+1}{2}\right)^{\frac{k+1}{k-1}}\right]^{\frac{1}{2}} \tag{2-16}$$

Equation (2-16) is strictly valid at any point in a flowing gas.

2.1.2 Mathematical Model of Valve

Equation (2-15) is commonly used to calculate mass flow through nozzles, orifices and valves. When a nozzle is discharging gas from a tank, and the nozzle area decreases monotonically, the flow process from a point in the tank to the exit of the nozzle may be considered isentropic. Since no energy loss occurs, the total pressure and temperature at the exit section are equal to the total pressure and temperature in the tank. If the diameter of the tank is large enough for the velocity approaching the nozzle, the static pressure in the tank is virtually the same as the static pressure in Equation (2-15). Therefore, the pressure P_0 in Equation (2-15) can be taken as the upstream total pressure P_u; T_0 can be taken as the upstream static or total temperature T_u; P_2 can be taken as the downstream static pressure P_d. Since the average exit velocity is less than the isentropic value, the calculated mass flow should be multiplied by a factor for velocity correction. However, this effect is usually lumped with the

discharge coefficient c_d in practice, whose range usually is from 0.6 to 1.0.

It is not convenient to measure static pressure at the exit section of the nozzle. If the nozzle discharges to the atmosphere, the exit static pressure is equal to atmospheric pressure provided that this is not lower than the critical pressure corresponding to the total pressure in the tank. If the ambient pressure at the exit is exactly critical, the gas will continue to expand after it leaves the nozzle. Under these conditions the nozzle is called sonic or choked.

If supply and exhaust pressures are assumed to be constant, then each port of the control valve acts like a standard orifice. Because P_0 in Equation (2-15) can be considered as P_u, P_2 as P_d and T_0 as T_u, according to the standard orifice theory, the mass flow rate through the valve orifice takes the form

$$M = c_d c_0 w X P_u \tilde{f}(P_r) / \sqrt{T_u} \tag{2-17}$$

where $P_r = P_d / P_u$

and $$\tilde{f}(P_r) = \begin{cases} 1, & P_{atm}/P_u < P_r \le c_r \\ c_k\left(P_r^{2/k} - P_r^{(k+1)/k}\right)^{1/2}, & c_r < P_r < 1 \end{cases} \tag{2-18}$$

Thus, for a valve component, the inputs to the valve from the previous components are supply pressure and valve displacement (regulated by electronic/electric signals) from its compressed air supply. The output to the next component is the mass flow rate to the two chambers of the cylinder, which can be called Chamber A and Chamber B (refer to Figure 2.1). There are also feedbacks from chambers A and B of the cylinder to valve, which are chamber pressures. Some parameters, such as valve port width and discharge coefficient, can be considered as inputs, constants, or variable parameters of the system.

The relationship between the valve's inputs and outputs are governed by the following equations (Blackburn *et al.*, 1960; Burrows, 1969; Andersen, 1976; Wang *et al.*, 1998; Wang *et al.*, 2000a):

$$M_a = c_d c_0 w_a X_a f_n(P_a, P_s, P_e) \tag{2-19.a}$$

$$M_b = c_d c_0 w_b X_b f_n(P_b, P_s, P_e) \tag{2 -19.b}$$

For the convenience of simulation and analysis, the following functions are introduced:

$$f_n(P_a, P_s, P_e) = \begin{cases} P_s \tilde{f}(P_a / P_s)/\sqrt{T_s}, & \text{Chamber A is drive chamber} \\ P_a \tilde{f}(P_e / P_a)/\sqrt{T_a}, & \text{Chamber B is drive chamber} \end{cases} \tag{2-20}$$

$$f_n(P_b, P_s, P_e) = \begin{cases} P_s \tilde{f}(P_b / P_s)/\sqrt{T_s}, & \text{Chamber B is drive chamber} \\ P_b \tilde{f}(P_e / P_b)/\sqrt{T_b}, & \text{Chamber A is drive chamber} \end{cases} \tag{2-21}$$

where $\tilde{f}(\cdot)$ is the function (2-18) with $P_r = \frac{P_a}{P_s}, \frac{P_e}{P_a}, \frac{P_e}{P_b}$ or $\frac{P_b}{P_s}$. The constants used in the system model are $k = 1.4$, $c_k = \left[\frac{2}{k-1}\left(\frac{k+1}{2}\right)^{\frac{k+1}{k-1}}\right]^{\frac{1}{2}} = 3.864$,

$c_r = \left(\frac{P_2}{P_0}\right)_{cr} = \left(\frac{2}{k+1}\right)^{\frac{k}{k-1}} = 0.528$, $c_0 = \left[\frac{k}{R}\left(\frac{2}{k+1}\right)^{\frac{k+1}{k-1}}\right]^{\frac{1}{2}} = 0.04$.

2.1.3 Mathematical Model of Cylinder

For the pneumatic cylinder, the inputs are mass flow rate from the valve and the feedback of the piston's position and velocity; the output is the pressures of the

two chambers. To derive the model for cylinders, the coordinate system is chosen as shown in Figure 2.1. This coordinate system will be used throughout the entire thesis.

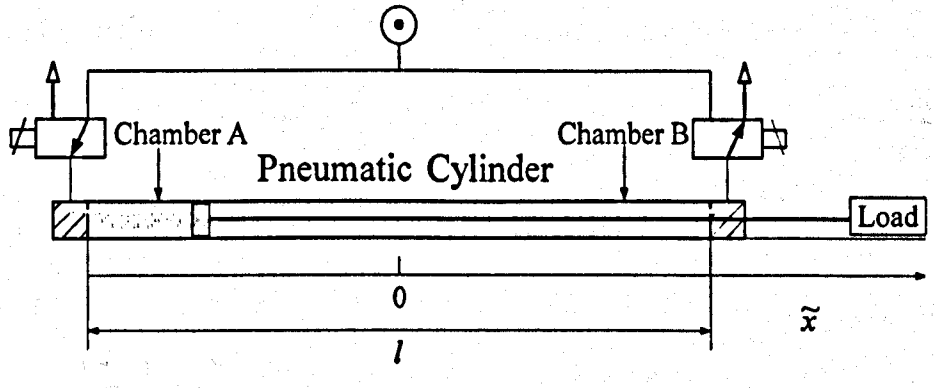

Figure 2.1 Coordinate system of a pneumatic cylinder

The model of the mass flowing into each of the cylinder chambers can be obtained from the energy conservation equation for the control volume bounded by the cylinder bore and piston (Blackburn *et al.*, 1960; Andersen, 1976; Ben-Dov and Salcudean, 1995). According to the first law of thermodynamics, the control volume energy is given by $c_v \rho_c V T_s$, where ρ_c is the cylinder air density, c_v is the specific heat of air at constant volume, V is chamber volume and T_s is cylinder air temperature. If the air flowing into the cylinder is assumed to be an adiabatic process of an ideal gas, the change in energy due to the mass transport equals

$$\frac{d}{dt}(c_v \rho_c V T_s) = M c_p T_s - P\dot{V} \tag{2-22}$$

where c_p is the specific heat of air at a constant pressure, m is P is the cylinder chamber pressure, Mc_pT_s is the change in internal gas energy, and $P\dot{V}$ is the work done by the cylinder. According to standard practice, the gas

kinetic energy term can be neglected since it is small.

Assuming an ideal gas $P = R\rho_c T_s$, where ρ_c can be eliminated in Equation (2-22) to obtain

$$M = \frac{P}{c_p T_s}\frac{dV}{dt} + \frac{1}{kRT_s}\frac{d}{dt}(PV) \tag{2-23}$$

where $k = c_p / c_v$ is the ratio of specific heats for air at the temperature T_s. For a perfect gas,

$$\frac{1}{R} = \frac{1}{c_p} + \frac{1}{kR} \tag{2-24}$$

Then $$M = (P\dot{V} + \dot{P}V/k)/(RT_s) \tag{2-25}$$

For the cylinder chambers A and B, the following equations hold

$$M_a = (P_a\dot{V}_a + \dot{P}_a V_a/k)/(RT_s) \tag{2-26}$$

$$M_b = (P_b\dot{V}_b + \dot{P}_b V_b/k)/(RT_s) \tag{2-27}$$

where V_a, V_b are the volumes of chamber A and B, $\dot{V}_a$, $\dot{V}_b$ are the volume rates and M_a, M_b are the mass flow rates.

For a pneumatic cylinder, the chamber volumes $\dot{V}_a$ and $\dot{V}_b$ are:

$$V_a = A_a(l/2 + \tilde{x} + \Delta) \tag{2-28}$$

$$V_b = A_b(l/2 - \tilde{x} + \Delta) \tag{2-29}$$

where Δ is the residual volume generated by connecting tubes. So $\dot{V}_a = A_a\dot{\tilde{x}}$ and $\dot{V}_b = -A_b\dot{\tilde{x}}$. From Equations (2-26) to (2-29), the cylinder can be modelled

by following equations:

$$\dot{P}_a = \frac{k}{(l/2+\tilde{x}+\Delta)}\left[-P_a\dot{\tilde{x}} + \frac{RT_s}{A_a}M_a\right] \tag{2-30.a}$$

$$\dot{P}_b = \frac{k}{(l/2-\tilde{x}+\Delta)}\left[P_b\dot{\tilde{x}} + \frac{RT_s}{A_b}M_b\right] \tag{2-30.b}$$

where $\tilde{x} \in (-l/2, l/2)$.

2.1.4 Mathematical Model of Payload

For the payload of the pneumatic cylinder system, the inputs are the pressures of two chambers, while the outputs are the piston's position and velocity. The relationship between its inputs and outputs can be derived as below. The load dynamics of pneumatic actuators are complex, primarily due to the nature of the associated friction characteristics. According to Newton's law, the following equation holds:

$$A_a P_a - A_b P_b - K_f\dot{\tilde{x}} - F_{S\text{-}C}(\tilde{x}) = m\ddot{\tilde{x}} \ , \tag{2-31}$$

where $\dot{\tilde{x}}$ represents velocity. $\ddot{\tilde{x}}$ denotes acceleration, K_f is viscous friction coefficient, $F_{S\text{-}C}(\tilde{x})$ represents the sum of static and Coulomb frictions, which are position dependent.

2.1.5 State-space Model of Pneumatic Actuator Systems

For convenience of analysis, the following state variables are introduced: $x_1 = \tilde{x}$, $x_2 = \dot{\tilde{x}}$, $x_3 = P_a$, $x_4 = P_b$. With the newly defined system variables in

state space, the system models can be rewritten as:

- Valve:

$$M_a = c_d c_0 w_a X_a f_n(x_3, P_s, P_e) \tag{2-32.a}$$

$$M_b = c_d c_0 w_b X_b f_n(x_4, P_s, P_e) \tag{2 -32.b}$$

Where

$$f_n(x_3, P_s, P_e) = \begin{cases} P_s \tilde{f}(x_3/P_s)/\sqrt{T_s}, & \text{Chamber A is drive chamber} \\ x_3 \tilde{f}(P_e/x_3)/\sqrt{T_a}, & \text{Chamber B is drive chamber} \end{cases} \tag{2-33}$$

$$f_n(x_4, P_s, P_e) = \begin{cases} P_s \tilde{f}(x_4/P_s)/\sqrt{T_s}, & \text{Chamber B is drive chamber} \\ x_4 \tilde{f}(P_e/x_4)/\sqrt{T_a}, & \text{Chamber A is drive chamber} \end{cases} \tag{2 -34}$$

and

$$\tilde{f}(P_r) = \begin{cases} 1, & P_{atm}/P_a < P_r \le c_r \\ c_k\left(P_r^{2/k} - P_r^{(k+1)/k}\right)^{1/2}, & c_r < P_r < 1 \end{cases} \tag{2-35}$$

- Cylinder

$$\dot{x}_3 = \frac{k}{(l/2 + x_1 + \Delta)}\left(-x_3 x_2 + \frac{RT_s}{A_a} M_a\right) \tag{2-36.a}$$

$$\dot{x}_4 = \frac{k}{(l/2 - x_1 + \Delta)}\left(x_4 x_2 + \frac{RT_s}{A_b} M_b\right) \tag{2 -36.b}$$

- Payload:

$$\dot{x}_1 = x_2 \tag{2-37.a}$$

$$\dot{x}_2 = \frac{1}{m}\left[-K_f x_2 - F_{S-C} + A_a x_3 - A_b x_4\right] \tag{2 -37.b}$$

Therefore, a complete pneumatic cylinder system model can be obtained with the system input, *i.e.* v alve displacements and the four state variables. Let $u_1 = X_a$ and $u_2 = X_b$, then:

$$\dot{x}_1 = x_2 \tag{2-38.a}$$

$$\dot{x}_2 = \frac{1}{m}\left[-K_f x_2 - K_{S\text{-}C} S(x_2, x_3, x_4) + A_a x_3 - A_b x_4\right] \tag{2-38.b}$$

$$\dot{x}_3 = \frac{k}{(l/2 + x_1 + \Delta)}\left[-x_3 x_2 + \frac{RT_s}{A_a} c_d c_0 w_a u_1 f_n(x_3, P_s, P_e)\right] \tag{2-38.c}$$

$$\dot{x}_4 = \frac{k}{(l/2 - x_1 + \Delta)}\left[x_4 x_2 + \frac{RT_s}{A_b} c_d c_0 w_b u_2 f_n(x_4, P_s, P_e)\right] \tag{2 -38.d}$$

The parameters and constants used in the system model are listed in the nomenclature and list of constants at the very beginning of the thesis. The term $-K_f x_2 - K_{S\text{-}C} S(x_2, x_3, x_4)$ in Equation (2-38.b) represents the summing effects of static and dynamic friction forces of the system, where

$$K_{S\text{-}C} S(x_2, x_3, x_4) := \begin{cases} (A_a x_3 - A_b x_4), & x_2 = 0 \quad and \quad |A_a x_3 - A_b x_4| \le F_S(x_2) \\ F_C(x_2)\,\mathrm{sign}(x_2), & x_2 \neq 0 \quad or \quad |A_a x_3 - A_b x_4| > F_S(x_2) \end{cases} \tag{2-39}$$

which describes the static friction. In the above formula, $F_S(x_2)$ repres ents static friction and $F_C(x_2)$ represents Coulomb friction. They are both dependent on the surface condition and the payload.

2.2 Friction Characteristics

In all machines incorporating parts with relative motion, friction is present. In most systems, friction has a negative influence on the performance of the system. Under certain conditions, friction in a system can result in effects like a steady state error, tracking errors, especially nearby velocity reversals (reversal bump effect: getting stuck when moving through zero velocity), limit cycles or stick-slip. To overcome these negative effects, insight into friction phenomena

and proper models of these frictions are useful. This section will address these aspects of friction and describe the friction models.

2.2.1 Introduction to Friction Phenomena

The first static friction model was the classic model of friction of Leonardo Da Vinci: friction force is proportional to load, opposes the direction of motion and is independent of contact area. In 1785, Coulomb further developed this model and the friction phenomena described by the model became known as Coulomb friction (Bowden and Tabor, 1974). Therefore, the Coulomb friction force can be described as: $F_C = F_n \cdot \mu_C \cdot \text{sign}(\dot{\tilde{x}})$, where μ_C is the Coulomb friction coefficient, F_n is the gravity of the object. The Coulomb friction model is often used because of its simplicity. It is also referred to as dynamic friction.

In 1833, Morin introduced the idea of static friction (Bowden and Tabor, 1974): friction force opposes the direction of motion when the sliding velocity is zero. The static friction force, is equal to the tensile forces until a maximum or minimum is reached: $F_{Smax} = F_n \cdot \mu_S$ and $F_{Smin} = -F_n \cdot \mu_S$, where μ_S is the static friction coefficient.

In 1866, Reynolds developed expressions for the friction force caused by the viscosity of lubricants (Bowden and Tabor, 1974). The term viscous friction is used for this friction phenomenon. The viscous friction force can be described as: $F_V = \mu_V \cdot F_n \cdot \dot{\tilde{x}}$, where μ_V is the viscous friction coefficient.

When the above three frictions join together, a friction model appears, which is commonly used in practice: the static plus Coulomb plus viscous friction model. This model is illustrated in Figure 2.2.

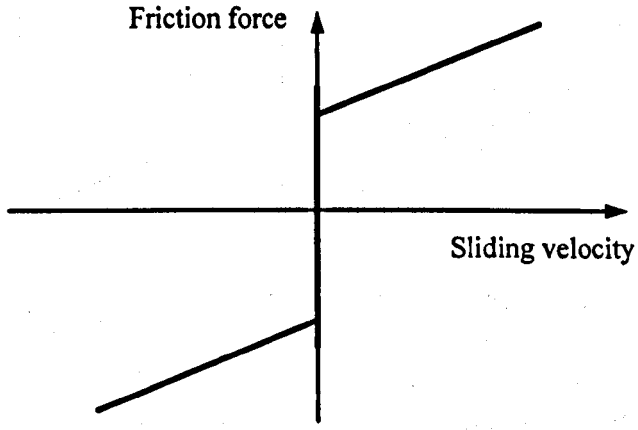

Figure 2.2 The static, Coulomb plus viscous friction model

In 1902, Stribeck observed that for low velocities, the friction force decreases continuously with increasing velocities and not in a discontinuous matter as described in Figure 2.2. This phenomenon of a decreasing friction at low, increasing velocities is called the Stribeck friction or Stribeck effect. The presence of nonlinear friction forces is unavoidable in high-performance motion control systems. The friction model has been widely studied by numerous researchers, who have attempted to understand its physics and dynamics (Kim and Lewis, 2000; Drakunov *et al.*, 1997). When considering the relationship between the velocity and static, Coulomb and fluid viscous frictions, the combination friction (Armstrong-Helouvry *et al.*, 1994), *i.e.* the friction model including static, Coulomb, viscous and Stribeck friction is given in Figure 2.3.

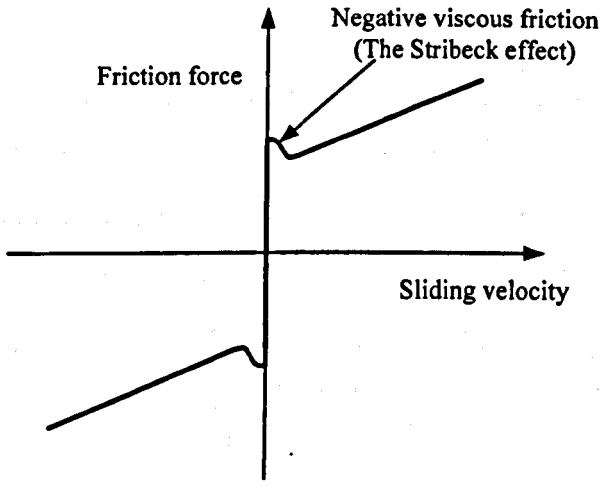

Figure 2.3 The static, Coulomb, viscous plus Stribeck friction model

Actually, the dynamic model of friction is far more complicated than that illustrated in Figure 2.3. There are four regimes of lubrication in a system with grease or oil: static friction, boundary lubrication, partial fluid lubrication and full lubrication. Each of four regimes contributes to the dynamics that a controller confronts as the machine accelerates away from zero velocity. Figure 2.4 is known as the Stribeck curve and shows the three moving regimes (Armstrong-Helouvry *et al.*, 1994).

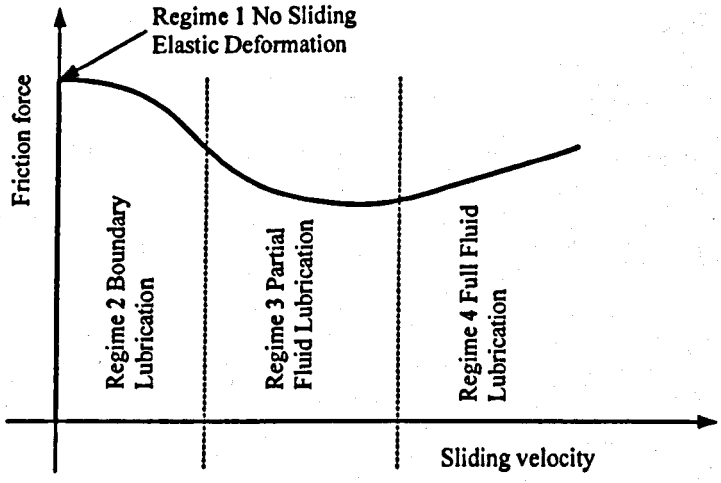

Figure 2.4 The generalized Stribeck curve

2.2.2 Simplified Friction Model

However, the friction model, which integrates the four regimes of the Stribeck curve shown in Figure 2.4, is far too complicated for the purpose of dynamic response investigation of pneumatic actuator systems. In this thesis, a simplified friction model will be used. The simplified friction model was proposed by some researchers, for example, Karnopp, 1985 and Wang *et al.*, 1998, which is shown below:

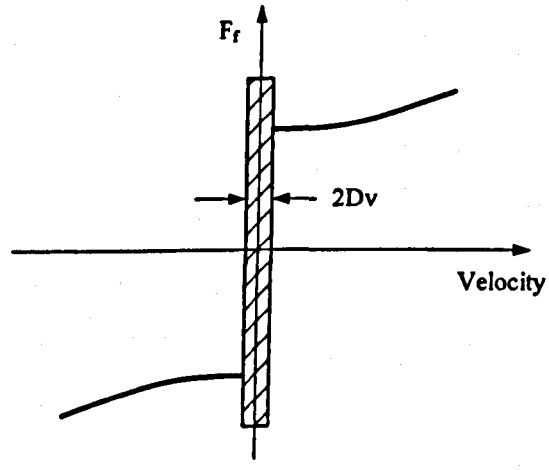

Figure 2.5 Static + Coulomb friction forces

A small neighbourhood of zero velocity is defined by D_v as shown in Figure 2.5. Inside the neighbourhood, velocity is considered to be zero and friction is force dependent. Similar dynamic analysis can be applied to machines with rotary motion. The torque plays an important role in dynamic analysis, which is similar to the force applied on the moving body. In modelling study of pneumatic cylinder systems, a simplified friction model is adopted and illustrated in Figure 2.6.

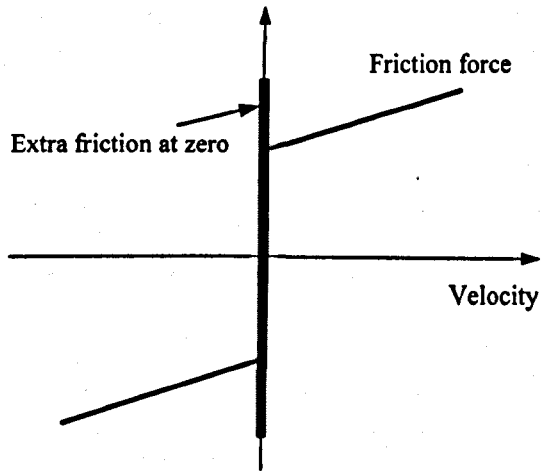

Figure 2.6 Simplified friction model

This model indicates that, when velocity is zero, the friction is classified as static friction. As soon as velocity is not equal to zero, the friction changes from static friction to dynamic friction, which combines coulomb and viscous friction. This simplified model can be expressed exactly as Equation (2-39).

2.3 Simulation Study of Pneumatic Cylinder Dynamic Characteristics

The open-loop simulation studies of the pneumatic cylinder actuating system have been conducted. The mathematical model has been implemented in Matlab to facilitate the simulation studies. This section will illustrate the simulation results and analysis of the open-loop responses with step input response of rodless and rodded pneumatic cylinders.

The Matlab programme shown in Appendix part A is developed to solve the

four differential equations that represent the cylinder model. The control inputs are the spool displacements of two control valves, which are proportional type. For the system model, the only difference between the rodless cylinder model and rodded cylinder model is the effective piston area of Chamber B, *i.e.* A_b. In the rodded cylinder model the effective piston area is less than that of the rodless cylinder model, due to the rod which connects the piston and the payload in rodded cylinder. The open-loop dynamics of the pneumatic cylinder actuating system can be observed from the simulation results. It is also known that the system dynamics are affected by design parameter variations.

2.3.1 Open-loop Simulation on Rodless Cylinder

Firstly, a simulation study has been conducted on the rodless cylinder model due to the symmetric structure. The simulation parameters are as follows:

- Cylinder: Rodless cylinder
- Stroke length: 1000mm
- Diameter of piston: 32mm
- Supply air pressure: 6 bars
- Exhaust pressure: 1 bar
- Initial chamber pressures: 3.5 bars for both chambers
- Temperature: 293K
- Valve spool displacements: 2mm and -2mm (valve half open)
- Payload mass: 1kg
- Static friction force: 60N
- Coulomb friction force: 2N
- Viscous frictional coefficient: 15Ns/m
- Simulation time: 2s

In the simulation studies, the cylinder has equal initial chamber pressures, $P_{a0} = P_{b0}$, in order to make the piston stop at the initial position. In addition, the symbols of control inputs are set to vary with the piston movement direction: when the piston moves towards to the positive direction (refer to Figure 2.1), $u_1 = 2$ mm, $u_2 = -2$ mm; when the piston moves towards to the negative direction, $u_1 = -2$ mm, $u_2 = 2$ mm.

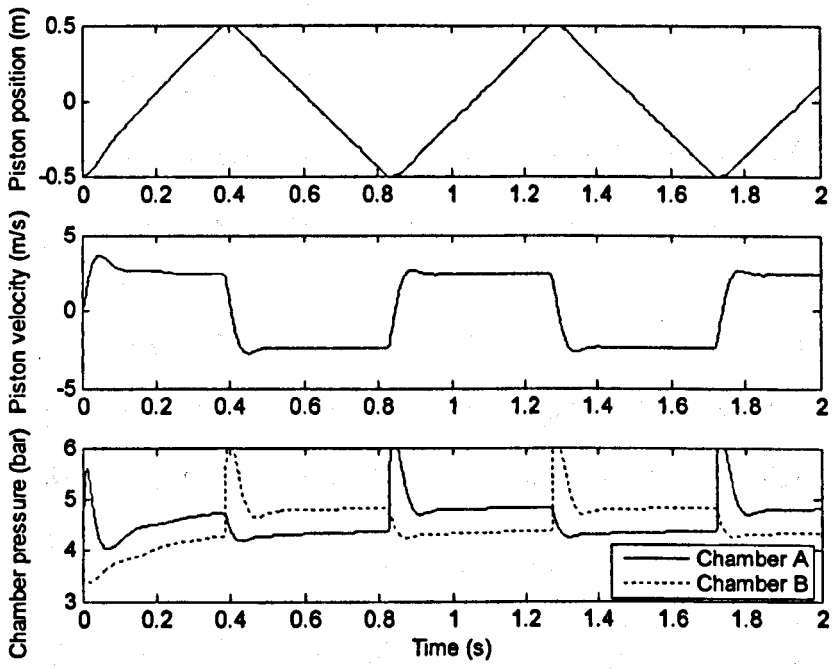

Figure 2.7 Open-loop simulation results of rodless cylinder

Figure 2.7 shows the cycle-to-cycle open-loop step input response. The dynamic piston position, piston velocity and chamber pressures are illustrated in the figure. From the figure, it can be seen that the cylinder completes two full cycles within 2 seconds. The piston goes from one end of the cylinder to the other (from -0.5 to 0.5 then goes back), which provides linear motion to the payload. When Chamber A pressure is greater than Chamber B pressure, Chamber A will be the working chamber, and the piston will drive the payload

in the right direction (refer to Figure 2.1); when the Chamber B pressure is greater than the Chamber A pressure, Chamber B will be the working chamber, and the piston will move in the left direction. A variety of simulation studies has been done to investigate the simulation parameters that influence to the system open-loop dynamics. Figure 2.7 will be compared with those results.

First of all, the effect of control inputs u_1 and u_2 has been investigated. With the same simulation conditions described at the beginning of this section, only the control inputs have been changed. Figure 2.8 shows the simulation results with 4mm valve spool displacement, which means the valve is fully opened, whilst Figure 2.9 shows the simulation results with 0.4mm valve spool displacement that means the valve only opens 10%. Comparing Figure 2.7, 2.8 and 2.9, it can be observed that with bigger control inputs, the piston can move faster, and the chamber pressures change dramatically accordingly. Therefore, for more stable movement of the payload, smaller control inputs should be applied with the compromise of the piston velocity.

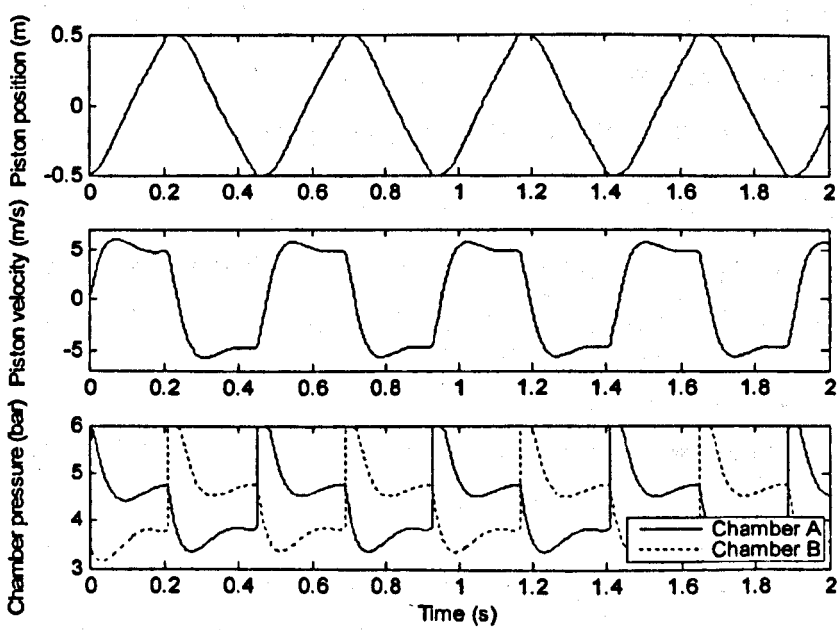

Figure 2.8 Open-loop simulation results with u_1 =4mm, u_2= -4mm

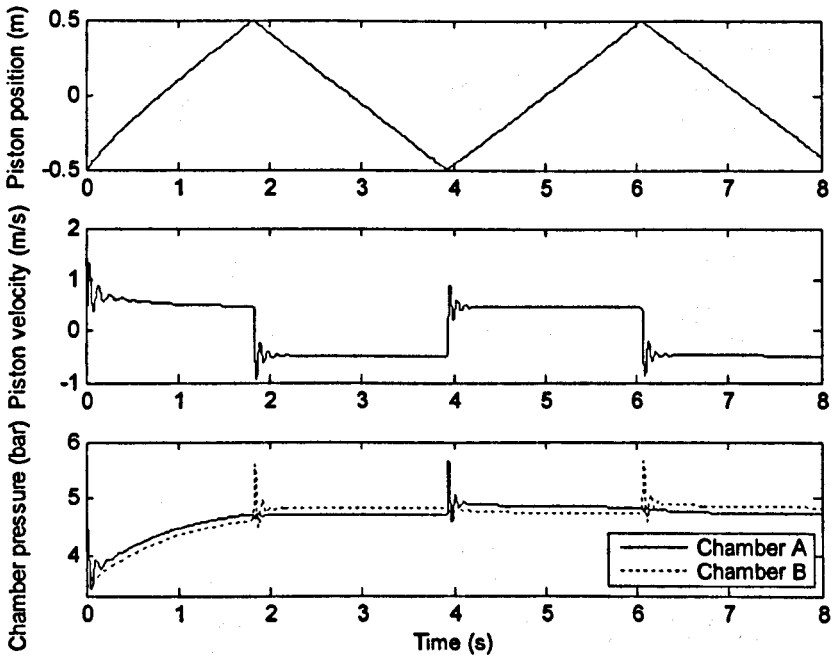

Figure 2.9 Open-loop simulation results with u_1 =0.4mm, u_2= -0.4mm

The effect of the compressed air supply pressure P_s has also been investigated. Under the same simulation conditions described at the beginning of this section, except for the compressed air supply pressure, Figure 2.10 shows the open-loop simulation results with 5 bars supply pressure, while Figure 2.11 and Figure 2.12 are with 8 bars and 10 bars supply pressures respectively. Comparing Figures 2.7 (6 bars), 2.10(5 bars), 2.11(8 bars) and 2.12(10 bars), it can be observed that with high compressed air pressure, the piston moves rapidly. For the first cycle although the initial acceleration seems increased with supply pressure, this is just due to the relative low initial chamber pressures, so after the first cycle the velocity becomes more stable. Apparently, high air supply pressure can make fast movement, but with more energy consumption.

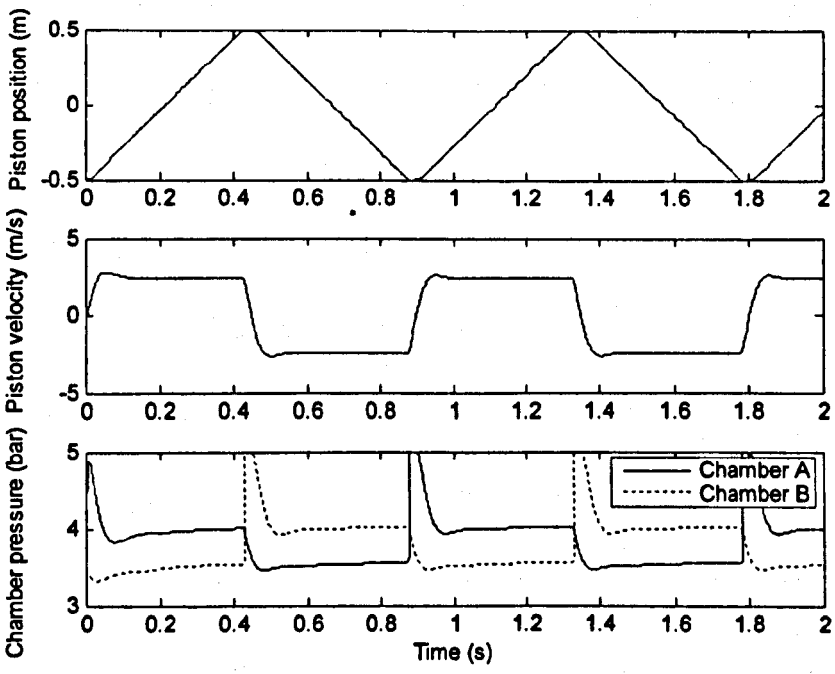

Figure 2.10 Open-loop simulation results with P_s =5bars

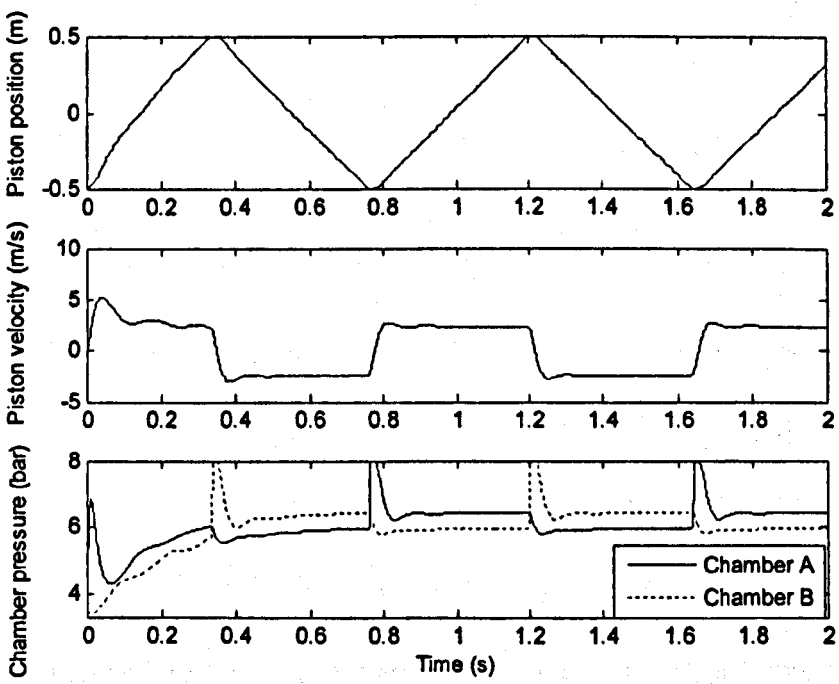

Figure 2.11 Open-loop simulation results with P_s =8bars

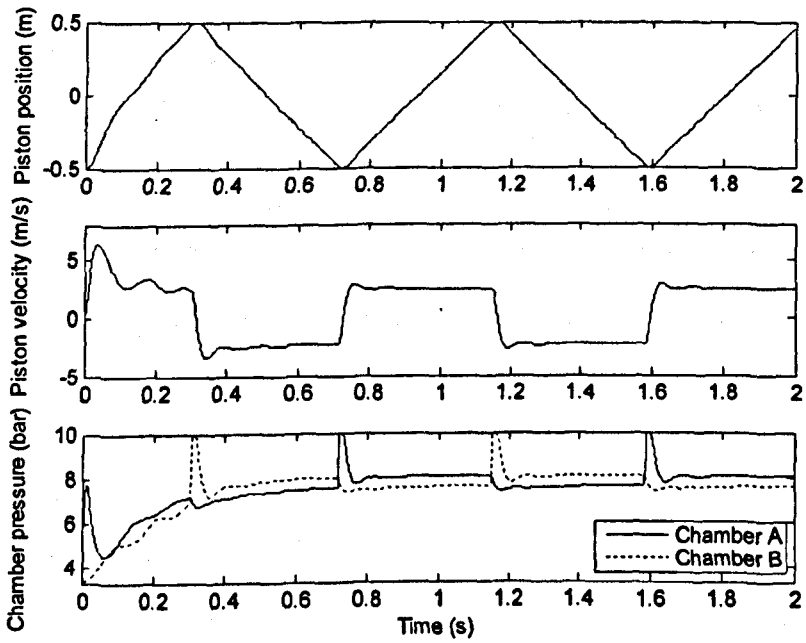

Figure 2.12 Open-loop simulation results with P_s =10bars

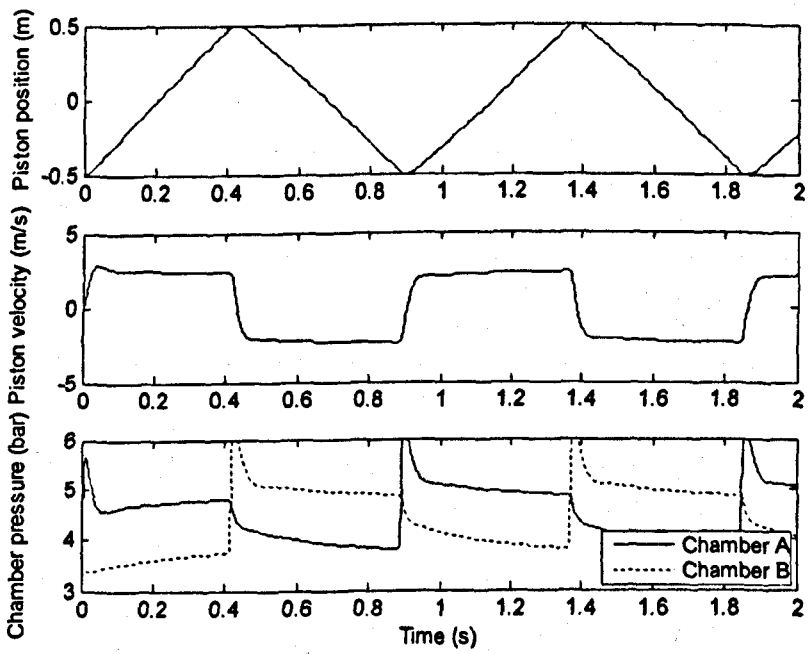

Figure 2.13 Open-loop simulation results with $K_f = 35\,\mathrm{Ns/m}$

When the lubrication is not good enough in the inner chambers of the cylinder, the viscous friction will increase. Figure 2.13 shows the effect of bigger viscous frictional coefficient K_f on the open-loop simulation results. Comparing with Figure 2.7($K_f = 15\text{Ns/m}$) and Figure 2.13($K_f = 35\text{Ns/m}$), it can be seen that with bigger viscous friction, the piston moves slower, and the piston starts more smoothly at each end of the stroke. However, from the energy saving point of view, the viscous friction should be kept to the minimum level.

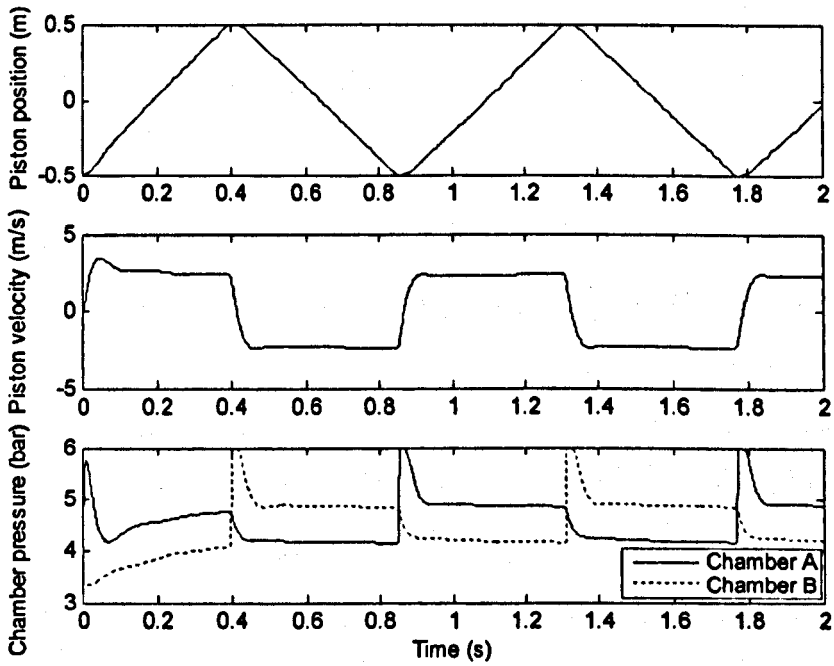

Figure 2.14 Open-loop simulation results with $F_s = 120\text{N}$, $F_c = 20\text{N}$

Static friction and Coulomb friction mainly depend on the contact surfaces and the mass of the object, which is in this case the mass of piston and the payload. When lubrication is not enough or the mass of payload increases, static and Coulomb frictions will increase. Figure 2.14 shows the open-loop simulation results with 120N static friction and 20N Coulomb friction. It should be noted

that in Figure 2.14 these frictions are extremely high for the cylinder system, so they are used here just for observation of the influence. Comparing Figure 2.7($F_S = 60\text{N}$, $F_C = 2\text{N}$) and Figure 2.14($F_S = 120\text{N}$, $F_C = 20\text{N}$), it can be seen that with bigger frictions the piston moves more slowly. Bigger static friction will increase counterwork against the start-up of the piston, whilst bigger Coulomb friction will slow down the piston through the entire cylinder stroke. From the energy saving point of view, all frictions should be kept to minimum levels.

2.3.2 Open-loop Simulation on Rodded Cylinder

The open-loop simulation is also conducted on the rodded cylinder model. The pneumatic cylinder showed in Figure 2.1 is a rodded type cylinder. The only difference between rodless and rodded cylinder is their effective piston area in Chamber B, because rodded cylinder has a rod to connect the payload. Therefore, for the rodded cylinder model used in this section most simulation parameters remain the same as those in Subsection 2.5.1; the only difference is the effective piston area in Chamber B, *i.e.* A_b. Assume the diameter of the rod connected to the piston in Chamber B is half of the piston diameter, d_r=0.5d, thus $A_r = \pi(d_r/2)^2 = \pi(0.5d/2)^2 = 0.25A_a$, then $A_b = A_a - A_r = 0.75A_a$. Therefore, the initial chamber pressures for Chamber A should be less than that of Chamber B to make the forces applied on the two sides of piston balanced, thus $P_{a0} = 0.75P_{b0}$. The initial chamber pressures are set as P_{a0} =3.5bar and P_{b0} =4.67bar.

Figures 2.15 and 2.16 show the open-loop dynamics of the rodded cylinder with step inputs u=2mm (valves half open) and u=4mm (valves fully open) respectively. Owing to the smaller effective piston area in Chamber B, for the majority of the time Chamber B pressure has to be higher than Chamber A pressure. And for the same reason, when Chamber B is the driving chamber, the cylinder uses a longer time to drive the load to the desired position than that time when Chamber A drives.

However, for the symmetric geometrical structure of the cylinder, the rodless cylinder model will be adopted and discussed throughout the entire thesis due to its convenience.

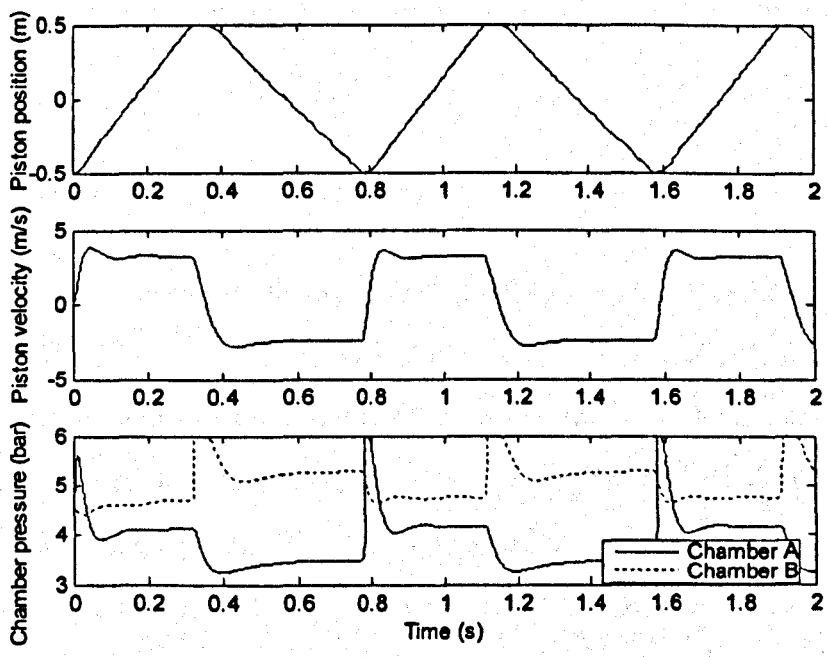

Figure 2.15 Open-loop simulation results on rodded cylinder with $u = 2$mm

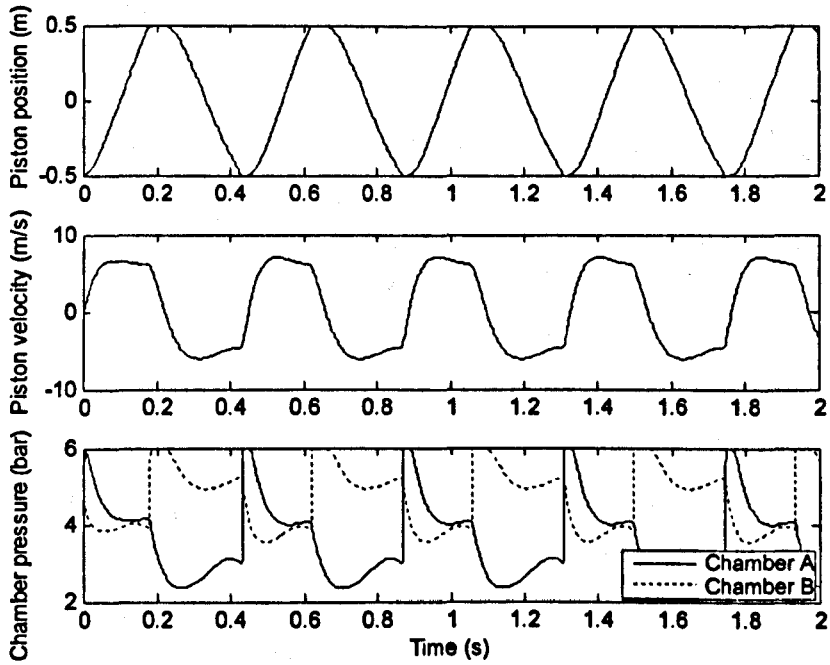

Figure 2.16 Open-loop simulation results on rodded cylinder with $u = 4\text{mm}$

2.4 Summary

This chapter focuses on the modelling of the pneumatic cylinder actuating system. Modelling of each system component has been discussed and then integrated. The mathematical model of the pneumatic cylinder actuating system has been worked out. One characteristic can not be neglected in pneumatic cylinder actuating systems: Friction phenomena have been introduced and a simplified friction model has been presented. In addition, the open-loop dynamics of rodless and rodded cylinder actuating systems are investigated by computer simulation work. The simulation results with a variety of different parameters are shown and analysed. However, the rodless cylinder will be adopted throughout the entire thesis due to its symmetric geometrical structure.

Chapter 3

Energy Efficient Optimal Control of Pneumatic Cylinder Systems

3.1 Introduction

This chapter addresses the issue of improvement of energy efficiency for servo-controlled pneumatic cylinder systems by using optimal control method. It is desired to find the optimal energy efficient profiles through optimal control of the pneumatic cylinder system, and then these optimal profiles can be tracked in practice. Even the users in industry do not use optimal controller, as long as they use the optimally energy efficient profiles, the pneumatic cylinder systems can save energy. So this chapter will start by introducing optimal control theory.

Optimal control theory has been proposed for over half a century, Kalman (1960) and Pontryagin (1962) *et al.* contributed extensively to this subject. The most successful achievement is to expand linear quadratic regulator (LQR) and Linear quadratic Gaussian (LQG) feedback control. In other cases, the optimal control is open-loop in nature which limited the application of optimal control theory. Although the work conducted in this chapter is to apply optimal control theory to pneumatic systems, the derivation of optimal control is not the main objective. Generalising energy efficient profiles or in other words predefined

tracking trajectories is the main aim of the work.

When optimal control theory is applied to the system model, an extra set of co-state differential equations will be generated. These co-state equations and the original system equations are coupled into a more complicated extended system model. Solving this extended system model, the energy optimal control law and the optimal profiles can then be obtained.

However, one may encounters difficulties in solving such a complicated system analytically. Numerical analysis usually can not be avoided, as the system has only partially known boundary and initial conditions. Shooting method (Lewis and Syrmos, 1995) and genetic algorithms can be adopted to search the unknown boundary and initial values. This will be discussed in later sections.

3.2 Introduction to Optimal Control Theory

The main objective of optimal control is to determine control signals that will cause a process or plant to satisfy some physical constraints and at the same time extremize (maximise or minimise) a chosen performance criterion (performance index or cost function). Finding the optimal control $u^*(t)$ (* indicates optimal condition) will drive the plant from the initial state to a final desired state with some constraints on controls and states and at the same time extremize the given performance index J.

The formulation of optimal control problem requires (Naidu, 2003):

1. A mathematical description or model of the process to be controlled (generally in state variable form);
2. A specification of the performance index;
3. A statement of boundary conditions and the physical constraints on the states and/or controls.

In this chapter, it is desired to minimise the energy consumed by the pneumatic cylinder system. Therefore, Pontryagin's minimum principle (1962) has been chosen and will be discussed in this section.

3.2.1 Calculus of Variations

Calculus of variations is a field of mathematics that deals with functionals, as opposed to ordinary calculus which deals with functions (Forsyth, 1927). The calculus of variations may be said to begin with a problem of Johann Bernoulli's, but Euler first elaborated the subject. His contributions began in 1733, and Lagrange contributed extensively to the theory (Forsyth, 1927).

If $x(t)$ is a continuous function of time t, $x \in C^2$, then the differentials $dx(t)$ and dt are not independent. However, a small change in $x(t)$ can be defined that is independent of dt. Let us define the variation in $x(t)$, *i.e.* $\delta x(t)$, as the incremental change in $x(t)$ when time t is fixed.

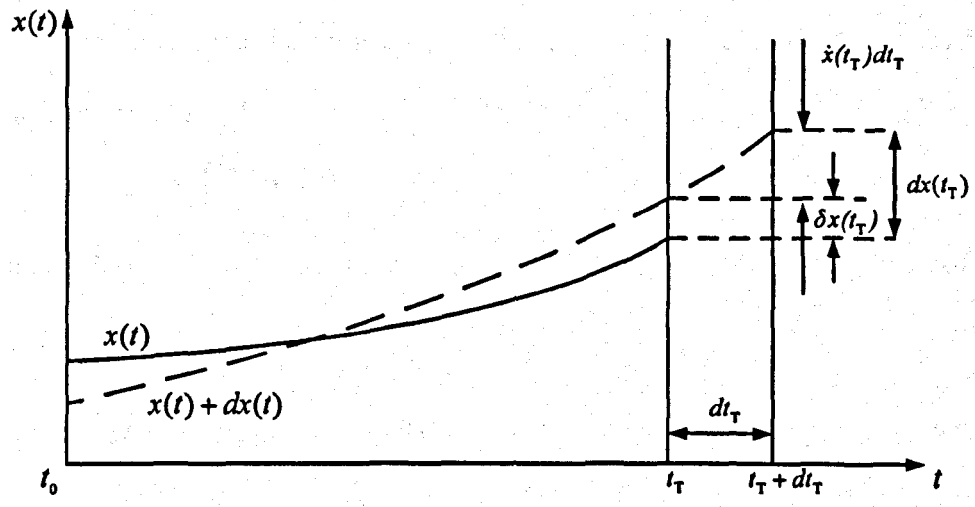

Figure 3.1 Relation between the variation δx and the differential dx (Figure courtesy of Lewis and Syrmos, 1995)

The relations among dx, δx, and dt are illustrated in Figure 3.1 (Lewis and Syrmos, 1995), which shows the original function $x(t)$ and a neighboring function $x(t)+dx(t)$ over an interval specified by initial time t_0 and final time T. In addition to the increment $dx(t)$ at each time t, the final time has been incremented by dt_T. It is clear from the illustration that the overall increment in x at t_T, $dx(t)$, depends on dt_T. According to the definition, the variation $\delta x(t)$ occurs at the fixed value of $t=t_T$ as shown and is independent of dt_T. Since $x(t)$ and $x(t)+dx(t)$ have approximately the same slope $\dot{x}(t_T)$ at $t=t_T$, and since dt_T is small, the following holds

$$dx(t_T) \doteq \delta x(t_T) + \dot{x}(t_T)dt_T \tag{3-1}$$

Another relation that is required is Leibniz's rule for functionals: if $x(t) \in \Re^n$ is a function of t and

$$J(x) = \int_0^T h(x(t),t)\, dt \tag{3-2}$$

where $J(\cdot)$ and $h(\cdot)$ are both real scalar functionals, *i.e.* functions of the function $x(t)$, then

$$dJ = h(x(t_T),t_T)\, dt_T - h(x(t_0),t_0)\, dt_0 + \int_0^T [h_x^T(x(t),t)\delta x]\, dt \tag{3-3}$$

Thus, the notation is $h_x = \dfrac{\partial h}{\partial x}$.

3.2.2 Solutions of the General Continuous Optimisation Problem

Pontryagin's principle is used in optimal control theory to find the best possible control for taking a dynamic system from one state to another, especially in the presence of constraints for the state or input controls (Pontryagin *et al.*, 1962). It has as a general case the Euler-Lagrange equation of the calculus of variations.

Suppose a system is described by the nonlinear model:

$$\dot{x}(t) = \hat{f}(x,u,t) \tag{3-4}$$

with state $x(t) \in \Re^n$ and control input $u(t) \in \Re^m$. With this system the performance index is associated as

$$J(t_0) = \phi(x(t_T),t_T) + \int_0^T L(x(t),u(t),t)\, dt \tag{3-5}$$

where $[t_0, t_T]$ is the time interval of interest. The final weighting function $\phi(x(t_T),t_T)$ depends on the final state and final time, and the weighting

function $L(x,u,t)$ depends on the state and input at intermediate times in $[t_0,t_T]$.

The performance index is selected to make the plant exhibit a desired type of performance. The optimal control problem is to find the input $u^*(t)$ on the time interval $[t_0,t_T]$ that drives the plant (3-4) along a trajectory $x^*(t)$ such that the cost function (3-5) is minimised, and such that the terminal condition

$$\psi(x(t_T),t_T)=0 \tag{3-6}$$

for a given function $\psi \in \Re^p$ (if there is a terminal condition).

The roles of the final weighting function ϕ and the fixed final function ψ should not be confused. $\phi(x(t_T),t_T)$ is a function of the final state, which is required to be minimised. An illustration might be the energy, which is $[x^T(t_T)S(t_T)x(t_T)]/2$, where $S(t_T)$ is a given weighting matrix. On the other hand, $\psi(x(t_T),t_T)$ is a function of the final state, which is required to be fixed at exactly zero.

To solve the continuous optimal control problem, Lagrange multipliers should be used to adjoin the constraints (3-4) and (3-6) to the performance index (3-5). Since the model (3-4) holds at each $t \in [t_0,t_T]$, an associated Lagrange multiplier $\lambda(t) \in \Re^n$ is required, which is a function of time. Since the terminal condition (3-6) holds only at one time, a constant associated multiplier $v \in \Re^p$

is required. The augmented performance index is thus

$$J' = \phi(x(t_T),t_T) + v^T \psi(x(t_T),t_T) + \int_0^T [L(x,u,t) + \lambda^T(t)(f(t)(x,u,t) - \dot{x})]\, dt \quad (3\text{-}7)$$

If the Hamiltonian function is defined as

$$H(x,u,t) = L(x,u,t) + \lambda^T f(x,u,t) \quad (3\text{-}8)$$

then Equation (3-7) can be rewritten as

$$J' = \phi(x(t_T),t_T) + v^T \psi(x(t_T),t_T) + \int_0^T [H(x,u,t) - \lambda^T \dot{x}]\, dt \quad (3\text{-}9)$$

Using Leibniz's rule, the increment in J' as a function of the increments in $x, \lambda, v, u,$ and t is

$$\begin{aligned} dJ' = {} & (\phi_x + \psi_x^T v)^T dx\big|_{t_T} + (\phi_t + \psi_t^T v)^T dt\big|_{t_T} + \psi^T\big|_{t_T} dv + (H - \lambda^T \dot{x})\, dt\big|_{t_T} \\ & - (H - \lambda^T \dot{x})\, dt\big|_{t_0} + \int_0^T [H_x^T \delta x + H_u^T \delta u - \lambda^T \delta \dot{x} + (H_\lambda - \dot{x})^T \delta\lambda]\, dt \end{aligned} \quad (3\text{-}10)$$

To eliminate the variation in $\dot{x}$, integrate by parts to see that

$$-\int_0^T \lambda^T \delta\dot{x}\, dt = -\lambda^T \delta x\big|_{t_T} + \lambda^T \delta x\big|_{t_0} + \int_0^T \dot{\lambda}^T \delta x\, dt \quad (3\text{-}11)$$

Substituting Equation (3-11) into Equation (3-10), the resulting terms at $t = t_T$ are dependent on both $dx(t)$ and $\delta x(t_T)$. $\delta x(t_T)$ can be expressed in terms of $dx(t)$ and dt_T using Equation (3-1). The result after these two substitutions is:

$$\begin{aligned} dJ = {} & (\phi_x + \psi_x^T v - \lambda)^T dx\big|_{t_T} + (\phi_t + \psi_t^T v + H - \lambda^T \dot{x} + \lambda^T \dot{x}) dt\big|_{t_T} + \psi^T\big|_{t_T} dv \\ & - (H - \lambda^T \dot{x} + \lambda^T \dot{x})\, dt\big|_{t_0} + \lambda^T dx\big|_{t_0} + \int_0^T [(H_x + \dot{\lambda})^T \delta x + H_u^T \delta u + (H_\lambda - \dot{x})^T \delta\lambda]\, dt \end{aligned} \quad (3\text{-}12)$$

According to the Lagrange theory, the constrained minimum of J is attained at the unconstrained minimum of J'. This is achieved when $dJ' = 0$ for all independent increments in its arguments. Setting to zero the coefficients of the

independent increments $dv, \delta x, \delta u$, and δv yields necessary conditions for a minimum as shown in Table 3-1. For this applications, t_0 and $x(t_0)$ are both fixed and known, so that dt_0 and $dx(t_0)$ are both zero. The two terms evaluated at $t = t_0$ in (3 -12) are thus automatically equal to zero.

Table 3.1 Continuous time optimal control with fixed final states

System model	$\dot{x} = \hat{f}(x,u,t), \quad t \geq t_0, \quad t_0$ fixed
Performance index	$J(t_0) = \phi(x(t_T),t_T) + \int_{t_0}^{T} L(x,u,t)\, dt$
Final-state constraint	$\psi(x(t_T),t_T) = 0$
Hamiltonian	$H(x,u,t) = L(x,u,t) + \lambda^T \hat{f}(x,u,t)$
State equation	$\dot{x} = \frac{\partial H}{\partial \lambda} = \hat{f}, \quad t \geq t_0$
Co-state equation	$-\dot{\lambda} = \frac{\partial H}{\partial x} = \frac{\partial f^T}{\partial x}\lambda + \frac{\partial L}{\partial x}, \quad t \leq t_T$
Stationarity condition	$0 = \frac{\partial H}{\partial u} = \frac{\partial f^T}{\partial u}\lambda + \frac{\partial L}{\partial u}$
Boundary condition	$x(t_0)$ given, $(\phi_x + \psi_x^T v - \lambda)^T\big\|_{t_T} dx(t_T) + (\phi_t + \psi_t^T v + H)\big\|_{t_T} dt_T = 0$ (3-13)

The boundary condition in Table 3.1 needs further discussion. It can be seen from Figure 3.1 that $dx(t_T)$ and dT are not independent. Therefore, the coefficients of the first two terms on the right hand side of Equation (3-12) cannot be simply set separately equal to zero. Instead, the entire expression

(3-13) must be zero at $t = t_T$. The time derivative of the Hamiltonian is

$$\dot{H} = H_t + H_x^T \dot{x} + H_u^T \dot{u} + \dot{\lambda}^T \hat{f} = H_t + H_u^T \dot{u} + (H_x + \dot{\lambda})^T \hat{f} \quad (3\text{-}14)$$

If $u(t)$ is an optimal control, then $\dot{H} = H_t$ (3-15)

Now, in the time-invariant case, $\hat{f}$ and L are not explicit functions of t, and so neither is H. In this situation $\dot{H} = 0$ (3-16)

Hence, for time-invariant systems and cost functions, the Hamiltonian is a constant on the optimal trajectory.

3.2.3 Solution of Two-point Boundary Value Problems

There are many computational methods for solving the optimal control problem. A few approaches that have immediate practical appeal are presented in this section (Lewis and Syrmos, 1995).

Suppose it is desired to solve the optimal control problem for the nonlinear plant (3-4) with quadratic performance index

$$J(t_0) = \frac{1}{2}(x(t_T) - r(t_T))^T S(t_T)(x(t_T) - r(t_T)) + \frac{1}{2}\int_{t_0}^{t_T} (x^T Q x + u^T R u)\, dt \quad (3\text{-}17)$$

where $S(t_T) \geq 0, Q \geq 0, R \geq 0$, and the desired final-state value $r(t_T)$ is given. Thus, the control $u(t)$ over the interval $[t_0, t_T]$ can be found to minimise $J(t_0)$. The final state is constrained to satisfy (3-6) for some given function $\psi \in \Re^p$. For simplicity, let the final time t_T be fixed.

According to Table 3.1, the state equation (3-4) and the Euler equations (3-18)

and (3-19) should be solved.

$$-\dot{\lambda} = \frac{\partial \hat{f}^T}{\partial x}\lambda + Qx \tag{3-18}$$

$$0 = \frac{\partial \hat{f}^T}{\partial u}\lambda + Ru \tag{3-19}$$

In general, the Jacobians $\partial \hat{f} / \partial x$ and $\partial \hat{f} / \partial u$ depend on the control $u(t)$, so that Equation (3-19) is an implicit equation for $u(t)$. If $\partial \hat{f} / \partial u$ is independent of $u(t)$, then the closed-loop feedback

$$u = -R^{-1}\frac{\partial \hat{f}^T}{\partial u}\lambda \tag{3-20}$$

which we can use to eliminate $u(t)$ in the state equation and the co-state equation (3-18), obtaining the Hamiltonian system

$$\dot{x} = \hat{f}\left(x, -R^{-1}\frac{\partial \hat{f}^T}{\partial u}\lambda, t\right) \tag{3-21.a}$$

$$-\dot{\lambda} = \frac{\partial \hat{f}^T}{\partial x}\lambda + Qx \tag{3-21.b}$$

The Hamiltonian system is a nonlinear ordinary differential equation in $x(t)$ and $\lambda(t)$ of order $2n$ with split boundary conditions, which are

n conditions: $x(t_0) = r(t_0)$ given, (3-22)

p conditions: $\psi(x(t_T), t_T) = 0$ (3-23)

n–p conditions: $\lambda(t_T) = S(t_T)(x(t_T) - r(t_T)) + \frac{\partial \psi^T}{\partial x}\Big|_{t_T} \nu$ (3-24)

The undetermined multipliers $\nu \in \Re^p$ allow some freedom, which means that

(3-24) provides only the required number n-p of final conditions (Lewis and Syrmos, 1995).

There are several ways to solve the Hamiltonian system numerically. An intensive discussion was provided by Bryson and Ho (1975). In numerical analysis, the shooting method is a method for solving a boundary value problem by reducing it to the solution of an initial value problem. This is done by assuming initial values that would have been given if the ordinary differential equation were a initial value problem. The boundary value obtained is compared with the actual boundary value. Using trial and error or some scientific approach, one tries to get as close to the boundary value as possible. The algorithm is given as follows (Lewis and Syrmos, 1995):

1. Guess the n unspecified initial conditions $\lambda(t_0)$.

2. Integrate the Hamiltonian system forward from t_0 to t_T.

3. Using the resulting values of $x(t_T)$ and $\lambda(t_T)$, evaluate

$$\psi(x(t_T), t_T) \tag{3-25}$$

$$\text{and } \lambda(t_T) - S(t_T)(x(t_T) - r(t_T)) - \frac{\partial \psi^T}{\partial x}\Big|_{t_T} v \tag{3-26}$$

4. If there is no $v \in \Re^p$ that makes constraint (3-25) and (3-26) equal to zero, determine changes in the final state and co-state $\delta x(t_T)$ and $\delta \lambda(t_T)$ to bring these functions closer to zero.

5. Find the sensitivity matrix

$$\left[\frac{\partial \tilde{\mu}(t_T)}{\partial \lambda(t_0)}\right] \quad \text{where } \tilde{\mu}(t_T) = \begin{bmatrix} x(t_T) \\ \lambda(t_T) \end{bmatrix}$$

$$\text{and } \delta\tilde{\mu}(t_T)=\begin{bmatrix}\delta x(t_T)\\ \delta\lambda(t_T)\end{bmatrix}=\frac{\partial\tilde{\mu}(t_T)}{\partial\lambda(t_0)}\delta\lambda(t_0) \tag{3-27}$$

6. Calculate the change in $\lambda(t_0)$ required to produce the desired changes in the final values $x(t_T)$, $\lambda(t_T)$ by solving (3-27).

7. Repeat steps 2 through 6 until (3-25), (3-26) are close enough to zero for the application.

Another way to solve the two-point boundary-value problem (3-21) to (3-24) for linear systems is first to solve several initial-condition problems and then solve a system of simultaneous equations. This unit solution method proceeds as follows (Lewis and Syrmos, 1995):

1. Integrate the Hamiltonian system using as initial conditions $\lambda(t_0)=0$ and $x(t_0)=r(t_0)$, where $r(t_0)$ is the given initial state. Call the resulting solutions.

2. Suppose $\lambda\in R^n$, and let $\tilde{e}_i$ represent the ith column of the $n\times n$ identity matrix. Determine n unit solutions by integrating the Hamiltonian system n times, using as initial conditions

$$\begin{aligned}&x(t_0)=0\\ &\lambda(t_0)=\tilde{e}_i, \qquad i=1,\ldots,n.\end{aligned} \tag{3-28}$$

Call the resulting unit solutions $x_i(t)$, $\lambda_i(t)$ for $i=1,\ldots,n$.

3. General initial conditions can be expressed as

$$\begin{aligned}&x(t_0)=r(t_0) \quad \text{given,}\\ &\lambda(t_0)=\sum_{i=1}^{n}\tilde{c}_i\tilde{e}_i\end{aligned} \tag{3-29}$$

For constants $\tilde{c}_i$ the overall solutions for these general initial conditions

$$x(t) = x_0(t) + \sum_{i=1}^{n} \tilde{c}_i x_i(t),$$

are

$$\lambda(t) = \lambda_0(t) + \sum_{i=1}^{n} \tilde{c}_i \lambda_i(t).$$

Evaluate these solutions at the final time $t = t_T$, and then solve for the initial co-state values $\tilde{c}_i$ required to ensure that the terminal conditions (3-22), (3-23) are satisfied. The unit solutions show the effect on $x(t_T)$, $\lambda(t_T)$ of each of the n individual components of $\lambda(t_0)$, and so they can be used to find the sensitivity matrix in (3-27).

3.3 Energy Optimal Control of Pneumatic Actuator Systems

In this section, optimal control theory presented in Section 3.2 will be applied to the pneumatic cylinder system. The detailed derivation procedure will be shown (Ke *et al.*, 2004). Similarly to Chapter 2, this section adopts the coordinate system illustrated in Figure 2.1. For the convenience of energy optimal control analysis, define functions $\hat{f}$ for system (2-38) as follows:

$$\dot{x}_1 = x_2 = \hat{f}_1(x,u)$$

$$\dot{x}_2 = \frac{1}{m}(-K_f x_2 + A_a x_3 - A_b x_4) = \hat{f}_2(x,u)$$

$$\dot{x}_3 = \frac{-k\left[x_3 x_2 - \dfrac{RT_s}{A_a} C_d C_0 w_a f_a(x_3, P_s, P_e) u_1\right]}{l/2 + x_1 + \Delta} = \hat{f}_3(x,u)$$

$$\dot{x}_4 = \frac{k\left[x_4 x_2 + \dfrac{RT_s}{A_b} C_d C_0 w_b f_a(x_4, P_s, P_e) u_2\right]}{l/2 - x_1 + \Delta} = \hat{f}_4(x,u)$$

where $x=[x_1 \ \ x_2 \ \ x_3 \ \ x_4]^T$, $u=[u_1 \ u_2]^T$, and the static and Coulomb frictions are neglected for the convenience of the optimal control development. The performance index for energy efficient optimal control is chosen as below:

$$J=\beta[x_3(t_T)-x_4(t_T)]^2+\frac{1}{2}\int_0^T u^T u dt \tag{3-30}$$

and define

$$\phi(x(t_T),t_T)=\beta[x_3(t_T)-x_4(t_T)]^2 \tag{3-31}$$

where $\beta>0$. The first part of the performance index (3-30) means that at the end of the cylinder it is desired to control the pressure difference as small as possible for energy saving; the second part is the standard format for optimal energy control. The boundary conditions are:

$$\begin{aligned} &x_1(0)=-l/2 \ or \ l/2 \\ &x_2(0)=0 \\ &x_3(0)=x_4(0)=P_{a0}=P_{b0} \\ &x_1(t_T)=l/2 \ or \ -l/2 \\ &x_2(t_T)=0 \end{aligned} \tag{3-32}$$

where the signs of initial and terminal conditions of piston position depend on the direction of piston movement (refer to Figure 2.1).

From the optimal control theory (Lewis and Syrmos, 1995), the Hamiltonian function is defined as (3-32) when co-states $\lambda=[\lambda_1 \ \ \lambda_2 \ \ \lambda_3 \ \ \lambda_4]^T$ are introduced.

$$H=\frac{1}{2}u^T u+\lambda^T \hat{f} \tag{3-33}$$

where $\hat{f}=[\hat{f}_1 \ \ \hat{f}_2 \ \ \hat{f}_3 \ \ \hat{f}_4]^T$. Applying the standard optimal control design procedure, the optimal control solution should satisfy the following equations:

State equation: $$\dot{x}=\frac{\partial H}{\partial \lambda}=\hat{f} \tag{3-34}$$

Stationary condition: $$0=\frac{\partial H}{\partial u}=\frac{\partial L}{\partial u}+\frac{\partial \hat{f}^T}{\partial u}\lambda \tag{3-35}$$

Co-state equation: $$-\dot{\lambda}=\frac{\partial H}{\partial x}=\frac{\partial \hat{f}^T}{\partial x}\lambda+\frac{\partial L}{\partial x} \tag{3-36}$$

L is a function of u only, so

$$-\dot{\lambda}=\frac{\partial H}{\partial x}=\frac{\partial \hat{f}^T}{\partial x}\lambda \tag{3-37}$$

where $$\frac{\partial \hat{f}^T}{\partial x}=\begin{bmatrix} \frac{\partial \hat{f}_1}{\partial x_1} & \frac{\partial \hat{f}_2}{\partial x_1} & \frac{\partial \hat{f}_3}{\partial x_1} & \frac{\partial \hat{f}_4}{\partial x_1} \\ \frac{\partial \hat{f}_1}{\partial x_2} & \frac{\partial \hat{f}_2}{\partial x_2} & \frac{\partial \hat{f}_3}{\partial x_2} & \frac{\partial \hat{f}_4}{\partial x_2} \\ \frac{\partial \hat{f}_1}{\partial x_3} & \frac{\partial \hat{f}_2}{\partial x_3} & \frac{\partial \hat{f}_3}{\partial x_3} & \frac{\partial \hat{f}_4}{\partial x_3} \\ \frac{\partial \hat{f}_1}{\partial x_4} & \frac{\partial \hat{f}_2}{\partial x_4} & \frac{\partial \hat{f}_3}{\partial x_4} & \frac{\partial \hat{f}_4}{\partial x_4} \end{bmatrix} \tag{3-38}$$

The elements of matrix (3-38) are shown as below:

1. The first row of matrix (3-38):

$$\frac{\partial \hat{f}_1}{\partial x_1}=0,\quad \frac{\partial \hat{f}_2}{\partial x_1}=0,$$

$$\frac{\partial \hat{f}_3}{\partial x_1}=\frac{k}{(l/2+x_1+\Delta)^2}\left[x_3x_2-\frac{RT_sC_dC_0w_af_a(x_3,P_s,P_e)u_1}{A_a}\right],$$

$$\frac{\partial \hat{f}_4}{\partial x_1}=\frac{k}{(l/2-x_1+\Delta)^2}\left[x_4x_2-\frac{RT_sC_dC_0w_bf_a(x_4,P_s,P_e)u_2}{A_b}\right]$$

2. The second row of matrix (3-38):

$$\frac{\partial \hat{f}_1}{\partial x_2}=1,\quad \frac{\partial \hat{f}_2}{\partial x_2}=\frac{-K_f}{m},$$

$$\frac{\partial \hat{f}_3}{\partial x_2}=-\frac{kx_3}{l/2+x_1+\Delta},$$

$$\frac{\partial \hat{f}_4}{\partial x_2}=-\frac{kx_4}{l/2-x_1+\Delta}$$

3. The third row of matrix (3-38):

$$\frac{\partial \hat{f}_1}{\partial x_3}=0,\quad \frac{\partial \hat{f}_2}{\partial x_3}=\frac{A_a}{m},$$
$$\frac{\partial \hat{f}_3}{\partial x_3}=-\frac{kx_2}{l/2+x_1+\Delta}+\frac{kRT_sC_dC_0w_a\bar{f}_n(x_3,P_s,P_e)u_1}{A_a(l/2+x_1+\Delta)},$$
$$\frac{\partial \hat{f}_4}{\partial x_3}=0$$

4. The fourth row of matrix (3-38):

$$\frac{\partial \hat{f}_1}{\partial x_4}=0,\quad \frac{\partial \hat{f}_2}{\partial x_4}=-\frac{A_b}{m},$$
$$\frac{\partial \hat{f}_3}{\partial x_4}=0,$$
$$\frac{\partial \hat{f}_4}{\partial x_4}=\frac{kx_2}{l/2-x_1+\Delta}+\frac{kRT_sC_dC_0w_b\bar{f}_n(x_4,P_s,P_e)u_2}{A_b(l/2-x_1+\Delta)}$$

From Equations (2-34) to (2-36), $f_n(x_3,P_s,P_e)$ and $f_n(x_4,P_s,P_e)$ can be rearranged in the following format:

$$f_n(x_3,P_s,P_e)$$
$$=\begin{cases} P_s/\sqrt{T_s}, & \frac{P_{atm}}{P_s}<\frac{x_3}{P_s}\le C_r \\ P_sC_k/\sqrt{T_s}\cdot\sqrt{\left(\frac{x_3}{P_s}\right)^{2/k}-\left(\frac{x_3}{P_s}\right)^{(k+1)/k}}, & C_r<\frac{x_3}{P_s}<1 \end{cases} \quad \text{Chamber A is drive chamber}$$
$$=\begin{cases} x_3/\sqrt{T_s}, & \frac{P_{atm}}{x_3}<\frac{P_e}{x_3}\le C_r \\ x_3C_k/\sqrt{T_s}\cdot\sqrt{\left(\frac{P_e}{x_3}\right)^{2/k}-\left(\frac{P_e}{x_3}\right)^{(k+1)/k}}, & C_r<\frac{P_e}{x_3}<1 \end{cases} \quad \text{Chamber B is drive chamber}$$

$$f_n(x_4,P_s,P_e)$$

$$= \begin{cases} x_4/\sqrt{T_b}, & \frac{P_{atm}}{x_4} < \frac{P_e}{x_4} \le C_r \\ x_4 C_k/\sqrt{T_b}\cdot\sqrt{\left(\frac{P_e}{x_4}\right)^{2/k}-\left(\frac{P_e}{x_4}\right)^{(k+1)/k}}, & C_r < \frac{P_e}{x_4} < 1 \end{cases} \quad \text{Chamber A is drive chamber}$$

$$= \begin{cases} P_s/\sqrt{T_s}, & \frac{P_{atm}}{P_s} < \frac{x_4}{P_s} \le C_r \\ P_s C_k/\sqrt{T_s}\cdot\sqrt{\left(\frac{x_4}{P_s}\right)^{2/k}-\left(\frac{x_4}{P_s}\right)^{(k+1)/k}}, & C_r < \frac{x_4}{P_s} < 1 \end{cases} \quad \text{Chamber B is drive chamber}$$

Due to $\tilde{f}_n(x_3,P_s,P_e)=\frac{\partial[f_n(x_3,P_s,P_e)]}{\partial x_3}$, $\bar{f}_n(x_4,P_s,P_e)=\frac{\partial[f_n(x_4,P_s,P_e)]}{\partial x_4}$, they can be expressed as follows:

$$\tilde{f}_n(x_3,P_s,P_e)$$

$$= \begin{cases} 0, & \frac{P_{atm}}{P_s} < \frac{x_3}{P_s} \le C_r \\ \frac{P_s C_k}{2kx_3\sqrt{T_s}}\cdot\frac{2\left(\frac{x_3}{P_s}\right)^{2/k}-(k+1)\left(\frac{x_3}{P_s}\right)^{(k+1)/k}}{\sqrt{\left(\frac{x_3}{P_s}\right)^{2/k}-\left(\frac{x_3}{P_s}\right)^{(k+1)/k}}}, & C_r < \frac{x_3}{P_s} < 1 \end{cases} \quad \text{Chamber A driving}$$

$$= \begin{cases} 1/\sqrt{T_s}, & \frac{P_{atm}}{x_3} < \frac{P_e}{x_3} \le C_r \\ \frac{C_k}{\sqrt{T_s}}\sqrt{\left(\frac{P_e}{x_3}\right)^{\frac{2}{k}}-\left(\frac{P_e}{x_3}\right)^{\frac{k+1}{k}}}\left\{1-\frac{2\left(\frac{P_e}{x_3}\right)^{\frac{2}{k}}-(k+1)\left(\frac{P_e}{x_3}\right)^{\frac{k+1}{k}}}{2k\left[\left(\frac{P_e}{x_3}\right)^{\frac{2}{k}}-\left(\frac{P_e}{x_3}\right)^{\frac{k+1}{k}}\right]}\right\}, & C_r < \frac{P_e}{x_3} < 1 \end{cases} \quad \text{Chamber B driving}$$

$$\bar{f}_n(x_4,P_s,P_e)$$

$$= \begin{cases} 1/\sqrt{T_b}, & \frac{P_{atm}}{x_4} < \frac{P_e}{x_4} \le C_r \\ \frac{C_k}{\sqrt{T_b}}\sqrt{\left(\frac{P_e}{x_4}\right)^{\frac{2}{k}} - \left(\frac{P_e}{x_4}\right)^{\frac{k+1}{k}}}\left\{1 - \frac{2\left(\frac{P_e}{x_4}\right)^{\frac{2}{k}} - (k+1)\left(\frac{P_e}{x_4}\right)^{\frac{k+1}{k}}}{2k\left[\left(\frac{P_e}{x_4}\right)^{\frac{2}{k}} - \left(\frac{P_e}{x_4}\right)^{\frac{k+1}{k}}\right]}\right\}, & C_r < \frac{P_e}{x_4} < 1 \end{cases} \quad \text{Chamber A driving}$$

$$= \begin{cases} 0, & \frac{P_{atm}}{P_s} < \frac{x_4}{P_s} \le C_r \\ \frac{P_s C_k}{2kx_4\sqrt{T_s}} \cdot \frac{2\left(\frac{x_4}{P_s}\right)^{2/k} - (k+1)\left(\frac{x_4}{P_s}\right)^{(k+1)/k}}{\sqrt{\left(\frac{x_4}{P_s}\right)^{2/k} - \left(\frac{x_4}{P_s}\right)^{(k+1)/k}}}, & C_r < \frac{x_4}{P_s} < 1 \end{cases} \quad \text{Chamber B driving}$$

From the co-state equation (3-37),

$$-\dot{\lambda}_1 = \frac{kx_3x_2}{(l/2+x_1+\Delta)^2}\lambda_3 + \frac{kx_4x_2}{(l/2-x_1+\Delta)^2}\lambda_4 - \frac{kRT_sC_dC_0w_a f_n(x_3,P_s,P_e)u_1}{A_a(l/2+x_1+\Delta)^2}\lambda_3 + \frac{kRT_sC_dC_0w_b f_n(x_4,P_s,P_e)u_2}{A_b(l/2-x_1+\Delta)^2}\lambda_4 \quad (3\text{-}39.a)$$

$$-\dot{\lambda}_2 = \lambda_1 - \frac{K_f}{m}\lambda_2 - \frac{kx_3}{l/2+x_1+\Delta}\lambda_3 + \frac{kx_4}{l/2-x_1+\Delta}\lambda_4 \quad (3\text{-}39.b)$$

$$-\dot{\lambda}_3 = \frac{A_a}{m}\lambda_2 - \frac{kx_2}{l/2+x_1+\Delta}\lambda_3 + \frac{kRT_sC_dC_0w_a\bar{f}_n(x_3,P_s,P_e)u_1}{A_a(l/2+x_1+\Delta)}\lambda_3 \quad (3\text{-}39.c)$$

$$-\dot{\lambda}_4 = -\frac{A_b}{m}\lambda_2 + \frac{kx_2}{l/2-x_1+\Delta}\lambda_4 + \frac{kRT_sC_dC_0w_b\bar{f}_n(x_4,P_s,P_e)u_2}{A_b(l/2-x_1+\Delta)}\lambda_4 \quad (3\text{-}39.d)$$

From the stationary condition (3-35),

$$\frac{\partial \hat{f}^T}{\partial u}=\begin{bmatrix} \frac{\partial \hat{f}_1}{\partial u_1} & \frac{\partial \hat{f}_2}{\partial u_1} & \frac{\partial \hat{f}_3}{\partial u_1} & \frac{\partial \hat{f}_4}{\partial u_1} \\ \frac{\partial \hat{f}_1}{\partial u_2} & \frac{\partial \hat{f}_2}{\partial u_2} & \frac{\partial \hat{f}_3}{\partial u_2} & \frac{\partial \hat{f}_4}{\partial u_2} \end{bmatrix}=\begin{bmatrix} 0 & 0 & \frac{kRT_sC_dC_0w_af_n(x_3,P_s,P_e)}{A_a(l/2+x_1+\Delta)} & 0 \\ 0 & 0 & 0 & \frac{kRT_sC_dC_0w_bf_n(x_4,P_s,P_e)}{A_b(l/2-x_1+\Delta)} \end{bmatrix}$$

and $\frac{\partial L}{\partial u}=\begin{bmatrix} \frac{\partial L}{\partial u_1} \\ \frac{\partial L}{\partial u_2} \end{bmatrix}=\begin{bmatrix} u_1 \\ u_2 \end{bmatrix}$. Therefore, the following optimal control law can be

derived $u_1=-\frac{kRT_sC_dC_0w_af_n(x_3,P_s,P_e)}{A_a(l/2+x_1+\Delta)}\lambda_3$ (3-40)

$$u_2=-\frac{kRT_sC_dC_0w_bf_n(x_4,P_s,P_e)}{A_b(l/2-x_1+\Delta)}\lambda_4 \tag{3-41}$$

From (3-13) and the chosen performance index (3-30),

$$J=\beta[x_3(t_T)-x_4(t_T)]^2+\frac{1}{2}\int_0^{t_T}u^Tudt=\phi(x(t_T),t_T)+\int_0^{t_T}L(x(t),u(t),t)dt$$

$$(\phi_x+\psi_x^Tv-\lambda)^T\Big|_{t_T}dx(t_T)+(\phi_t+\psi_t^Tv+H)\Big|_{t_T}dt_T=0$$

The terminal time is fixed, so the second part of (3-13), that is, $(\phi_t+\psi_t^Tv+H)\Big|_{t_T}dt_T=0$. And then it is desired that the first part of (3-13) also equal to zero, which is $(\phi_x+\psi_x^Tv-\lambda)^T\Big|_{t_T}=0$.

$$\begin{aligned}\phi_x\Big|_{t_T}&=\frac{\partial\phi}{\partial x}\Big|_{t_T}=\begin{bmatrix} \frac{\partial\phi}{\partial x_1}\Big|_{t_T} & \frac{\partial\phi}{\partial x_2}\Big|_{t_T} & \frac{\partial\phi}{\partial x_3}\Big|_{t_T} & \frac{\partial\phi}{\partial x_4}\Big|_{t_T} \end{bmatrix}^T \\ &=[0 \quad 0 \quad 2\beta[x_3(t_T)-x_4(t_T)] \quad -2\beta[x_3(t_T)-x_4(t_T)]]^T\end{aligned} \tag{3-42}$$

As for the final state constraint $\varphi(x(t_T),t_T)=\begin{bmatrix} x_1(t_T)-x_{1T} \\ x_2(t_T)-0 \end{bmatrix}=\begin{bmatrix} \varphi_1 \\ \varphi_2 \end{bmatrix}$,

$$\varphi_x\big|_{t_T} = \frac{\partial \phi}{\partial x}\bigg|_{t_T} = \begin{bmatrix} \dfrac{\partial \phi_1}{\partial x_1}\bigg|_{t_T} & \dfrac{\partial \phi_2}{\partial x_1}\bigg|_{t_T} \\ \dfrac{\partial \phi_1}{\partial x_2}\bigg|_{t_T} & \dfrac{\partial \phi_2}{\partial x_2}\bigg|_{t_T} \\ \dfrac{\partial \phi_1}{\partial x_3}\bigg|_{t_T} & \dfrac{\partial \phi_2}{\partial x_3}\bigg|_{t_T} \\ \dfrac{\partial \phi_1}{\partial x_4}\bigg|_{t_T} & \dfrac{\partial \phi_2}{\partial x_4}\bigg|_{t_T} \end{bmatrix} = \begin{bmatrix} 1 & 0 \\ 0 & 1 \\ 0 & 0 \\ 0 & 0 \end{bmatrix} \tag{3-43}$$

Thus, $\varphi_x^T \tilde{\gamma} = [\tilde{\gamma}_1(t_T) \quad \tilde{\gamma}_2(t_T) \quad 0 \quad 0]^T$. From $\phi_x(t_T) + \varphi_x^T \tilde{\gamma} - \lambda(t_T) = 0$, the terminal conditions for co-states are derived as

$$\lambda(t_T) = [0 \quad 0 \quad 2\beta[x_3(t_T) - x_4(t_T)] \quad -2\beta[x_3(t_T) - x_4(t_T)]]^T \tag{3-44}$$

Thus, when optimal control theory is applied to the pneumatic cylinder system, a set of co-state differential equations (3-39.a-d) is derived. The energy optimal control law and state trajectories can be obtained by solving these eight differential equations with the partially known boundary conditions. However, it presents a great challenge in solving the equations and obtaining the solutions. Numerical analysis is the only way forward for this problem. The major difficulty in obtaining numerical solutions will be the imperfectly known boundary conditions (3-42) to (3-44). Two possible methods, genetic algorithms and shooting method can be applied to search the boundary conditions of the co-states.

3.4 Numerical Solution and Challenges

The search for solutions started from the shooting method presented in Subsection 3.2.3 initially. But no good results were obtained after spending

quite a long period of time. Then the search turned to genetic algorithms. The general algorithm structure is illustrated in Figure 3.2. As shown in Figure 3.2, the shooting method and genetic algorithm can be implemented in Matlab working with the ODE solver programmed for the eighth-order expanded system equations.

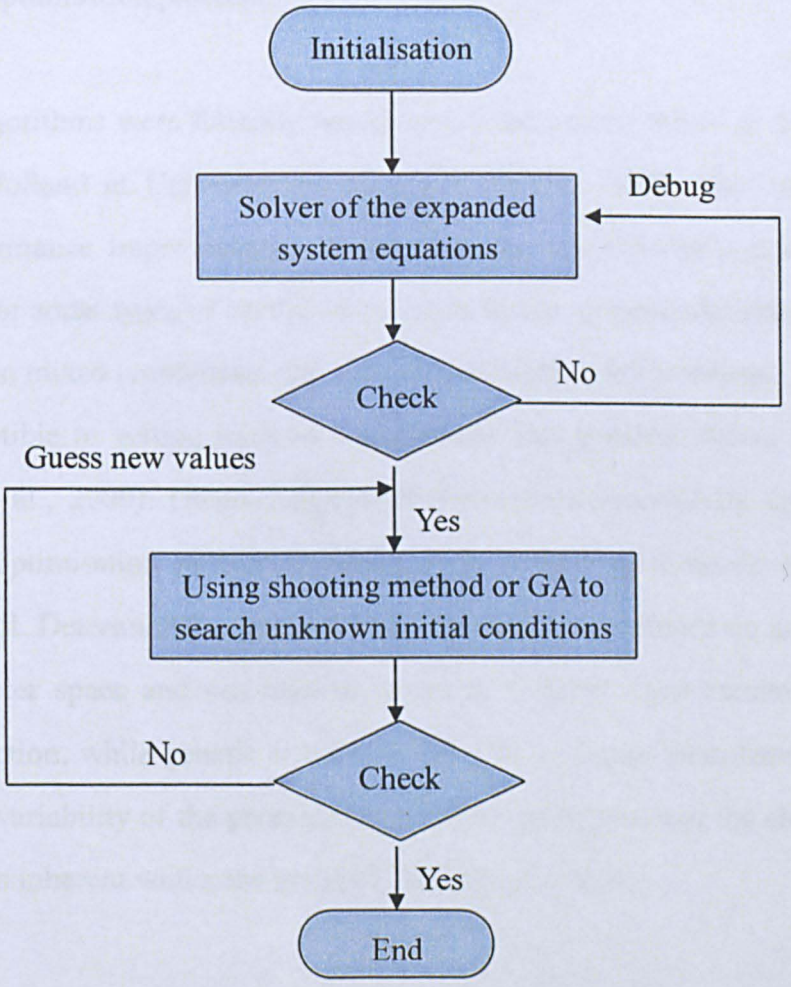

Figure 3.2 Block diagram of the algorithm structure

3.4.1 Brief Introduction to Genetic Algorithms

In this subsection, a brief introduction of genetic algorithms will be given.

There exists a large number of different approximation methods for solving differential equations. The advent of the powerful digital computer has significantly increased the ability to carry out the numerical solution of very complicated group of equations. With the development of the popular powerful calculation software, Matlab, the genetic algorithm approach has been chosen to solve this optimisation problem.

Genetic algorithms were formally introduced in the United States in the 1970s by John Holland at University of Michigan (Davis, 1987). The continuing price/performance improvements of computational systems have made them attractive for some types of optimisation. In particular, genetic algorithms work very well on mixed (continuous and discrete), combinatorial problems. They are less susceptible to getting stuck at local optima than gradient search methods (Hsiung et al., 2000). Genetic algorithms have been successfully applied to nonlinear optimisation problems, where more traditional methods are often found to fail. Deterministic, gradient based optimisation methods do not search the parameter space and can tend to converge towards local extrema of the fitness function, while genetic algorithms are able to depart from local optima due to the variability of the parameters within the gene pool and the element of randomness inherent within the methods (Mera *et al.*, 2004).

Genetic algorithms (GA) are basically algorithms based on natural biological evolution. A GA functions by generating a large set of possible solutions to a given problem. It then evaluates each of those solutions, and decides on a fitness level for each solution set. These solutions then breed new solutions. The parent solutions that are more fit are more likely to reproduce, while those that

are less fit are less likely to do so. To use a genetic algorithm, the user must represent a solution to the problem as a genome or chromosome. The genetic algorithm then creates a population of solutions and applies genetic operators such as mutation and crossover to evolve the solutions in order to find the best one. The possible applications of genetic algorithms are immense. Any problem that has a large search domain can be suitable tackled by GAs. Genetic algorithms now can be used easily thanks to the powerful software Matlab with GA as one of its toolboxes.

3.4.2 Implementation of GA in Matlab and Searching Difficulties

To search the reasonable ranges of the partially unknown boundary conditions of the eighth-order expanded system equations presented in Section 3.3, a genetic algorithm is implemented in Matlab. The programme consists of two parts: one part includes the ordinary differential equation (ODE) solver and the expanded adjoint system equations which describe the pneumatic cylinder system. The other is the genetic algorithm, which calls the ODE solver every time to search possible boundary condition values. The genetic algorithm programme includes a main programme and two functions which describe the GA options and fitness function.

The unknown boundary conditions of system states, which indicate piston position, velocity and pressures of both chambers, are assumed according to common knowledge in industry. However, the range of boundary conditions of co-states can not be estimated or predicted. It needs the genetic algorithm to search a reasonable range of the unknown boundary conditions of four co-states.

The simulation conditions are as follows:

- Cylinder: Rodless cylinder
- Stroke length: 1000mm
- Diameter of piston: 32mm
- Supply air pressure: 6 bars
- Exhaust pressure: 1 bar
- Temperature: 293K
- Payload mass: 1kg
- Static friction forces: ignored
- Viscous frictional coefficient: 15Ns/m
- Initial piston position: -0.5m
- Initial piston velocity: 0m/s
- Initial chamber pressures: 3.5 bars for both chambers
- Initial condition of four co-states: guessed values
- Simulation time: 2s
- GA generation size: 100
- GA population size: 30
- GA mutation shrink rate: 0.5

In the adopted genetic algorithm, there are 4 variables to be processed. The fitness function is defined as

$$\text{Fit} = |x_1(t_T) - l/2| + |x_2(t_T)| + |u_1(t_T)| + |u_2(t_T)| + 10^{-5}|x_3(t_T) - x_4(t_T)| \quad (3\text{-}45)$$

The fitness function (3-45) means it is desired that a minimum value can be achieved for the combination of terminal piston position, terminal piston velocity, terminal spool displacements of two control valves and the difference between the two terminal chamber pressures. In fitness function (3-45), 10^{-5} is the weighting of the chamber pressures, because of their 10^5 order of magnitude.

In other words, it is hoped that when the piston arrives at the desired terminal position, *i.e.* the other end of the stroke, the piston velocity can slow down to zero, and will not collide the end of cylinder hard. At the same time, it is also hoped the two control valves are shut off indicating there is no extra compressed air waste.

The initial values of boundary conditions of the four system states are chosen as $x_{10} \sim x_{40} \in$ [-0.5 0.0 3.5×10^5 3.5×10^5]. As for the initial conditions of the system co-states $\lambda_{10} \sim \lambda_{40}$, an extensive range has been tried, from 10^{-25} to 10^{25}. However, since the simulation results seem not to be convergent, and the dynamic responses under those boundary conditions are not consistent with the common knowledge of the industrial process, the simulation results will not be included in the thesis. The incorrect ranges of the four co-states λ_{10} to λ_{40} result in the incorrect simulation results, which is also due to the inherent nonlinearity of the system model, especially the functions $\bar{f}_n(x_3, P_s, P_e)$ and $\bar{f}_n(x_4, P_s, P_e)$ in the co-state equations. The reason of the non-convergent simulation results may be the functions $\bar{f}_n(x_3, P_s, P_e)$ and $\bar{f}_n(x_4, P_s, P_e)$ can not be differentiable. Therefore, solving this problem by linearisation of the pneumatic cylinder model will be proposed in Chapter 4.

3.5 Summary

In this chapter, optimal control theory for continuous-time systems has been briefly introduced and applied to find the energy efficient control and state

trajectories. When the optimal control theory is applied to the system model, an extra set of co-state differential equations are generated. These co-state equations and the original system equations extend the original system model. However, this derived set of system equations are too complicated to be solved analytically, numerical solutions is the only choice. A great effort has been put into solving the optimal control problem in together with some mathematicians. However, the complexity of the system model and the extreme nonlinear characteristics result in the difficulty to search the unknown co-state initial values. This motivated the finding of an alternative way to solve this challenging problem. Chapter 4 describes an alternative way for solving this optimal control problem by input/output feedback linearisation.

Chapter 4

Development of Energy Efficient Optimal Control Based on the Linearised System Model

4.1 Introduction

As described in Chapter 3, it is difficult to obtain numerical solutions for the optimal control problem, which motivated to investigate if there is an alternative way for energy efficient control or optimisation. This chapter presents an optimal control design and analysis in a mapped linear space.

Simulation studies have indicated that different quantities of compressed air are consumed for one cycle of piston movement when the same controller is adopted but with different velocity profiles for servo pneumatic actuators (Wang *et al*, 2000b). This gives a motivation to investigate the shapes of velocity profiles to identify a particular one which may lead the system to use the least amount of compressed air, *i.e.* the most energy efficient profile. In this chapter, an energy efficient optimal control strategy is developed for the servo controlled pneumatic cylinder actuating system by using input/output feedback linearisation.

As detailed in Chapter 2, the pneumatic cylinder system is modelled by four first order non-linear differential equations. Applying optimal control methods on this system directly will result in a group of eight first order nonlinear differential equations with partially known boundary conditions, which is derived in Chapter 3. This seems impossible to solve analytically. Numerical solution may be the only way to find energy efficient control and state trajectories. In this chapter, an alternative way to develop an energy efficient control strategy in order to avoid the problems of solving the eight complicated nonlinear differential equations has been investigated, which employs input/output state feedback linearisation.

The method adopted in this chapter can be broken down into three stages:

1. The pneumatic cylinder model is linearised by regular static state feedback and state coordinate transformation.
2. Applying the optimal control theory with the linearised system model, a generalised energy efficient control strategy is developed and the optimal trajectories are obtained with respect to the state variables after the transformation. In this way, an analytic solution of energy efficient control can be obtained.
3. The generalised energy efficient feedback control is then substituted back to the original system control input variable. Then simulation work is conducted to verify if the optimal trajectories obtained from stage 2 are still optimally energy efficient in the original pneumatic system.

For servo systems the critical issue is the profile, which the state variable needs to follow. After the controller is developed, a set of reliable energy efficient

system state trajectories can be obtained. Then these trajectories can be used as energy efficient optimal profiles for servo-controlled pneumatic cylinders.

4.2 Feedback Linearisation

The basic idea of feedback linearisation is to transform a nonlinear system model into a linear system model and then well developed linear control system design techniques can be applied for the nonlinear system control design (Franklin *et al.*, 1994). This methodology has converted many previously intractable nonlinear problems into simpler solvable forms. The techniques have two main themes: the input/state linearisation, where the full state equation is linearised, and the input/output linearisation, where linearising the map from input to output is emphasized even if the state equations are only partially linearisable (Wang *et al.*, 2007). The feedback linearisation method has been used to solve a number of nonlinear control problems but many engineers still think that this method is quite naive for practical applications. This is mainly due to the exact feedback cancellation, which is very difficult or almost impossible to be conducted in the practical world. If the un-cancelled nonlinear dynamics are classified as part of the uncertainties and robustness is taken into account in the controller design, the problem may be solved (Wang *et al.*, 2007). In some cases, the uncertainties can be estimated using a nonlinear observer and the estimated variables can be used in feedback control. On the other hand, the controller designed using the feedback linearisation method can be used as a guideline for system optimisation.

4.2.1 Theory of Feedback Linearisation

Feedback linearisation is a common approach used in controlling nonlinear systems. The approach involves finding a transformation of the nonlinear system into an equivalent linear system, through a change of variables and a suitable control input (Isidori, 1995). The feedback linearisation of a single-input single-output (SISO) system will be discussed in this section. The general mathematical formulation for a SISO system is shown below:

$$\dot{x} = \hat{f}(x) + \hat{g}(x)u \tag{4-1.a}$$

$$y = \hat{h}(x) \tag{4 -1.b}$$

where $x \in \Re^n$ is the state vector, $u \in \Re$ represents the input, and $y \in \Re$ is the system output. In Equations (4-1), $\hat{f}$ and $\hat{g}$ are C^∞ vector fields on $\Re^n$ and $\hat{h}$ is a C^∞ function on $\Re^n$. The goal of feedback linearisation is to develop a control input u that renders either the input-output map linear, or results in a linearisation of the full state of the system (Isidori, 1995).

Before we proceed with developing the feedback linearising control law, a couple of important notions must be introduced. The first one is the Lie derivative. Consider the time derivative of Equation (4-1.b), which can be computed using the chain rule,

$$\dot{y} = \frac{d\hat{h}(x)}{dx}\dot{x} = \frac{d\hat{h}(x)}{dx}\hat{f}(x) + \frac{d\hat{h}(x)}{dx}\hat{g}(x)u$$

Now the Lie derivative of $\hat{h}(x)$ with respect to $\hat{f}(x)$ is defined as,

$$L_f\hat{h}(x) = \frac{d\hat{h}(x)}{dx}\hat{f}(x)$$

And similarly, the Lie derivative of $\hat{h}(x)$ with respect to $\hat{g}(x)$ is,

$$L_g\hat{h}(x) = \frac{d\hat{h}(x)}{dx}\hat{g}(x)$$

With this new notation, $\dot{y}$ ma y be expressed as,

$$\dot{y} = L_f\hat{h}(x) + L_g\hat{h}(x)u$$

Note that the notation of Lie derivatives is convenient when it takes multiple derivatives with respect to either the same vector field, or a different one. For example, $L_f^2\hat{h}(x) = L_f L_f\hat{h}(x) = \frac{d(L_f\hat{h}(x))}{dx}\hat{f}(x)$ and

$$L_g L_f\hat{h}(x) = \frac{d(L_f\hat{h}(x))}{dx}\hat{g}(x)$$

The second notion is the relative degree (Isidori, 1995). The SISO nonlinear system (4-1) is said to have relative degree r at a point x^0 if

(i) $L_g L_f^k\hat{h}(x) = 0$ for all x in a neighborhood of x^0 and all $k < r-1$

(ii) $L_g L_f^{r-1}\hat{h}(x^0) \neq 0$

Note that there may be points where a relative degree cannot be defined. This occurs, in fact, when the first function of the sequence $L_g\hat{h}(x), L_g L_f\hat{h}(x), \ldots, L_g L_f^k\hat{h}(x), \ldots$ which is not identically zero (in a neighborhood of x^0) has a zero exactly at the point $x = x^0$. However, the set of points where a relative degree can be defined is clearly an open and dense subset of the set $\tilde{U}$ where System (4-1) is defined.

A simple interpretation of the notion of relative degree is illustrated below. Assume the system at some time t^0 is the state $x(t^0)=x^0$ and suppose the value of the output $y(t)$ and of its derivatives with respect to time $y^{(k)}(t)$, for $k=1,2,...,$ at $t=t^0$. For $y(t^0)=\hat{h}(x(t^0))=\hat{h}(x^0)$ and

$$y^{(1)}(t)=\frac{\partial \hat{h}}{\partial x}\frac{dx}{dt}=\frac{\partial \hat{h}}{\partial x}(\hat{f}(x(t))+\hat{g}(x(t))u(t))=L_f\hat{h}(x(t))+L_g\hat{h}(x(t))u(t)$$

If the relative degree r is larger than 1, for all t such that $x(t)$ is near x^0, *i.e.* for all t near t^0, $L_g\hat{h}(x(t))=0$ and therefore $y^{(1)}(t)=L_f\hat{h}(x(t))$.

This yields

$$y^{(2)}(t)=\frac{\partial L_f\hat{h}}{\partial x}\frac{dx}{dt}=\frac{\partial L_f\hat{h}}{\partial x}(\hat{f}(x(t))+\hat{g}(x(t))u(t))=L_f^2\hat{h}(x(t))+L_gL_f\hat{h}(x(t))u(t)$$

Again, if the relative degree is larger than 2, for all t near t^0, $L_gL_f\hat{h}(x(t))=0$ and therefore $y^{(2)}(t)=L_f^2\hat{h}(x(t))$. Continuing in this way,

$$y^{(k)}(t)=L_f^k\hat{h}(x(t)) \quad \text{for all } k<r \text{ and all } t \text{ near } t^0 \tag{4-2}$$

and

$$y^{(k)}(t^0)=L_f^k\hat{h}(x^0)+L_gL_f^{r-1}\hat{h}(x^0)u(t^0) \tag{4-3}$$

Thus, the relative degree r is exactly equal to the number of times one has to differentiate the output $y(t)$ at time $t=t^0$ in order to have the value $u(t^0)$ of the input explicitly appearing.

Note also that if $L_gL_f^k\hat{h}(x(t))=0$ for all x in a neighborhood of x^0 and all $k\geq 0$, then the output of the system is not affected by the input, for all t near t^0. The previous calculations show that the Taylor series expansion of $y(t)$ at the

point $t=t^0$ has the form $y(t)=\sum_{k=0}^{\infty} L_f^k \hat{h}(x^0)\frac{(t-t^0)^k}{k!}$, *i.e.* $y(t)$ is a function depending only on the initial state and not on the input.

The system will be called static state feedback input-output linearisable by regular static state feedback and coordinate transformation, if there exists an invertible feedback, *i.e.*

$$u=\tilde{\alpha}(x)+\tilde{\beta}(x)v \tag{4-4}$$

where v is the external reference input, with $\frac{\partial\tilde{\beta}(x)}{\partial x} \not\equiv 0$ and a coordinate change $z=\Phi(x)$, such that, under the z-coordinates and the new input v, system (4-1) becomes

$$\begin{aligned}\dot{z}^1 &= \tilde{A}z^1+\tilde{b}v\\ \dot{z}^2 &= \hat{f}^2(z^1,z^2)+\hat{g}^2(z^1,z^2)v\\ y &= \tilde{c}^T z^1\end{aligned} \tag{4-5}$$

where $\tilde{A},\tilde{b},\tilde{c}$ are constant matrices of proper dimension (Isidori, 1995).

For a single input single output system, if the system has a relative degree $r\le n$, the local co-ordinate transformation can be chosen as (Isidori, 1995):

$$\left.\begin{aligned}&\Phi_1(x)=\hat{h}(x)\\ &\Phi_2(x)=L_f\hat{h}(x)\\ &\cdots\\ &\Phi_r(x)=L_f^{r-1}\hat{h}(x)\end{aligned}\right\} \tag{4-6}$$

i.e. the function $\hat{h}(x)$ and its first $n-1$ derivatives along $\hat{f}(x)$. It is always possible to find $n-r$ more functions $[\Phi_{r+1}(x)\ \Phi_{r+2}(x)\ \cdots\ \Phi_n(x)]$ such that the

mapping $\Phi_{r+1}(x)\ \Phi_{r+2}(x)\ \cdots\ \Phi_n(x)$ qualifies as a local coordinate transformation in a neighbourhood of x^0. Note that $[\Phi_{r+1}(x)\ \Phi_{r+2}(x)\ \cdots\ \Phi_n(x)]$ can be arbitrarily chosen, and the choice is highly dependent on the individual systems.

In the new coordinates $z_i = \Phi_i(x) = L_f^{i-1}\hat{h}(x) \quad 1 \le i \le n$, the system will appear described by equations of the form:

$$\begin{aligned} \dot{z}_1 &= L_f\hat{h}(x) = z_2 \\ \dot{z}_2 &= L_f^2\hat{h}(x) = z_3 \\ &\cdots \\ \dot{z}_{n-1} &= L_f^{n-1}\hat{h}(x) = z_n \\ \dot{z}_n &= L_f^n\hat{h}(x) + L_g L_f^{n-1}\hat{h}(x)u \end{aligned} \tag{4-7}$$

Suppose now the following state feedback control law is chosen

$$u = \frac{1}{L_g L_f^{n-1}\hat{h}(x)}(-L_f^n\hat{h}(x) + v) \tag{4-8}$$

which indeed exists and is well-defined in a neighborhood of z^0. The resulting closed loop system is governed by the equations:

$$\begin{aligned} \dot{z}_1 &= z_2 \\ \dot{z}_2 &= z_3 \\ &\cdots \\ \dot{z}_{n-1} &= z_n \\ \dot{z}_n &= v \end{aligned} \tag{4-9}$$

which is linear and controllable. Thus it can be concluded that any nonlinear system with relative degree n at some point x^0 can be transformed into a system which, in a neighborhood of the point $z^0 = \Phi(x^0)$, is linear and controllable.

However, the basic feature of the system that makes it possible to change it into a linear and controllable one is the existence of an output function $\hat{h}(x)$ for which the system had relative degree exactly n. The existence of such a function is not only a sufficient but also a necessary condition for the existence of a state feedback and a change of coordinates transforming a given system into a linear and controllable one.

For a multi-input system, in Equation (4-1), $u \in \Re^m$ represents the input, and $\hat{g}(x) = (\hat{g}_1(x) \quad \hat{g}_2(x) \quad \cdots \quad \hat{g}_m(x)) \in \Re^{n \times m}$. In this case, the static state feedback has the same form as shown in Equation (4-4) with $\tilde{\alpha}(x) \in \Re^m$, $\tilde{\beta}(x) \in \Re^{m \times m}$ with $\tilde{\beta}(x)$ being an invertible matrix. As there is only one output in this case, the local co-ordinate transformation can be chosen in the same way as the one used for the case of single input and single output systems.

4.2.2 Linearisation of the System Model

When applying the above theory to servo pneumatic cylinder actuating systems, for the convenience of finding the suitable set of new co-ordinates, the static frictions are ignored initially and will be brought back in a later section. The servo pneumatic actuators can be driven by a single five-port proportional valve or two separate three-port proportional valves. In this section, only the two three-port proportional valves case will be discussed.

The main purpose is to use the feedback linearisation method to linearise the

nonlinear pneumatic system model and then apply optimal control theory. When the pneumatic actuator system adopts two separate three-port valves, $\hat{f},\hat{g}$ and $\hat{h}$ of the system are, comparing with the general formulation (4-1), as follows:

$$\hat{f}(x)=\begin{bmatrix} x_2 \\ (-K_f x_2+A_a x_3-A_b x_4)/m \\ \dfrac{-kx_3x_2}{l/2+x_1+\Delta} \\ \dfrac{-kx_4x_2}{l/2-x_1+\Delta} \end{bmatrix},\ \hat{g}(x)=\begin{bmatrix} 0 & 0 \\ 0 & 0 \\ \dfrac{kRT_sC_dC_0wf_n(x_3,P_s,P_e)}{A_a(l/2+x_1+\Delta)} & 0 \\ 0 & \dfrac{kRT_sC_dC_0wf_n(x_4,P_s,P_e)}{A_b(l/2-x_1+\Delta)} \end{bmatrix}$$

and $y=\hat{h}(x)=x_1$, where $\hat{f}$ is C^∞ vector field on the set $\Omega\subset\Re^4$ (there are some constraints on the system variables and parameters in practice), $\hat{g}\in\Omega\subset\Re^{4\times2}$, $y=\hat{h}(x)\in(-l/2,\ l/2)\subset\Re$.

Since $L_{g_i}L_f^{\,k}\hat{h}(x)=0\ \ (i=1,2)$, for all $k<3$ and $L_{g_i}L_f^{\,k}\hat{h}(x)\neq0\ \ (i=1,2)$ for all $k=3$ ($\forall$), then the relative degree of the system is also 3, while the order of system $n=4$. The system is a multi-input and single-output system. Applying the formulae (4-6),

$$\Phi_1(x)=\hat{h}(x)=x_1$$

$$\Phi_2(x)=L_f\hat{h}(x)=\frac{d\hat{h}(x)}{dx}\cdot\hat{f}(x)=[1\ 0\ 0\ 0]\cdot\hat{f}(x)=x_2$$

$$\Phi_3(x)=L_f^{\,2}\hat{h}(x)=L_fL_f\hat{h}(x)=\frac{d\phi_2(x)}{dx}\cdot\hat{f}(x)=[0\ 1\ 0\ 0]\cdot\hat{f}(x)$$

$$=-\frac{K_f}{m}x_2+\frac{A_a}{m}x_3-\frac{A_b}{m}x_4$$

and $\Phi_4(x)$ can be chosen as x_4. Then the following co-ordinate transform to linearise the system is obtained:

$$\left.\begin{aligned} z_1 &= x_1 \\ z_2 &= x_2 \\ z_3 &= -\frac{K_f}{m}x_2 + \frac{A_a}{m}x_3 - \frac{A_b}{m}x_4 \\ z_4 &= x_4 \end{aligned}\right\} \tag{4-10}$$

or $z = \bar{T}x$ and $\bar{T} = \begin{bmatrix} 1 & 0 & 0 & 0 \\ 0 & 1 & 0 & 0 \\ 0 & -\frac{K_f}{m} & \frac{A_a}{m} & -\frac{A_b}{m} \\ 0 & 0 & 0 & 1 \end{bmatrix}$.

Applying the transformation (4-10), the pneumatic system is transformed into:

$$\left.\begin{aligned} \dot{z}_1 &= z_2 \\ \dot{z}_2 &= z_3 \\ \dot{z}_3 &= -\frac{K_f}{m}z_3 - \frac{k(z_2z_3 + A_bz_2z_4/m + K_fz_2^2/m)}{l/2+z_1+\Delta} + \frac{kRT_sC_dC_0w_a\hat{f}_n(z_3,P_s,P_e)}{m(l/2+z_1+\Delta)}u_1 \\ &\quad - \frac{A_bkz_4z_2}{m(l/2-z_1+\Delta)} - \frac{kRT_sC_dC_0w_b\hat{f}_n(z_4,P_s,P_e)}{m(l/2-z_1+\Delta)}u_2 \\ \dot{z}_4 &= \frac{kz_4z_2}{l/2-z_1+\Delta} + \frac{kRT_sC_dC_0w_b\hat{f}_n(z_4,P_s,P_e)}{A_b(l/2-z_1+\Delta)}u_2 \end{aligned}\right\} \tag{4-11}$$

Let $$u_1 = \frac{m(l/2+z_1+\Delta)}{kRT_sC_dC_0w_a\hat{f}_n(z_3,P_s,P_e)}\left[\frac{k(z_2z_3 + A_bz_2z_4/m + K_fz_2^2/m)}{l/2+z_1+\Delta} + \frac{K_f}{m}z_3 + v_3\right] \tag{4-12}$$

$$u_2 = \frac{A_b(l/2-z_1+\Delta)}{kRT_sC_dC_0w_b\hat{f}_n(z_4,P_s,P_e)}\left(\frac{-kz_2z_4}{l/2-z_1+\Delta} + v_2\right) \tag{4-13}$$

and define $v_1 = v_3 - A_bv_2/m$. Substitute u_1 and u_2 back into (4-11), there are

$$\left.\begin{aligned} \dot{z}_1 &= z_2 \\ \dot{z}_2 &= z_3 \\ \dot{z}_3 &= v_1 \\ \dot{z}_4 &= v_2 \\ y &= z_1 \end{aligned}\right\} \tag{4-14}$$

Then System (4-14) is completely a linear system with two equivalent inputs v_1 and v_2.

4.3 Development of Energy Efficient Optimal Control

The original nonlinear pneumatic cylinder model is linearised by using a set of new state variables as a coordinate transformation as shown in Section 4.2. In this section, the energy efficient optimal control of pneumatic system with two three-port valves will be discussed (Ke *et al.*, 2005).

The purpose of the energy efficient control on the pneumatic cylinder actuating system is to move a piston from one position to another within a pre-specified time period limit and the motion consumes the least compressed air. Choosing $y = z_1$ as the system output, the linear system (4-14) can be rewritten in matrix form as follows:

$$\begin{aligned} \dot{z} &= \hat{A}z + \hat{B}V \\ y &= z_1 \end{aligned} \tag{4-15}$$

where $z = [z_1 \quad z_2 \quad z_3 \quad z_4]^T$, $v = [v_1 \quad v_2]^T$, $\hat{A} = \begin{bmatrix} 0 & 1 & 0 & 0 \\ 0 & 0 & 1 & 0 \\ 0 & 0 & 0 & 0 \\ 0 & 0 & 0 & 0 \end{bmatrix}$, and $\hat{B} = \begin{bmatrix} 0 & 0 \\ 0 & 0 \\ 1 & 0 \\ 0 & 1 \end{bmatrix}$.

The aim of energy efficient control is to derive a feedback control $v(z)$, for system (4-15) to minimize the following performance index:

$$J = \alpha z_3^2(t_T) + \int_0^{t_T} v^T v dt \tag{4-16}$$

where $\alpha z_3^2(t_T)$ means the squared final acceleration and $\int_0^T v^T v dt$ represents

the integration of the control effort or the energy consumption. As the piston will stop at the desired position, it is certainly expected that the final acceleration $z_3(t_T)$ is as small as possible. If the piston is assumed to move from one end to the other end of the cylinder, the boundary conditions are $z_1(0) = -l/2$ or $z_1(0) = l/2$, $z_1(t_T) = l/2$ or $z_1(t_T) = -l/2$, which depends on the directions of the piston movement, $z_2(0) = 0$, $z_2(t_T) = 0$, $z_3(0) = z_3^0$, and $z_4(0) = z_4^0$. $z_3(t_T)$ and $z_4(t_T)$ are free boundary conditions. Here, the boundary conditions all have real meanings in the pneumatic cylinder: z_1 denotes the piston position; z_2 is the piston velocity, for the sake of energy saving the initial and terminal values are set to zero; z_3 is the piston acceleration while z_4 is the Chamber B pr essure.

This control problem can be considered as a class of continuous time optimal control problem with a partially fixed final state function. To obtain the optimal control solution, the first step is to construct a Hamiltonian function, $H(z,v,t,\lambda)$ with an associated multiplier $\lambda \in R^4$ below (Lewis and Syrmos, 1995):

$$H(z,v,t,\lambda) = v^T v + \lambda^T(\hat{A}z + \hat{B}v) \tag{4-17}$$

Then, there are

$$\dot{z} = \frac{\partial H}{\partial \lambda} = \hat{A}z + \hat{B}V \tag{4-18}$$

$$-\dot{\lambda} = \frac{\partial H}{\partial z} = \hat{A}^T\lambda \tag{4-19}$$

$$0 = \frac{\partial H}{\partial v} = 2v + \hat{B}^T \lambda \tag{4-20}$$

From Equation (4-20), the optimal control will be obtained as

$$v_1 = -\frac{1}{2}\lambda_3 \tag{4-21}$$

$$v_2 = -\frac{1}{2}\lambda_4 \tag{4-22}$$

Expend Equation (4-19), the following equations can be derived

$$\begin{aligned} \dot{\lambda}_1 &= 0 \\ \dot{\lambda}_2 &= -\lambda_1 \\ \dot{\lambda}_3 &= -\lambda_2 \\ \dot{\lambda}_4 &= 0 \end{aligned} \tag{4-23}$$

While the solutions for Equations (4-23) are

$$\begin{aligned} \lambda_1 &= \mu_1 \\ \lambda_2 &= -\mu_1 t + \mu_2 \\ \lambda_3 &= \frac{1}{2}\mu_1 t^2 - \mu_2 t + \mu_3 \\ \lambda_4 &= \mu_4 \end{aligned} \tag{4-24}$$

where μ_1 to μ_4 are the constants to be determined. Substitute Equations (4-24) into optimal controls (4-21) and (4-22), then substitute (4-21) and (4-22) back to the system (4-15), there are:

$$\dot{z}_4 = v_2 = -\frac{1}{2}\lambda_4 \text{ then } z_4 = -\frac{1}{2}\mu_4 t + \mu_5 \tag{4-25}$$

$$\dot{z}_3 = v_1 = -\frac{1}{2}\lambda_3 \text{ then } z_3 = -\frac{1}{2}\left(\frac{1}{6}\mu_1 t^3 - \frac{1}{2}\mu_2 t^2 + \mu_3 t + \mu_6\right) \tag{4-26}$$

$$\dot{z}_2 = z_3 \text{ then } z_2 = -\frac{1}{2}\left(\frac{1}{24}\mu_1 t^4 - \frac{1}{6}\mu_2 t^3 + \frac{1}{2}\mu_3 t^2 + \mu_6 t + \mu_7\right) \tag{4-27}$$

$$\dot{z}_1 = z_2 \text{ then } z_1 = -\frac{1}{240}\mu_1 t^5 + \frac{1}{48}\mu_2 t^4 - \frac{1}{12}\mu_3 t^3 - \frac{1}{4}\mu_6 t^2 - \frac{1}{2}\mu_7 t + \mu_8 \tag{4-28}$$

where μ_5 to μ_8 are the constants to be determined. Suppose the piston

moves to the positive direction and substitute the boundary and initial conditions into the solutions (4-25) to (4-28), part of the unknown constants can be determined to have the following values: $\mu_5 = z_4(0)$, $\mu_4 = \frac{2}{T}[z_4(0) - z_4(t_T)]$, $\mu_6 = 0$, $\mu_7 = 0$, $\mu_8 = -l/2$, and

$$z_1(t_T) = \frac{l}{2} = -\frac{1}{240}\mu_1 t_T^{\,5} + \frac{1}{48}\mu_2 t_T^{\,4} - \frac{1}{12}\mu_3 t_T^{\,3} - \frac{l}{2}$$

$$z_2(t_T) = 0 = -\frac{1}{2}\left(\frac{1}{24}\mu_1 t_T^{\,4} - \frac{1}{6}\mu_2 t_T^{\,3} + \frac{1}{2}\mu_3 t_T^{\,2}\right)$$

$$z_3(t_T) = -\frac{1}{2}\left(\frac{1}{6}\mu_1 t_T^{\,3} - \frac{1}{2}\mu_2 t_T^{\,2} + \mu_3 t_T\right)$$

$$\mu_1 = -\frac{1440l}{t_T^{\,5}} - \frac{120}{t_T^{\,3}} z_3(t_T)$$

Then $$\mu_2 = \frac{-720l}{t_T^{\,4}} - \frac{48}{t_T^{\,2}} z_3(t_T)$$

$$\mu_3 = \frac{-120l}{t_T^{\,3}} - \frac{6}{t_T} z_3(t_T)$$

Finally, equations (4-25) to (4-28) become

$$z_1 = \left(\frac{6l}{t_T^{\,5}} + \frac{z_3(t_T)}{2t_T^{\,3}}\right)t^5 - \left(\frac{15l}{t_T^{\,4}} + \frac{z_3(t_T)}{t_T^{\,2}}\right)t^4 + \left(\frac{10l}{t_T^{\,3}} + \frac{z_3(t_T)}{2t_T}\right)t^3 - \frac{l}{2} \quad (4\text{-}29.a)$$

$$z_2 = \left(\frac{30l}{t_T^{\,5}} + \frac{5z_3(t_T)}{2t_T^{\,3}}\right)t^4 - \left(\frac{60l}{t_T^{\,4}} + \frac{4z_3(t_T)}{t_T^{\,2}}\right)t^3 + \left(\frac{30l}{t_T^{\,3}} + \frac{3z_3(t_T)}{2t_T}\right)t^2 \quad (4\text{-}29.b)$$

$$z_3 = \left(\frac{120l}{t_T^{\,5}} + \frac{10z_3(t_T)}{t_T^{\,3}}\right)t^3 - \left(\frac{180l}{t_T^{\,4}} + \frac{12z_3(t_T)}{t_T^{\,2}}\right)t^2 + \left(\frac{60l}{t_T^{\,3}} + \frac{3z_3(t_T)}{t_T}\right)t \quad (4\text{-}29.c)$$

$$z_4 = \frac{t}{t_T}[z_4(t_T) - z_4(0)] + z_4(0) \quad (4\text{-}29.d)$$

Then the analytic solutions of this optimal control problem can be obtained by solving Equations (4-29).

When the chosen input controls (4-12) and (4-13) are substituted back to the state feedback transform (4-11), from the defined equation $v_1 = v_3 - A_b v_2 / m$, the nonlinear controls with respect to the state variables z become:

$$u_1 = \frac{m(l/2+z_1+\Delta)}{kRT_s C_d C_0 w_a \hat{f}_n(z_3,P_s,P_e)}\left[\frac{k(z_2z_3+A_bz_2z_4/m+K_fz_2^2/m)}{l/2+z_1+\Delta}+\frac{K_f}{m}z_3+\left(\frac{360}{t_T^5}\right)t^2l-\left(\frac{360}{t_T^4}\right)tl+\frac{60}{t_T^3}l+\frac{A_b}{mt_T}[z_4(t_T)-z_4(0)]\right] \quad (4\text{-}30)$$

$$u_2 = \frac{A_b(l/2-z_1+\Delta)}{kRT_s C_d C_0 w_b \hat{f}_n(z_4,P_s,P_e)}\left[\frac{-kz_2z_4}{l/2-z_1+\Delta}+\frac{1}{T}[z_4(t_T)-z_4(0)]\right] \quad (4\text{-}31)$$

4.4 Energy Efficient Optimal Trajectories and Analysis

When applying the analytic solutions obtained from the linearised model (4-29), simulation studies have been conducted. A group of optimal trajectories are obtained. Investigation of the effects in using different parameters has also been done. The conditions specified for the simulations are:

- Cylinder: Rodless cylinder
- Stroke length: 1000mm
- Diameter of piston: 32mm
- Supply air pressure: 6 bars
- Exhaust pressure: 1 bar
- Temperature: 293K
- Payload mass: 1kg
- Static friction forces: ignored
- Viscous frictional coefficient: 15Ns/m
- Initial piston position: -0.5m

- Initial piston velocity: 0m/s
- Initial chamber pressures: 3.5 bars for both chambers
- Simulation time: 2s

From the analytic solutions (4-29) for the energy efficient optimal control problem of the pneumatic cylinder, it can be seen that $z_3(t_T)$ and $z_4(t_T)$, *i.e.* the terminal piston acceleration and terminal Chamber B pressure, should be specified. From the performance index (4-16), we already know that $z_3(t_T)$ is desired to be as small as possible. In the optimal case, $z_3(t_T)$ is expected to be zero, while terminal Chamber B pressure $z_4(t_T)$ is set to 2.5 bars initially. Since the piston will stop ultimately, Chamber A terminal pressure should equal the Chamber B terminal pressure under the assumption of ignored static frictions. The simulation dynamic responses are presented in Figure 4.1 and 4.2.

Then the optimal trajectories from Figure 4.1 and 4.2 are obtained with the 2.5 bars terminal pressures of Chamber A and B. To test if the simulation results are correct, the shooting method (refer to Section 3.2.3) has been used on the linearised model, and exactly the same results have been obtained. However, a question emerges, whether or not the optimal trajectories obtained always are optimal with different conditions. First of all, the effect of different terminal pressures conditions is investigated. In the simulation study, the terminal pressures of Chamber A and B vary from 2.0 bars to 6.0 bars with the same initial chamber pressure 3.5 bars. Figure 4.3 and 4.4 show the optimal trajectories obtained with 20 different terminal chamber pressures.

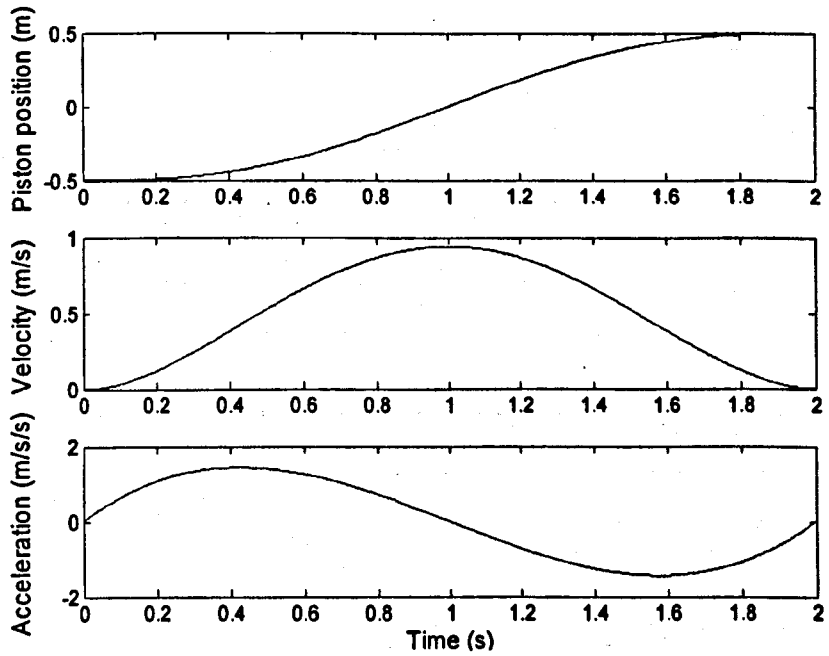

Figure 4.1 Optimal trajectories of piston position, velocity and acceleration with terminal pressures of 2.5 bars

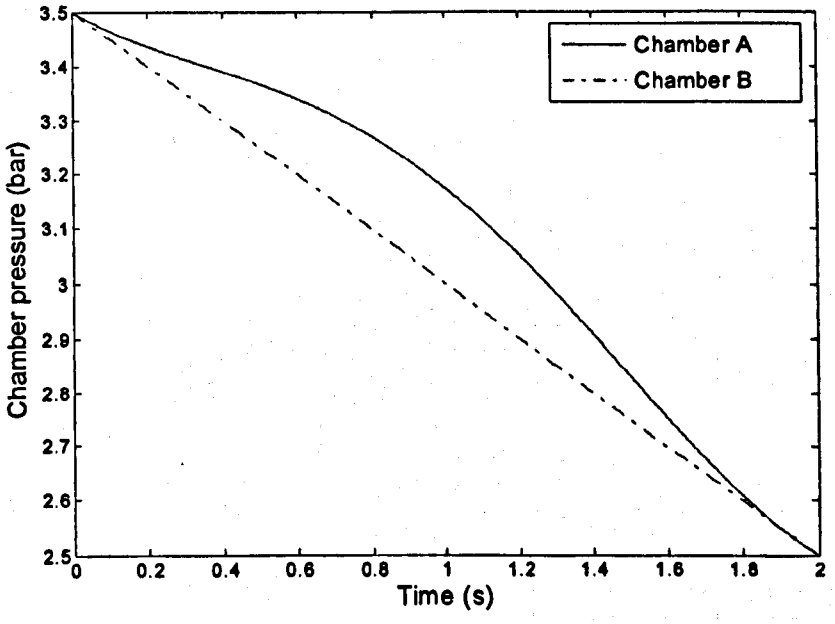

Figure 4.2 Optimal chamber pressure trajectories with terminal pressures of 2.5 bars

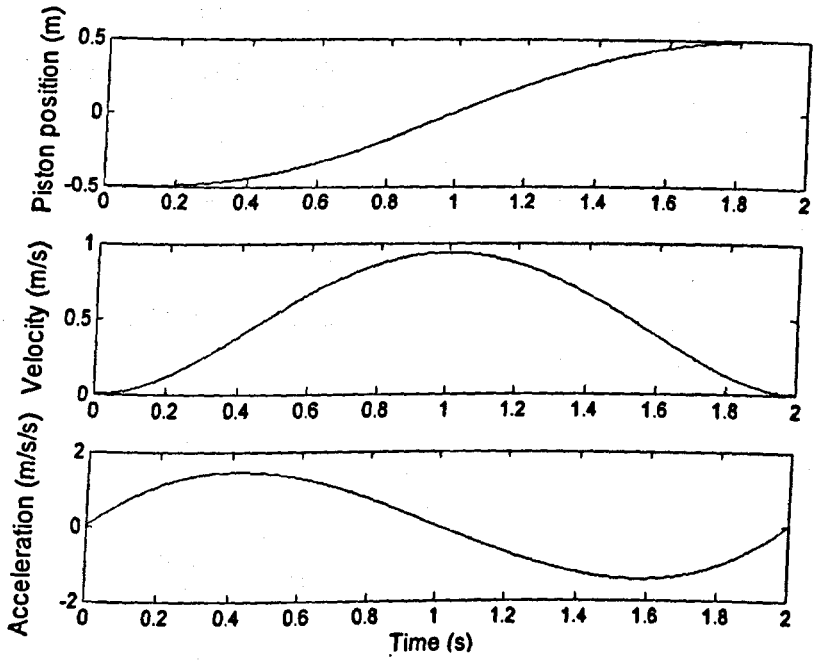

Figure 4.3 Optimal trajectories of piston position, velocity and acceleration with 20 different terminal pressures

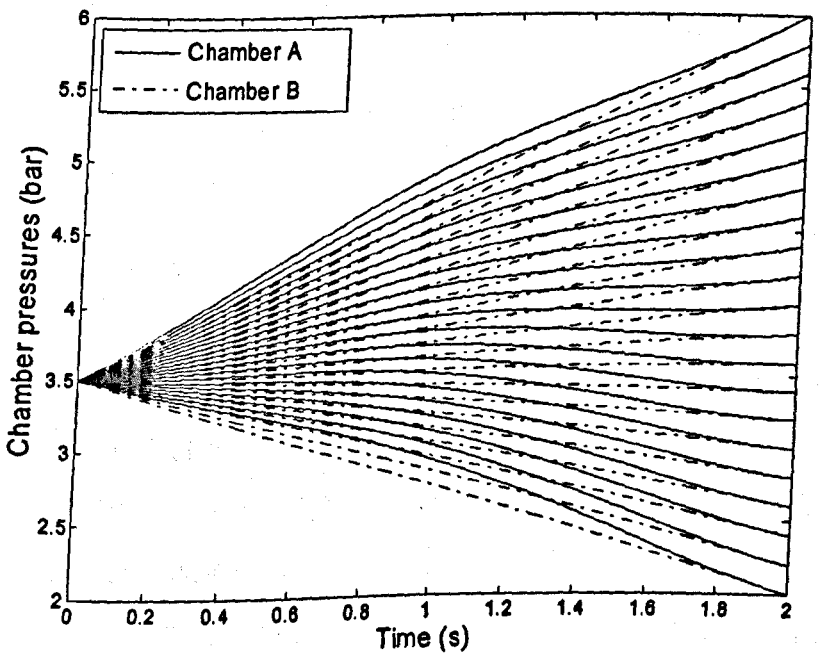

Figure 4.4 Optimal chamber pressure trajectories with 20 different terminal pressures

It can be easily seen that Figure 4.3 is exactly same as Figure 4.1, which means with different terminal pressure conditions, the piston position, velocity and acceleration retain the same pattern. In Figure 4.4, which shows 20 different chamber pressure patterns, the Chamber A pressure is always higher than Chamber B pressure apart from the beginning and end part, which assures the piston can move from one end of the stroke to the other end smoothly.

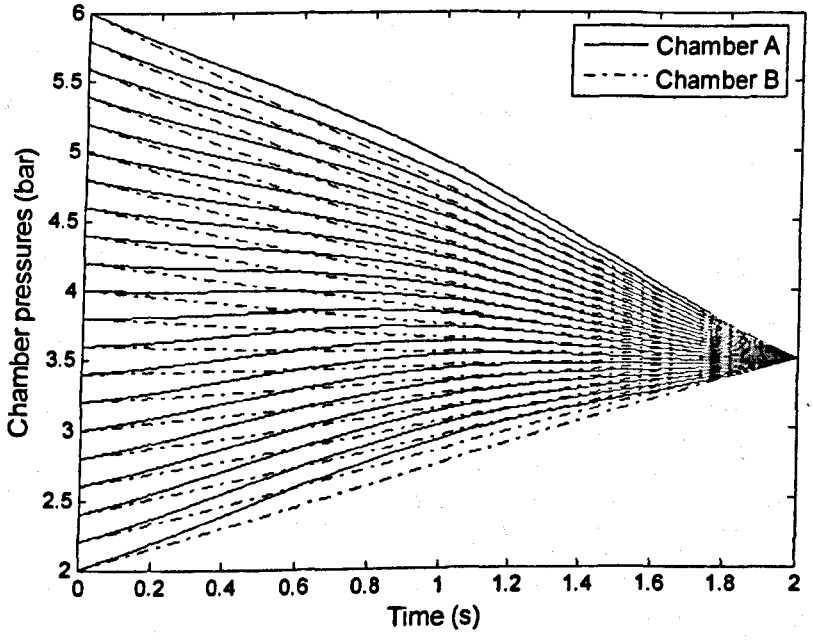

Figure 4.5 Optimal chamber pressure trajectories with 20 different initial pressures

As different terminal pressure conditions do not affect the group of optimal trajectories, will different initial pressures affect them? An investigation with fixed terminal chamber pressures, 3.5 bars, and 20 different initial pressures, from 2.0 bars to 6.0 bars, has been done. It is found that even with different initial chamber pressures the optimal trajectories of piston position, piston velocity and acceleration still remain the same. Figure 4.5 shows the 20

different chamber pressure patterns.

The obtained analytic solutions of the energy efficient optimal control problem (4-29) can explain why the initial and terminal chamber pressures do not affect the optimal trajectories. From the equations (4-29.a-c), z_1, z_2 and z_3, which denote the piston position, velocity and acceleration, depend only on the stroke length l, simulation time T and the terminal piston acceleration $z_3(t_T)$, which is set to zero in the simulation for the sake of energy saving. So Equation (4-29.b) becomes

$$z_2 = \left(\frac{30l}{t_T^5}\right)t^4 - \left(\frac{60l}{t_T^4}\right)t^3 + \left(\frac{30l}{t_T^3}\right)t^2 \qquad (4\text{-}32)$$

The equation (4-32) is the energy efficient optimal piston velocity profile, which could be quite useful in applications of servo-controlled pneumatic actuator systems in industry.

In 2001, Wang *et al.* discovered that the servo pneumatic system used less compressed air when a sine wave shape piston velocity profile was adopted comparing with the situation of using trapezoidal and parabolic shape velocity profiles, which was obtained through the simulation study using a PID controller. It was also predicted that there exists an optimal energy efficient profile for servo control pneumatic systems based on the simulation results (Wang *et al.*, 2001). Comparing the optimal velocity trajectory presented in Figure 4.1 and the result from Wang *et al.* 2001, Figure 4.6 is illustrated below. Obviously, the sinusoidal shape profile is very close to the energy efficient optimal profile obtained above, in particular, they have same variation trend. This result is encouraging as it has verified the findings at a certain level in

Wang *et al.*, 2001. The curve also informs that it requires a lower maximum velocity to move a piston from one position to another within the same length of time period compared with the sine wave.

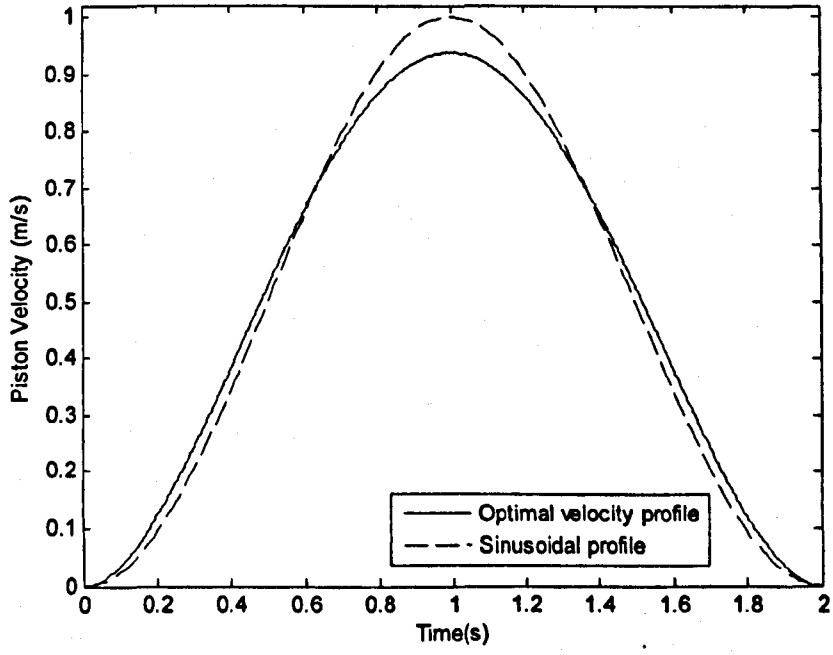

Figure 4.6 The optimal velocity trajectory comparing with a sine wave profile

For the generalised nonlinear controls (4-12) and (4-13) applied to the transformed system (4-11), the same set of simulation work as above has been done. The key issue is to investigate if the generalised optimal controls in the original nonlinear system model are still the pair of most energy efficient controls for the pneumatic actuator system. It is found that the piston position, velocity, acceleration and both chamber pressures optimal trajectories are exactly the same as those obtained directly from the linearised model, which are shown in Figure 4.1 to Figure 4.5 with the same simulation conditions. This validates that the analytic solutions obtained for the linearised model and confirms that the generalised nonlinear controls (4-12) and (4-13) are energy

efficient optimal controls for the original nonlinear pneumatic cylinder system indeed. Figure 4.7 shows a pair of energy efficient optimal controls, which represent the displacements of the two valves.

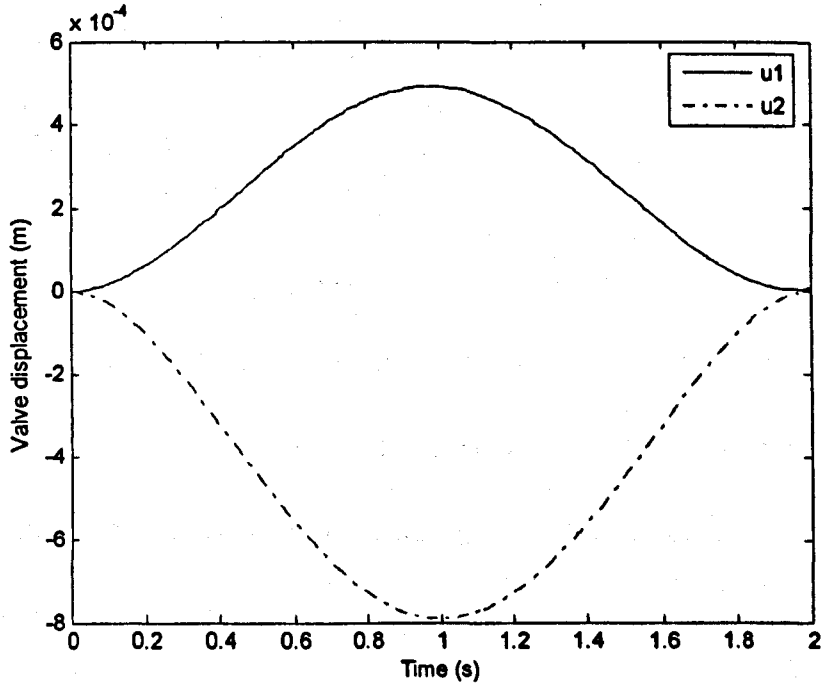

Figure 4.7 Typical control variables for the nonlinear control

4.5 Energy Efficient Optimal Control Design with Consideration of Static and Coulomb Frictions

The energy efficient optimal control design presented in the above sections ignores the static and Coulomb frictions for the convenience of finding the suitable set of transformations to linearise the original system. In this section, the static and Coulomb frictions are included in the system. Since the same transformation (4-10) will be used again, the influence of frictions will be included in the design of the optimal controller.

With the transformation (4-10) and the original system (2-38)

$$\begin{cases} \dot{z}_1 = \dot{x}_1 = x_2 = z_2 \\ \dot{z}_2 = \dot{x}_2 = \dfrac{1}{m}\left[-K_f x_2 - K_{S\text{-}C} S(x_2, x_3, x_4) + A_a x_3 - A_b x_4\right] = z_3 - \dfrac{K_{S\text{-}C} S(z_2, z_3, z_4)}{m} \\ \dot{z}_3 = -\dfrac{K_f}{m}\dot{x}_2 + \dfrac{A_a}{m}\dot{x}_3 - \dfrac{A_b}{m}\dot{x}_4 \\ \dot{z}_4 = \dot{x}_4 = \dfrac{k z_4 z_2}{l/2 - z_1 + \Delta} + \dfrac{k R T_s C_d C_0 w_b \hat{f}_n(z_4, P_s, P_e)}{A_b(l/2 - z_1 + \Delta)} u_{f2} \end{cases}$$

Comparing with the system (4-11), there are two differences when considering the frictions: one is $\dot{z}_2$, the other is the $-K_f \dot{x}_2 / m$ item in $\dot{z}_3$. In the equations, only $\dot{z}_3$ and $\dot{z}_4$ can affect the optimal controllers with consideration of the frictions u_{f1} and u_{f2}. So for finding suitable optimal controllers, the $\dot{z}_3$ expression needs to be altered. $-K_f \dot{x}_2 / m$ item in $\dot{z}_3$ becomes:

$$\begin{aligned} -\frac{K_f}{m}\dot{x}_2 &= -\frac{K_f}{m}\cdot\frac{1}{m}\left[-K_f x_2 - K_{S\text{-}C} S(x_2, x_3, x_4) + A_a x_3 - A_b x_4\right] \\ &= \begin{cases} -\dfrac{K_f}{m^2}\left[-K_f x_2 - (A_a x_3 - A_b x_4) + A_a x_3 - A_b x_4\right], & x_2 = 0 \\ -\dfrac{K_f}{m^2}\left[-K_f x_2 - F_C \operatorname{sign}(x_2) + A_a x_3 - A_b x_4\right], & x_2 \neq 0 \end{cases} \\ &= \begin{cases} \dfrac{K_f^2}{m^2} x_2, & x_2 = 0 \\ -\dfrac{K_f}{m^2}\left[-K_f x_2 - F_C \operatorname{sign}(x_2) + A_a \dfrac{m z_3 + K_f x_2 + A_b x_4}{A_a} - A_b x_4\right], & x_2 \neq 0 \end{cases} \\ &= \begin{cases} 0, & z_2 = 0 \\ \dfrac{K_f}{m^2} F_C \operatorname{sign}(z_2) - \dfrac{K_f}{m} z_3, & z_2 \neq 0 \end{cases} \end{aligned}$$

in which $x_3 = \dfrac{m z_3 + K_f x_2 + A_b x_4}{A_a}$ from the transform (4-10). Finally, the

original system with consideration of frictions can be transformed as:

$$\begin{cases} \dot{z}_1 = z_2 \\ \dot{z}_2 = z_3 - \dfrac{K_{S\text{-}C} S(z_2, z_3, z_4)}{m} \\ \dot{z}_3 = \begin{cases} \gamma, & z_2 = 0 \\ \dfrac{K_f}{m^2} F_C \operatorname{sign}(z_2) - \dfrac{K_f}{m} z_3 + \hat{\gamma}, & z_2 \neq 0 \end{cases} \\ \dot{z}_4 = \dfrac{k z_4 z_2}{l/2 - z_1 + \Delta} + \dfrac{k R T_s C_d C_0 w_b \hat{f}_n(z_4, P_s, P_e)}{A_b (l/2 - z_1 + \Delta)} u_2 \end{cases} \tag{4-33}$$

where

$$\begin{aligned} \hat{\gamma} = & -\frac{k(z_2 z_3 + A_b z_2 z_4 / m + K_f z_2^2 / m)}{l/2 + z_1 + \Delta} + \frac{k R T_s C_d C_0 w_a \hat{f}_n(z_3, P_s, P_e)}{m(l/2 + z_1 + \Delta)} u_1 \\ & - \frac{A_b k z_4 z_2}{m(l/2 - z_1 + \Delta)} - \frac{k R T_s C_d C_0 w_b \hat{f}_n(z_4, P_s, P_e)}{m(l/2 - z_1 + \Delta)} u_2 \end{aligned} \tag{4-34}$$

Therefore, the optimal controllers with consideration of frictions can be selected as:

$$u_{f1} = \begin{cases} \dfrac{m(l/2 + z_1 + \Delta)}{k R T_s C_d C_0 w_a \hat{f}_n(z_3, P_s, P_e)} \left[\dfrac{k(z_2 z_3 + A_b z_2 z_4 / m + K_f z_2^2 / m)}{l/2 + z_1 + \Delta} + v_3 \right], & z_2 = 0 \\ \dfrac{m(l/2 + z_1 + \Delta)}{k R T_s C_d C_0 w_a \hat{f}_n(z_3, P_s, P_e)} \left[\begin{array}{l} -\dfrac{K_f}{m^2} F_C \operatorname{sign}(z_2) + \dfrac{K_f}{m} z_3 + \\ \dfrac{k(z_2 z_3 + \dfrac{A_b z_2 z_4}{m} + \dfrac{K_f z_2^2}{m})}{l/2 + z_1 + \Delta} + v_3 \end{array} \right], & z_2 \neq 0 \end{cases} \tag{4-35}$$

$$u_{f2} = \frac{A_b (l/2 - z_1 + \Delta)}{k R T_s C_d C_0 w_b \hat{f}_n(z_4, P_s, P_e)} \left(\frac{-k z_2 z_4}{l/2 - z_1 + \Delta} + v_2 \right) \tag{4-36}$$

where $v_1 = v_3 - A_b v_2 / m$ as defined in those defined in Equations (4-30) and (4-31). It can be seen that u_{f2} is the same as u_2, which is the optimal controller without consideration of static and Coulomb frictions; while there are two cases that need to be discussed regarding u_{f1}, *i.e.* when the piston stops

and the piston moves. Although simulation work is still on-going, it can be predicted that a similar optimal trajectory set would be obtained.

4.6 Test of the Optimal Velocity Profile

In this section, the optimal velocity trajectory obtained from Section 4.4 will be validated by a set of simulation studies, which is implemented in Simulink. A simple conventional PI controller plus velocity feedback control strategy is introduced to the pneumatic cylinder actuating system, in order to make the system follow four different shape velocity profiles respectively, including the obtained optimal velocity profile (4-32) and three other velocity profiles, which are trapezoidal, sinusoidal and parabolic profiles. All of these velocity profiles are calculated to make sure the piston start moving from one end of the stroke and stopping at the other end exactly at the terminal time. In other words, all of these profiles are reasonable and applicable for real industrial application.

To examine the most energy-saving profile amongst these velocity profiles, under the same control strategy and simulation parameters, a comparison is conducted. The controller parameters are tuned based on a trial and error method. The tracking errors are limited in 0.2%. The parameters of the controller are selected as: K_p=0.08, K_i=0.002, the velocity feedback derivative coefficient K_v is 0.0002. The schematic of the control system structure is shown in Figure 4.8, while the adopted velocity profiles are shown in Figure 4.9. The simulation study is conducted under the same conditions as those in Section 4.4. Full cycle is measured, thus the simulation time is 4 seconds.

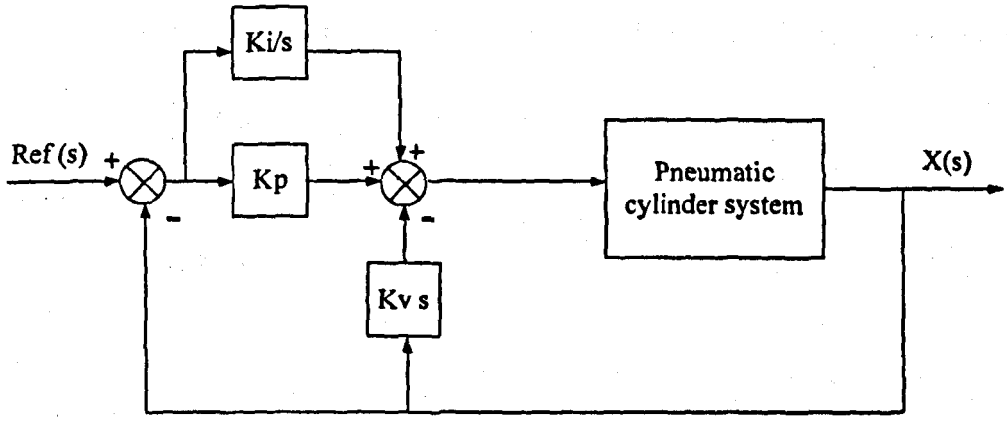

Figure 4.8 Schematic of the controller structure

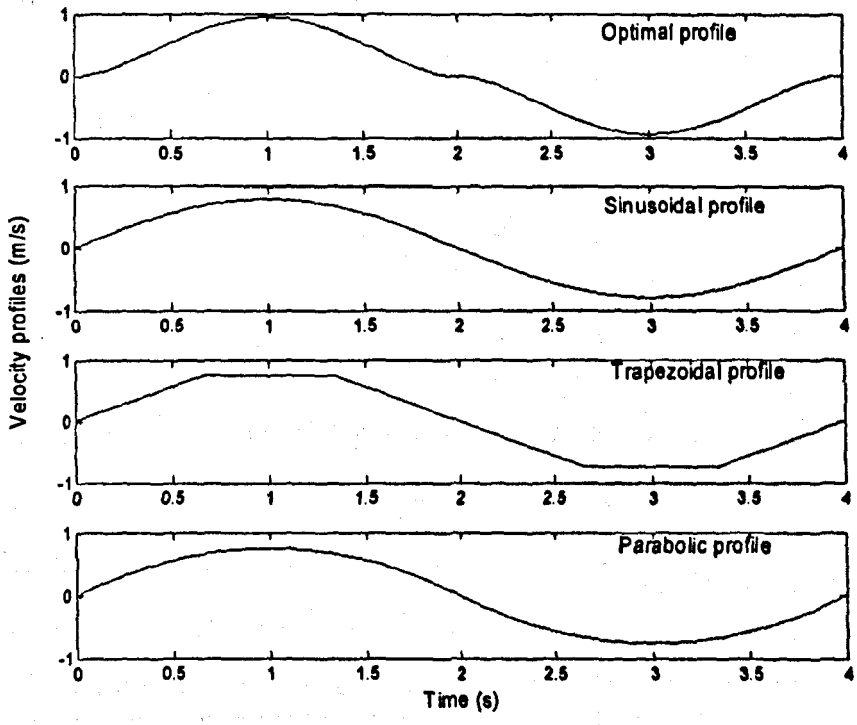

Figure 4.9 Four different shape velocity profiles tracked by the controller

In the simulation study, only the intake of the air consumption will be considered, in the first half cycle, valve A is the inlet valve, but in the second half cycle, valve B takes compressed air from the air tank. Therefore, the compressed air consumption is calculated by the following equations:

$$m_a = \int_0^{0.5t_T} \dot{m}_a dt = \int_0^{0.5t_T} c_d c_0 w_a u_1 f_n(x_3, P_s, P_e)\, dt \tag{4-37}$$

$$m_b = \int_{0.5t_T}^{t_T} \dot{m}_b dt = \int_{0.5t_T}^{t_T} c_d c_0 w_b u_2 f_n(x_4, P_s, P_e)\, dt \tag{4-38}$$

So for the air consumption of the full cycle,

$$m = m_a + m_b \tag{4-39}$$

Through simulation study, it has been found the system uses different amounts of compressed air with different velocity profiles. The results are listed in Table 4.1. It can be noticed that when the system follows the optimal profile (4-32), it uses the least amount of compressed air compared to other profiles. This validates that the optimal velocity profile obtained from Section 4.4 is indeed optimal.

There is not a big difference in the air consumption for one cycle associated with those velocity profiles. However, considering a pneumatic cylinder will operate thousands of cycles a day, the amount of cylinders in a plant and the huge amount of users in the world, it is not negligible. The optimal control could deliver significant savings in the amount of electricity the world needs to generate.

Table 4.1 Comparison of air consumption with different velocity profiles

Velocity profiles tracked by the same controller	Mass of compressed air consumption (g)
Optimal profile	9.091
Sinusoidal profile	9.097
Trapezoidal profile	9.098
Parabolic profile	9.099

4.7 Conditions to Attain Minimum Value of Performance Index

In optimal control theory, when the optimal control $u^*(t)$ drives the plant from the initial state to final state, at the same time it will extremize the chosen performance criterion, *i.e.* performance index. The performance index can be chosen for different purposes. In this case, it is chosen for minimise the energy usage for pneumatic cylinder actuating systems.

4.7.1 Conditions to Attain Minimum Value of Performance Index in the Linearised Model

Since the terminal piston acceleration is set to zero in the simulation, in the linearised model, the performance index (4-16) adopted in Section 4.4 becomes

$$J = \int_0^{t_T} v^T v dt \tag{4-40}$$

where the vector $v = [v_1 \quad v_2]^T$ and

$$\begin{aligned} v_1 &= -\frac{1}{2}\lambda_3 = -\frac{1}{2}\left(\frac{1}{2}\mu_1 t^2 - \mu_2 t + \mu_3\right) \\ &= \left(\frac{360l}{t_T^5} + \frac{30z_3(t_T)}{t_T^3}\right)t^2 - \left(\frac{360l}{t_T^4} + \frac{24z_3(t_T)}{t_T^2}\right)t + \frac{60l}{t_T^3} + \frac{3z_3(t_T)}{t_T} \\ &= \left(\frac{360l}{t_T^5}\right)t^2 - \left(\frac{360l}{t_T^4}\right)t + \frac{60l}{t_T^3} \end{aligned} \tag{4-41}$$

$$v_2 = -\frac{1}{2}\lambda_4 = -\frac{1}{2}\mu_4 = \frac{1}{t_T}[z_4(t_T) - z_4(0)] \tag{4-42}$$

v_1 and v_2 are the control inputs of the system after linearisation. v_1 denotes the acceleration changing rate of the piston movement; v_2 denotes the changing rate of the pressure in Chamber B. It is quite reasonable using the combination of piston acceleration changing rate and chamber pressure changing rate as the performance index, which means the system with the least changing rates saves

the most energy.

The situation when the value of performance index value can achieve its minimum will be discussed in this section. From the simulation work, it has been found that the performance index value changes with different chamber pressure values. To investigate the condition under which the minimum value of performance index J occurs, the initial chamber pressure is fixed firstly, whereas the terminal chamber pressure is free. Figure 4.10 shows the value of performance index J against different terminal chamber pressures P_{Ta}, P_{Tb}, which range from 2 bars to 6 bars, with fixed initial pressures of both chambers, 3.5 bars. It can be seen from Figure 4.10 that the performance index has a minimum value when the terminal pressures are 3.5 bars, which is coincidently equal to the initial pressures. It should be noted that at the minimum point, the performance index is not zero, although it seems to be zero from Figure 4.10.

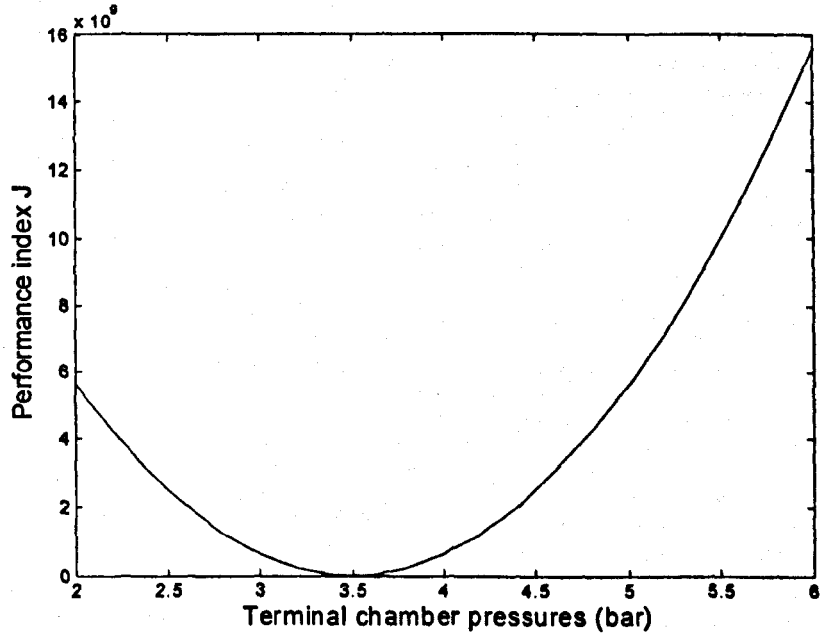

Figure 4.10 Performance index value against terminal chamber pressures with $P_0 = 3.5$ bar

The performance index also can be affected by initial chamber pressures P_{0a}, P_{0b}. Figure 4.11 shows the relationship between performance index J and terminal chamber pressures with different initial chamber pressures, 2.5 bars, 3.5 bars and 4.5 bars. It can be seen that the performance index reaches minimum at exactly where the terminal pressures are 2.5 bars, 3.5 bars and 4.5 bars respectively. This finding means the condition of the occurrence of minimum performance index is the equality of the initial chamber pressures and terminal chamber pressures, *i.e.*

$$P_{0a,b} = P_{Ta,b} \tag{4-43}$$

More simulation work has already been done to support this result. This result would be very useful in practical controller design as it implies that the controller should aim at driving the chamber to reach the same initial and terminal chamber pressures.

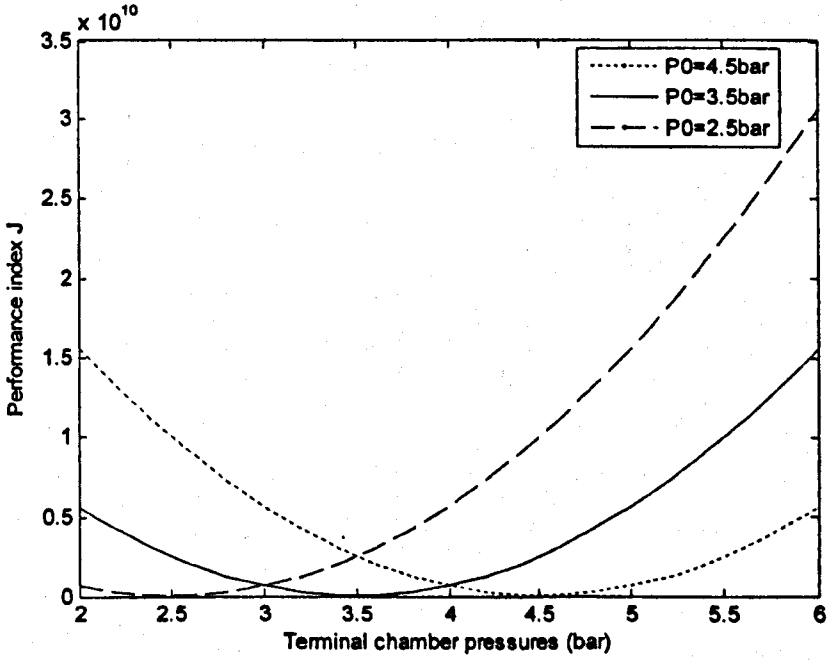

Figure 4.11 Performance index value against terminal chamber pressures with different initial chamber pressures

The condition of the occurrence of minimum performance index (4-43) has been obtained under the same compressed air supply pressure, 6 bars. So what will happen if the supply pressure is changed? To investigate if the supply pressure affects this condition, simulation study has been conducted under different air supply pressures. The results are shown in Figure 4.12. The simulation adopts different air supply pressures, 4 bars, 5 bars, 6 bars, 9 bars and 12 bars with fixed initial pressures of both chambers, 3.5 bars. It can be seen that the minimum performance index J still occurs when terminal pressures of both chambers are 3.5 bars, that is, when the terminal pressures are the same as the initial pressures no matter how high/low the supply pressure is. Because the exact linearisation via feedback eliminates the items containing air supply pressure P_s, the compressed air supply pressure does not affect the condition (4-43).

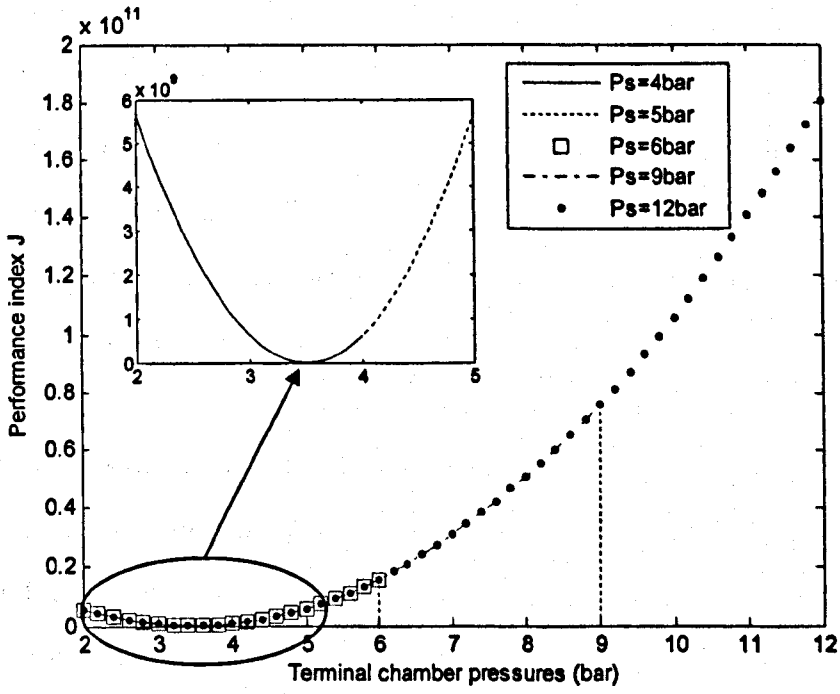

Figure 4.12 Performance indices against terminal chamber pressures with different air supply pressures

4.7.2 Conditions to Attain Minimum Value of Performance Index Based in Original System

Certainly, the simulation results in Subsection 4.7.1 and the condition (4-43) are obtained from the optimal control design on the linearised system model under the exact linearisation and theoretical optimal control method. However, in the practical engineering environment, are the results obtained from the theoretical calculation still appropriate? This section will examine if the condition (4-43) is still tenable in the practical case, *i.e.*, the original nonlinear system and the influence from the compressed air supply pressure.

The simulation study is conducted to find out if the minimum value of the performance index still happens under the same conditions derived from the linearised systems. For practical purpose a performance index, which determines the minimum fuel consumption of the system, can be set also as:

$$J_1 = \int_0^{t_f} (|u_1| + |u_2|)dt \tag{4-44}$$

The new performance index J_1 can be interpreted as the total spool displacement of the two valves on the pneumatic cylinder is minimized, that is, the integration of the control effort or the energy consumption is minimized.

Similar to the simulation conducted on the linearised system model, by fixing the initial chamber pressures but varying the terminal pressures, the relationship between the values of new performance index J_1 and the terminal pressures with different initial chamber pressures and air supply pressures are shown in Figure 4.13. The results are obtained under initial chamber pressures at 2.5 bars, 3.5 bars and 4.5 bars, respectively. And three different air supply pressures, 6 bars,

9 bars, and 12 bars, are adopted for each group. It should be noted that the minimum value of J_1 does not happen at the point of the terminal pressures same as the initial pressures. The minimum J_1 appears when the terminal pressure is slightly lower or higher than the initial values. Also the air supply pressure variations affect the trends of the curves in Figure 4.13 obviously. If the supply pressures increase, the terminal pressures increase to achieve the point of minimum J_1. Therefore, in principle, the condition (4-43) reached in Subsection 4.7.1 still correlates with the original nonlinear system. It is realistic to set up the initial and terminal chamber pressures to have same value. But, in this case, only sub-optimal control can be achieved as the minimum J_1 happens at the point slightly away from the optimal terminal pressures. In practice, this will guide the profile design. Once the initial pressure is determined the terminal pressure will settle at the same level as its initial pressure.

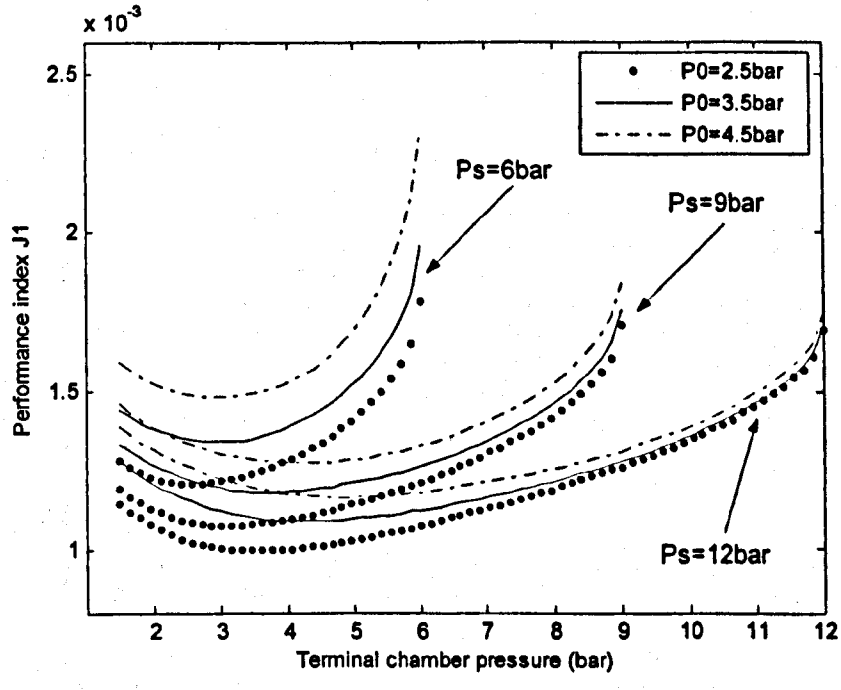

Figure 4.13 The performance index J_1 as functions of terminal chamber pressures with different initial chamber pressures and air supply pressures

Then investigation of the relation between the condition of occurrence of minimum J_1 and initial chamber pressures and air supply pressures has been undertaken. The integrated results through plenty of simulation work are shown in Figure 4.14, which shows the relationship between the initial chamber pressures and the terminal chamber pressure, when the performance index J_1 achieves minimum, under conditions of different air supply pressures. The results indicated that the initial chamber pressures should be chosen about 10% to 20% lower than the 50% of the supply pressure.

All the simulation results obtained in this subsection are under the adoption of the performance index J_1. If other forms of performance index are used, for example, air mass flow rate or combination of mass flow rate and valve displacement, the relations obtained will be changed.

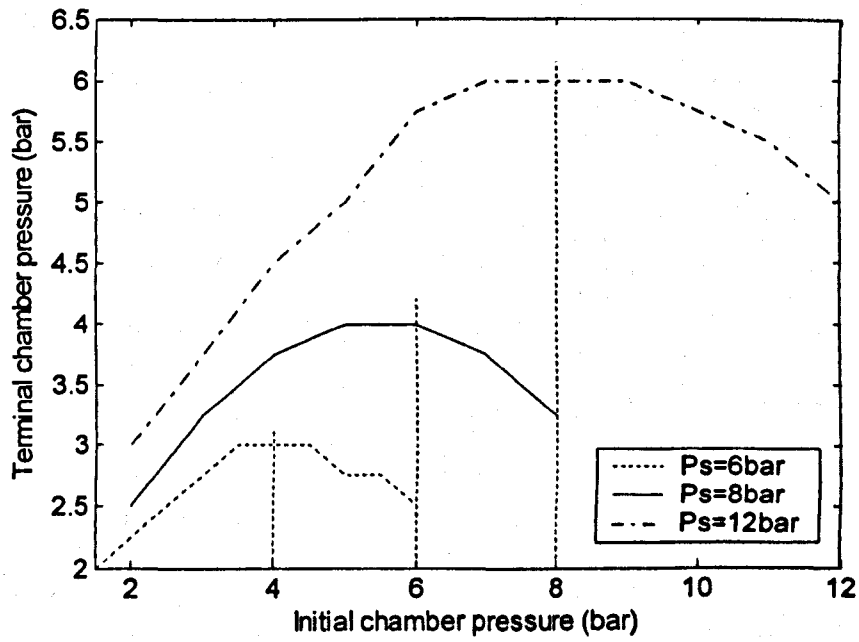

Figure 4.14 The terminal chamber pressure when the minimum J_1 value is achieved as a function of initial chamber pressures with different air supply pressures

4.8 Summary

In this chapter, an energy efficient optimal control strategy of servo pneumatic cylinder actuating systems is presented. To avoid solving the set of complicated nonlinear differential equations with unknown boundary conditions, the pneumatic cylinder system is linearised through input/output state feedback. The feedback linearisation control law and the detailed method are explained.

Then optimal control theory is applied to the linearised system. An optimal control strategy is developed with respect to the transformed states of the linearised system. The solution of the state trajectory results in a group of energy efficient piston position, velocity, acceleration and chamber pressure trajectories. Through simulation studies, it is found that the energy efficient optimal trajectories of piston position, velocity and acceleration are not affected by the initial and terminal chamber pressures and compressed air supply pressure; they are only dependent on the length of the stroke and the preset time period. After the generalised nonlinear controls are substituted back into the transformed system, the same group of trajectories is obtained through plenty of simulation work, which proves the obtained trajectories are energy efficient indeed optimal trajectories. The simulation study also validates that the energy efficient optimal profile worked out by this method will lead the cylinder to use the least quantity of compressed air compared with the three other different velocity profiles.

The performance index of the energy efficient control based on the linearised model is also investigated. It is found that under the condition, that is, as long as the initial chamber pressures are the same as the terminal chamber pressures,

the performance index can reach minimum value, and this condition is independent with respect to the air supply pressure. However, this condition will be slightly changed, however, still correlated when a new practical performance index is adopted in the original nonlinear system. The relations of initial and terminal chamber pressures, air supply pressures and occurrence of minimum performance index also depend on the selection of the performance index.

These results suggest that the industry may need to reform their traditional trapezoidal velocity profile to the newly developed velocity profile (4-32) and make an effort to make the terminal chamber pressures the same level of the initial chamber pressures. One system may not save a great amount of energy consumption but with the huge numbers of pneumatic actuators in use, optimal control could deliver significant savings in the amount of electricity the nation needs to generate.

Chapter 5

Tracking Control of Pneumatic System Using Input/Output Linearisation by State Feedback

5.1 Introduction

With the development of pneumatic components and microprocessors, pneumatic actuators can be employed to accomplish more sophisticated motion control tasks. Servo controlled pneumatic actuator system can follow any preset position/velocity profiles, which can be classified as tracking control systems. However, enormous difficulties are encountered in servo pneumatic system control due to the inherent nonlinearities associated with the compressibility of air and complex friction distributions along the cylinders. With the advantage of linearisation derived in Chapter 4, this chapter will discuss the tracking control of pneumatic cylinder actuating systems based on the linearised model. It is well known that with better and more precise tracking control, no doubt energy can be saved.

The tracking control strategy will be initially developed for the linearised model. Since there exists an inverse transformation for the new coordinate system, the

designed tracking control can be transformed back to the original state coordinates with the original input variables. Two different cases will be discussed in this chapter, that is, the pneumatic cylinder driven by a single five-port proportional valve and by two three-port proportional valves. At the initial stage, for the convenience of analysis, the static friction forces are ignored and then the friction forces are treated as uncertainties of the system in a later section.

However, the derived servo controller is still too complicated for online implementation, thus the controller needs to be simplified. Some approximations have been investigated, and the simplified controller requires only position and velocity state variables in its feedback. The simulation results indicate that the simplified controller can drive the pneumatic actuators to follow a desired profile within the accuracy requirement.

5.2 Input/Output Feedback Linearisation Applied on Pneumatic Cylinder Actuating System

As explained in Section 4.2, a suitable set of new coordinates can be found, and then the original system can be mapped into a different space. After selecting suitable control inputs, the nonlinear items can be eliminated by exact linearisation via feedback, *i.e.* the system becomes a linear system. For the convenience of finding the suitable set of coordinates, the static frictions are ignored initially and will be brought in as uncertainties in the later sections.

The servo pneumatic actuators can be driven by a single five-port proportional valve or two separate three-port proportional valves. Therefore, the analysis covers two different cases: a nonlinear pneumatic cylinder actuating system with a single input and two independent inputs.

5.2.1 Pneumatic Cylinder System with a Single Five-port Valve

The main purpose is to use the feedback linearisation method to achieve the high performance tracking control. When a pneumatic actuator system adopts a single five-port valve, the inlet and outlet ports are not independent inputs. The control inputs will be $u_1 = u$ and $u_2 = -u$. In the linearisation procedure adopted in Section 4.2, comparing with the general formulation (4-1), $\hat{f}, \hat{g}, \hat{h}$ of the system are as follows :

$$\hat{f}(x) = \begin{bmatrix} x_2 \\ (-K_f x_2 + A_a x_3 - A_b x_4)/m \\ \dfrac{-k x_3 x_2}{l/2 + x_1 + \Delta} \\ \dfrac{-k x_4 x_2}{l/2 - x_1 + \Delta} \end{bmatrix}, \hat{g}(x) = \begin{bmatrix} 0 \\ 0 \\ \dfrac{kRT_s C_d C_0 w f_n(x_3, P_s, P_e)}{A_a(l/2 + x_1 + \Delta)} \\ -\dfrac{kRT_s C_d C_0 w f_n(x_4, P_s, P_e)}{A_b(l/2 - x_1 + \Delta)} \end{bmatrix} \quad \text{and } y = \hat{h}(x) = x_1$$

where $\hat{f}$ and $\hat{g}$ are C^∞ vector fields on the set $\Omega \subset \Re^4, y = \hat{h}(x) \in (-l/2,\ l/2) \subset \Re$.

For this system, $L_g L_f^{\,k} \hat{h}(x) = 0$, for all $k < 3$; and $L_g L_f^{\,k} \hat{h}(x) \neq 0$ for all $k = 3\,(\forall x)$. Then the relative degree of the system is 3. As explained in Section 4.2, the coordinate transformation to linearise the pneumatic system (4-10) also can be used in this case, which is as follows:

$$\left.\begin{aligned} z_1 &= x_1 \\ z_2 &= x_2 \\ z_3 &= -\frac{K_f}{m}x_2 + \frac{A_a}{m}x_3 - \frac{A_b}{m}x_4 \\ z_4 &= x_4 \end{aligned}\right\}$$

Applying this transformation, the pneumatic system is transformed into:

$$\left.\begin{aligned} \dot{z}_1 &= z_2 \\ \dot{z}_2 &= z_3 \\ \dot{z}_3 &= -\frac{K_f}{m}z_3 - \frac{k(z_2z_3 + K_f z_2^2/m)}{l/2 + z_1 + \Delta} - \frac{A_b k(l+2\Delta)}{(l/2+\Delta)^2 - z_1^2} z_2 z_4 + \hat{\psi}(z)u \\ \dot{z}_4 &= \frac{kz_4z_2}{l/2 - z_1 + \Delta} - \frac{kRT_sC_dC_0w\hat{f}_n(z_4,P_s,P_e)}{A_b(l/2 - z_1 + \Delta)}u \end{aligned}\right\} \quad (5\text{-}1)$$

where $\hat{\psi}(z) = kRT_sC_dC_0w\dfrac{(l/2 - z_1 + \Delta)\hat{f}_n(z_3,P_s,P_e) + (l/2 + z_1 + \Delta)\hat{f}_n(z_4,P_s,P_e)}{m[(l/2+\Delta)^2 - z_1^2]}$.

Let $u = \dfrac{1}{\hat{\psi}(z)}\left[\dfrac{k(z_2z_3 + K_f z_2^2/m)}{l/2 + z_1 + \Delta} + \dfrac{A_b k(l+2\Delta)z_2z_4}{(l/2+\Delta)^2 - z_1^2} + v\right]$. Substitute u into (5-1), then

$$\left.\begin{aligned} \dot{z}_1 &= z_2 \\ \dot{z}_2 &= z_3 \\ \dot{z}_3 &= -\frac{K_f}{m}z_3 + v \end{aligned}\right\} \quad (5\text{-}2.a)$$

$$\dot{z}_4 = \frac{kz_4z_2}{l/2 - z_1 + \Delta} - \left[\frac{1}{\hat{\psi}(z)}\frac{kRT_sC_dC_0w_b\hat{f}_n(z_4,P_s,P_e)}{A_b(l/2 - z_1 + \Delta)}\right]$$

and

$$\left[\frac{k(z_2z_3 + \frac{K_f}{m}z_2^2)}{l/2 + z_1 + \Delta} + \frac{A_b k(l+2\Delta)z_2z_4}{(l/2+\Delta)^2 - z_1^2} + v\right] \quad (5\text{-}2.b)$$

$$y = z_1 \quad (5\text{-}2.c)$$

Subsystem (5-2.a) is linear with respect to z and v, and its I/O map is also linear.

5.2.2 Pneumatic Cylinder System with Two Three-port Valves

When the pneumatic cylinder adopts two three-port valves, as shown in Section 4.2, and applying the same set of coordinates transformation, the pneumatic system can be transformed into:

$$\left.\begin{aligned}
\dot{z}_1 &= z_2 \\
\dot{z}_2 &= z_3 \\
\dot{z}_3 &= -\frac{K_f}{m} z_3 - \frac{k(z_2 z_3 + A_b z_2 z_4 / m + K_f z_2^2 / m)}{l/2 + z_1 + \Delta} + \frac{kRT_s C_d C_0 w_a \hat{f}_n(z_3, P_s, P_e)}{m(l/2 + z_1 + \Delta)} u_1 \\
&\quad - \frac{A_b k z_4 z_2}{m(l/2 - z_1 + \Delta)} - \frac{kRT_s C_d C_0 w_b \hat{f}_n(z_4, P_s, P_e)}{m(l/2 - z_1 + \Delta)} u_2 \\
\dot{z}_4 &= \frac{k z_4 z_2}{l/2 - z_1 + \Delta} + \frac{kRT_s C_d C_0 w_b \hat{f}_n(z_4, P_s, P_e)}{A_b(l/2 - z_1 + \Delta)} u_2
\end{aligned}\right\} \quad (5\text{-}3)$$

However, for tracking control design, there is a slight difference from the energy efficient control inputs derived in Section 4.2. Let

$$u_1 = \frac{m(l/2 + z_1 + \Delta)}{kRT_s C_d C_0 w_a \hat{f}_n(z_3, P_s, P_e)} \left[\frac{k(z_2 z_3 + A_b z_2 z_4 / m + K_f z_2^2 / m)}{l/2 + z_1 + \Delta} - q z_4 + v_1 \right]$$

$$u_2 = \frac{A_b(l/2 - z_1 + \Delta)}{kRT_s C_d C_0 w_b \hat{f}_n(z_4, P_s, P_e)} \left[\frac{-k z_2 z_4}{l/2 - z_1 + \Delta} - q z_4 + v_2 \right]$$

where q is a design parameter with a positive real value. Substitute u_1 and u_2 back into system (5-3),

$$\begin{aligned}
\dot{z}_1 &= z_2 \\
\dot{z}_2 &= z_3 \\
\dot{z}_3 &= -\frac{K_f}{m} z_3 + v_1 - v_2 \\
\dot{z}_4 &= -q z_4 + v_2 \\
y &= z_1
\end{aligned} \quad (5\text{ -}4)$$

So the system (5-4) is linear with two equivalent inputs v_1 and v_2, and its I/O map is obviously also linear.

5.3 Tracking Control of the Pneumatic Actuator System

Similarly, the discussion of the tracking control design method will start from the case of using a single five-port valve. The linearised subsystem (5-2.a) can be rewritten in a matrix format as follows:

$$\dot{z} = \tilde{A}_1 z + \tilde{B}_1 v, \tag{5-5}$$

where $z = \begin{bmatrix} z_1 \\ z_2 \\ z_3 \end{bmatrix}$, $\tilde{A}_1 = \begin{bmatrix} 0 & 1 & 0 \\ 0 & 0 & 1 \\ 0 & 0 & -\frac{K_f}{m} \end{bmatrix}$, and $\tilde{B}_1 = \begin{bmatrix} 0 \\ 0 \\ 1 \end{bmatrix}$.

For a tracking problem, suppose that it requires the system output z_1 to accurately follow the trajectory $\varphi(t)$. It can be shown that $(\tilde{A}_1, \tilde{B}_1)$ is a controllable pair, $\varphi(t)$ can be normally generated by the same structured linear system as equation (5-5). Let $\theta_1(t) = \varphi(t)$ and $\theta = [\theta_1 \quad \theta_2 \quad \theta_3]^T$, z_1, z_2 and z_3 track θ_1, θ_2 and θ_3, there is

$$\begin{bmatrix} \dot{\theta}_1 \\ \dot{\theta}_2 \\ \dot{\theta}_3 \end{bmatrix} = \begin{bmatrix} 0 & 1 & 0 \\ 0 & 0 & 1 \\ 0 & 0 & -\frac{K_f}{m} \end{bmatrix} \begin{bmatrix} \theta_1 \\ \theta_2 \\ \theta_3 \end{bmatrix} \tag{5-6}$$

With equation (5-6), the tracking problem can be converted to an asymptotical stability problem. Let the errors $e(t) = \theta(t) - z(t)$, then

$$\dot{e} = \dot{\theta} - \dot{z} = \tilde{A}_1(\theta - z) + \tilde{B}_1 v = \tilde{A}_1 e + \tilde{B}_1 v \qquad (5\text{-}7)$$

A feedback controller can be developed to drive the error state $e(t)$ to zero. The controller has a structure of $v = -Ke$, where $K = [K_1 \quad K_2 \quad K_3]$. The closed-loop system is then written as $\dot{e} = (\tilde{A}_1 - \tilde{B}_1 K)e$. If the feedback control can be designed to guarantee that $\sigma(\tilde{A}_1 - \tilde{B}_1 K) \in C^-$, the tracking error $e(t)$ will eventually approach zero within a finite time period.

Substituting the tracking control v back into the original system control u, the following equation is obtained:

$$\begin{aligned} u = & \frac{k(z_2 z_3 + K_f z_2^2 / m)}{\psi(z)(l/2 + z_1 + \Delta)} + \frac{A_b k(l + 2\Delta) z_2 z_4}{\psi(z)[(l/2 + \Delta)^2 - z_1^2]} \\ & + \frac{1}{\psi(z)}[K_1(\theta_1 - z_1) + K_2(\theta_2 - z_2) + K_3(\theta_3 - z_3)] \end{aligned} \qquad (5\text{-}8)$$

By substituting $z = \overline{T}x$ into (5-8), the final feedback control $u(x)$ will be derived, which is quite straightforward:

$$\begin{aligned} u = & \frac{kx_2\left(\frac{A_a}{m}x_3 - \frac{A_b}{m}x_4\right)}{\psi(x)(l/2 + x_1 + \Delta)} + \frac{A_b k(l + 2\Delta) x_2 x_4}{\psi(x)[(l/2 + \Delta)^2 - x_1^2]} \\ & + \frac{1}{\psi(x)}\left[K_1(\theta_1 - x_1) + K_2(\theta_2 - x_2) + K_3(\theta_3 + \frac{K_f}{m}x_2 - \frac{A_a}{m}x_3 + \frac{A_b}{m}x_4)\right] \end{aligned}$$

where $\psi(x) = kRT_s C_d C_0 w \dfrac{(l/2 - x_1 + \Delta) f_n(x_3, P_s, P_e) + (l/2 + x_1 + \Delta) f_n(x_4, P_s, P_e)}{m[(l/2 + \Delta)^2 - x_1^2]}$.

For the case of using two three-port valves, the system is linearised as shown in (5-4). Letting $v_2 = -K_4 z_4$, $\dot{z}_4$ in (5-4) becomes $\dot{z}_4 = -qz_4 - K_4 z_4 = -(q + K_4)z_4$. This means that if the design parameter q has been properly chosen, v_2 can

be simply set to zero ($v_2 = 0$). In this case, the system (5-4) would be identical to (5-2.a), which implies that the same feedback control design procedure can be applied to this case. Therefore, the controller with respect to the state variables z is as follows:

$$u_1 = \frac{mz_2z_3 + A_b z_2 z_4 + K_f z_2^2}{RT_s C_d C_0 w_a \hat{f}_n(z_3, P_s, P_e)} - \frac{mqz_4(l/2 + z_1 + \Delta)}{kRT_s C_d C_0 w_a \hat{f}_n(z_3, P_s, P_e)} - \frac{m(l/2 + z_1 + \Delta)[K_1(\theta_1 - z_1) + K_2(\theta_2 - z_2) + K_3(\theta_3 - z_3)]}{kRT_s C_d C_0 w_a \hat{f}_n(z_3, P_s, P_e)} \quad (5\text{-}9)$$

$$u_2 = \frac{l/2 - z_1 + \Delta}{kRT_s C_d C_0 w_b \hat{f}_n(z_4, P_s, P_e)}\left[\frac{-kz_2 z_4}{l/2 - z_1 + \Delta} - qz_4\right] \quad (5\text{-}10)$$

Similarly, by substituting $z = \bar{T}x$ into u_1 and u_2, the final feedback control $u_1(x)$ and $u_2(x)$ can be derived for the second case:

$$u_1 = \frac{A_a x_2 x_3}{RT_s C_d C_0 w_a f_n(x_3, P_s, P_e)} - \frac{mqx_4(l/2 + x_1 + \Delta)}{kRT_s C_d C_0 w_a f_n(x_3, P_s, P_e)} - \frac{m(l/2 + x_1 + \Delta)\left[K_1(\theta_1 - x_1) + K_2(\theta_2 - x_2) + K_3(\theta_3 + \frac{K_f}{m}x_2 - \frac{A_a}{m}x_3 + \frac{A_b}{m}x_4)\right]}{kRT_s C_d C_0 w_a f_n(x_3, P_s, P_e)}$$

$$u_2 = \frac{l/2 - x_1 + \Delta}{kRT_s C_d C_0 w_b f_n(x_4, P_s, P_e)}\left[\frac{-kx_2 x_4}{l/2 - x_1 + \Delta} - qx_4\right]$$

5.4 Simplified Tracking Control Design and Simulation Results

The tracking controls (5-8) to (5-10) might be too complicated for real-time implementation, so it is desired to simplify the feedback tracking control. From the analysis of the characteristics of the function $\tilde{f}(P_r)$, we notice that the value of the function is in the interval (0, 1] and the average is around 0.75. If

the $\tilde{f}(P_r)$ function is replaced by 0.75, the controller designed in Section 5.3 can be simplified significantly. Then $0.75P_s/\sqrt{T_s}$ is used to approximate the functions $f_a(x_3,P_s,P_e)$ and $f_a(x_4,P_s,P_e)$. The approximation process is described below.

For the system using a single five-port valve, let $\tilde{C}=1/\left(0.75P_sR\sqrt{T_s}C_dC_0w(l+2\Delta)\right)$, then

$$\begin{aligned} u=&\tilde{C}x_2\left[A_ax_3(l/2+\Delta-x_1)+A_bx_4(l/2+\Delta+x_1)\right]\\ &-\tilde{C}Kem\left[(l/2+\Delta)^2-x_1^2\right]/k \end{aligned} \tag{5-11}$$

It is obviously noticed that all the denominators in controller (5-11) are constants. The controller is much simpler than the original control structure shown in Equation (5-8).

For the system using two three-port valves, let $\tilde{C}_1=1/\left(0.75P_skR\sqrt{T_s}C_dC_0w_a\right)$ and $\tilde{C}_2=1/\left(0.75P_skR\sqrt{T_s}C_dC_0w_b\right)$, then

$$u_1=\tilde{C}_1[kA_ax_2x_3-m(l/2+\Delta+x_1)qx_4-Kem(l/2+\Delta+x_1)] \tag{5-12}$$

$$u_2=\tilde{C}_2[-kx_2x_4-q(l/2+\Delta-x_1)x_4] \tag{5-13}$$

Similarly, the above controllers (5-12) and (5-13) are simpler than (5-9) and (5-10).

However, it is unknown if the simplification is reasonable. In other words, it is unknown if the controllers (5-11), (5-12) and (5-13) can give a satisfactory tracking precision. Simulation studies are carried out to compare the tracking accuracy of using controller (5-8) with the results of using controller (5-11). The

conditions specified for the simulations are:

- Cylinder: Rodless cylinder
- Stroke length: 1000mm
- Diameter of piston: 32mm
- Supply air pressure: 6 bars
- Exhaust pressure: 1 bar
- Temperature: 293K
- Payload mass: 1kg
- Static friction forces: ignored
- Viscous frictional coefficient: 15Ns/m
- Initial piston position: -0.5m
- Initial piston velocity: 0m/s
- Initial chamber pressures: 4.0 bars for both chambers
- Simulation time: 2s
- Tracking trajectory: $\theta_1(t) = -0.5\cos(0.5\pi t), 0 \le t \le 2\text{s}$

In Figure 5.1 and Figure 5.2, the simulation results using the controllers (5-8) and (5-11) are shown respectively. It is necessary to point that the simulation is conducted for the case of using a single five-port valve because it is adopted in a wider range of applications in practice.

From the simulation results shown in Figures 5.1 and 5.2, it can be observed that the approximate feedback control has a position tracking accuracy similar to the original control. The maximum error is less than 2mm, which means the relative error is less than 0.2%. But the dynamical responses are more volatile using the approximate feedback controller. In practice, the choice of feedback control must be a compromise with the tracking accuracy, smoothness of responses, and the complexity of controller structure.

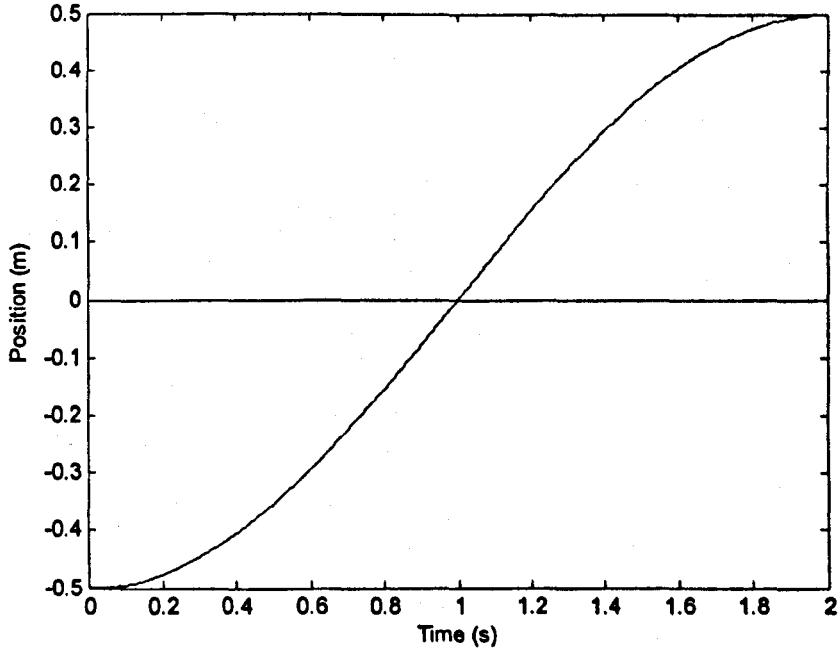

(a) Position

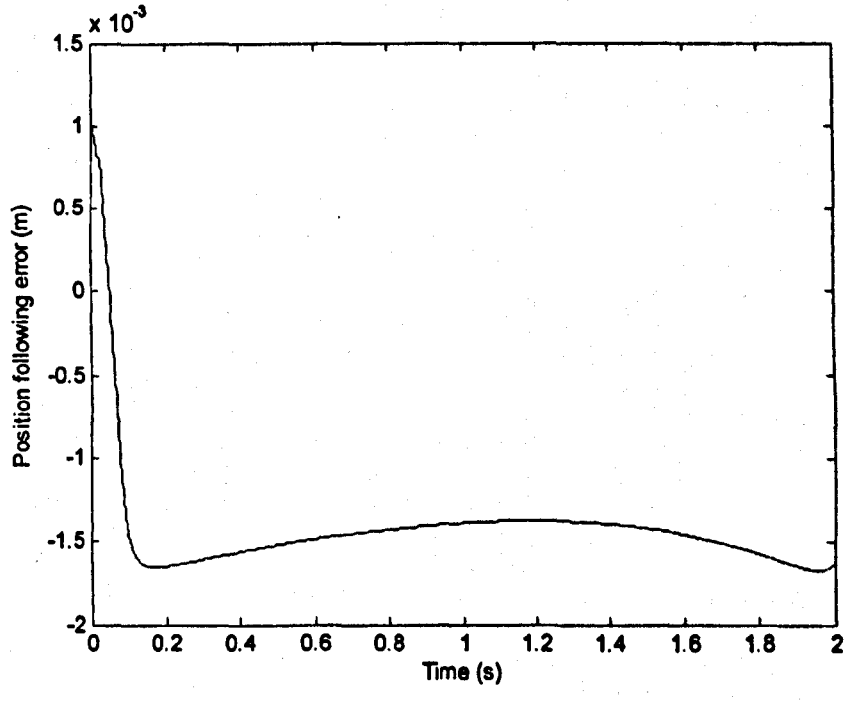

(b) Position following error

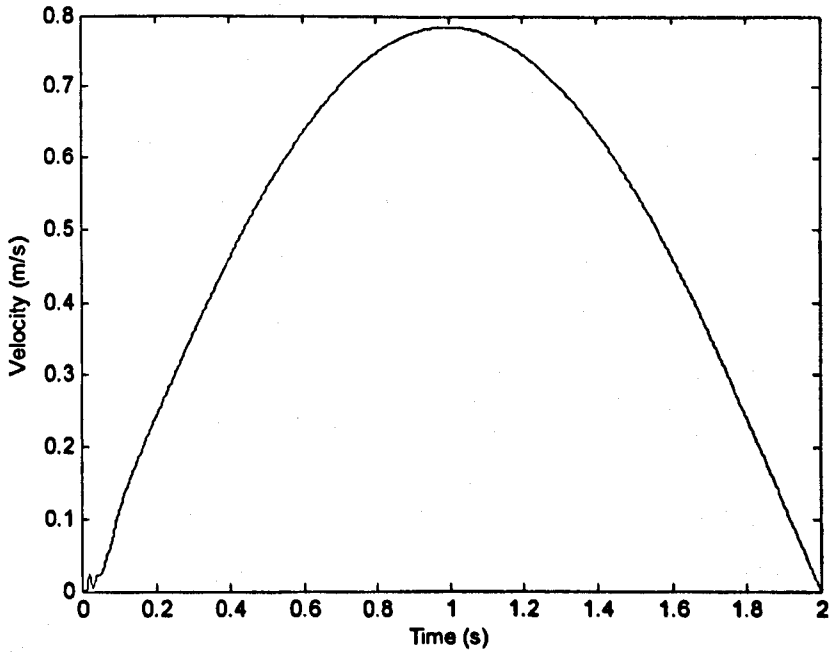

(c) Velocity

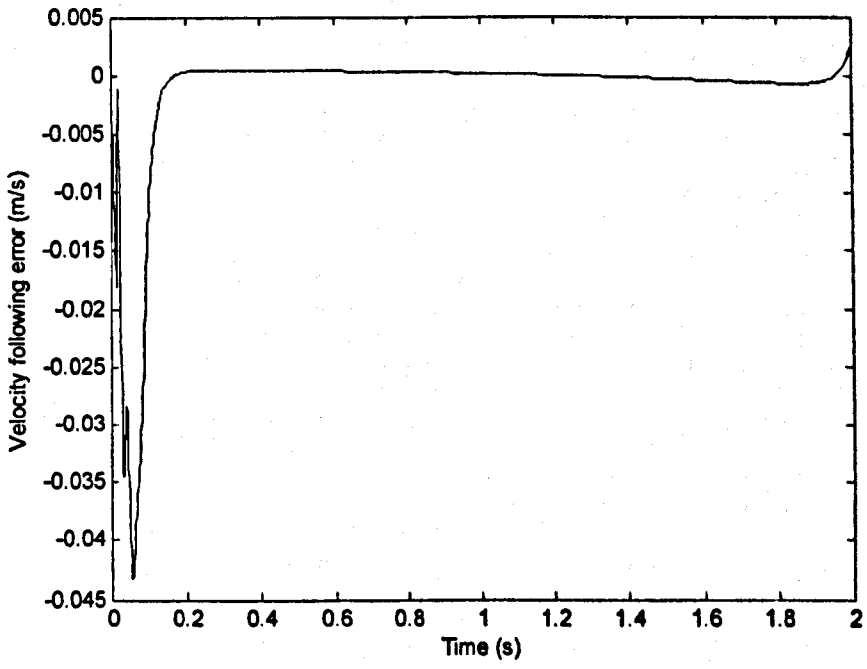

(d) Velocity following error

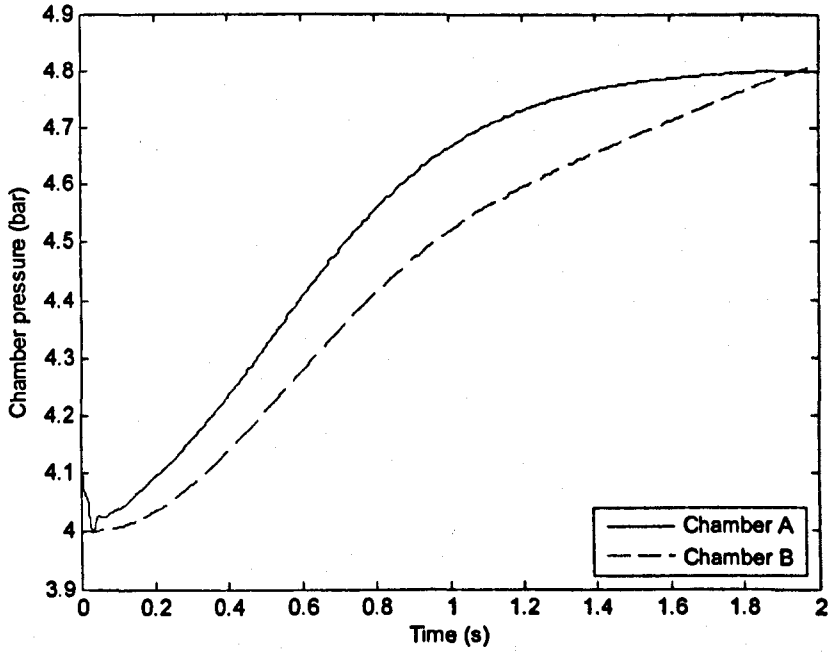

(e) Chamber pressures

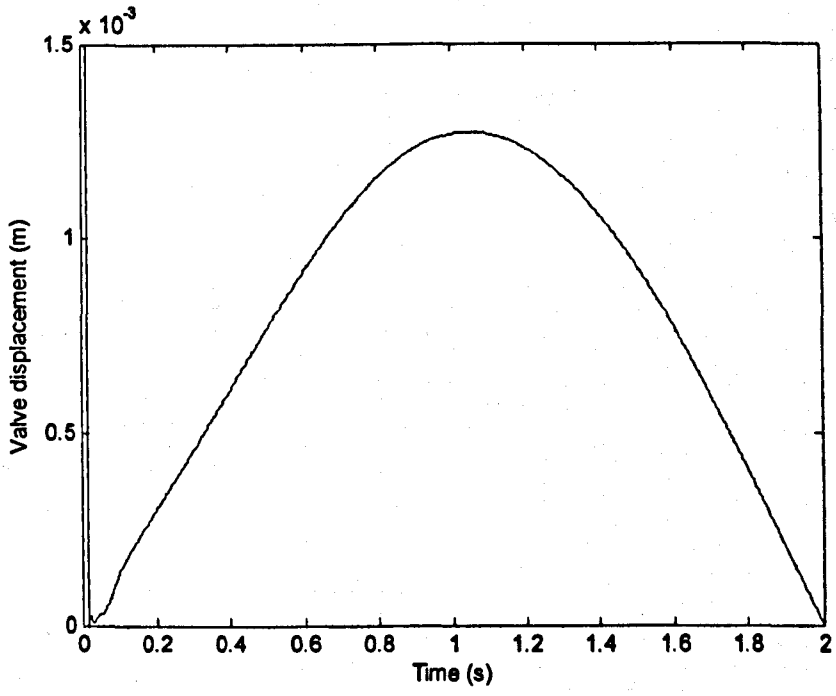

(f) Valve displacement (control input)

Figure 5.1 Simulation results using the feedback tracking control described in Equation (5-8)

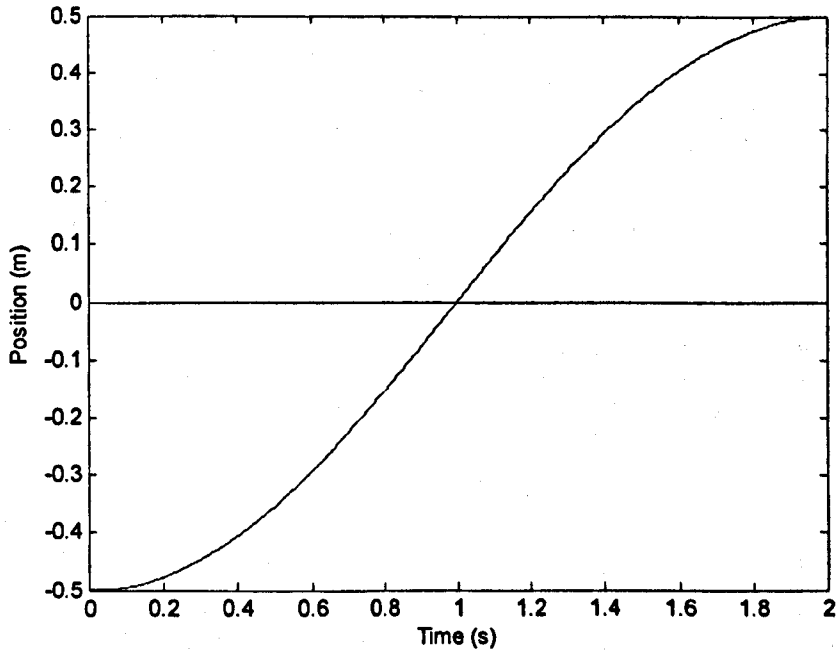

(a) Position

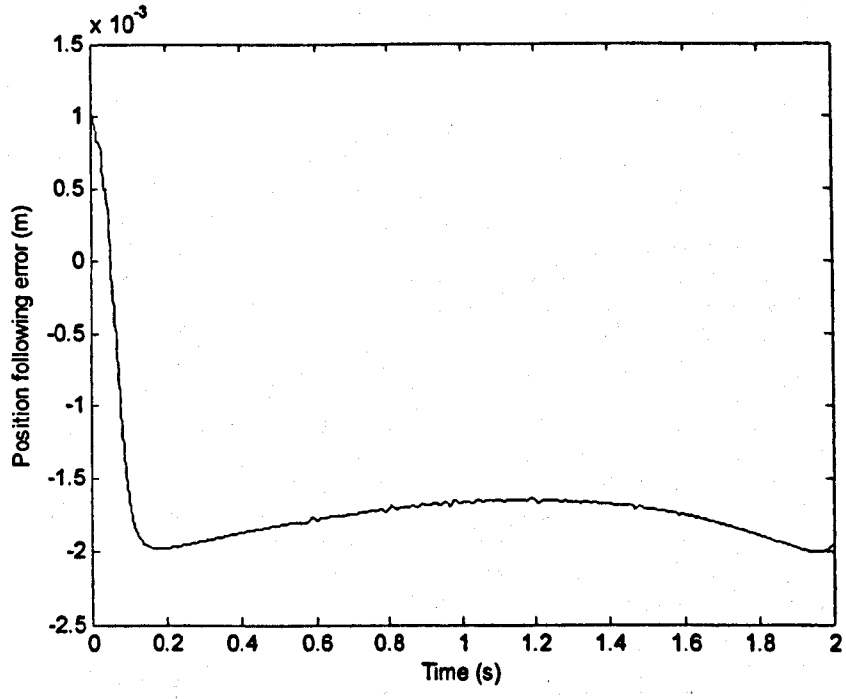

(b) Position following error

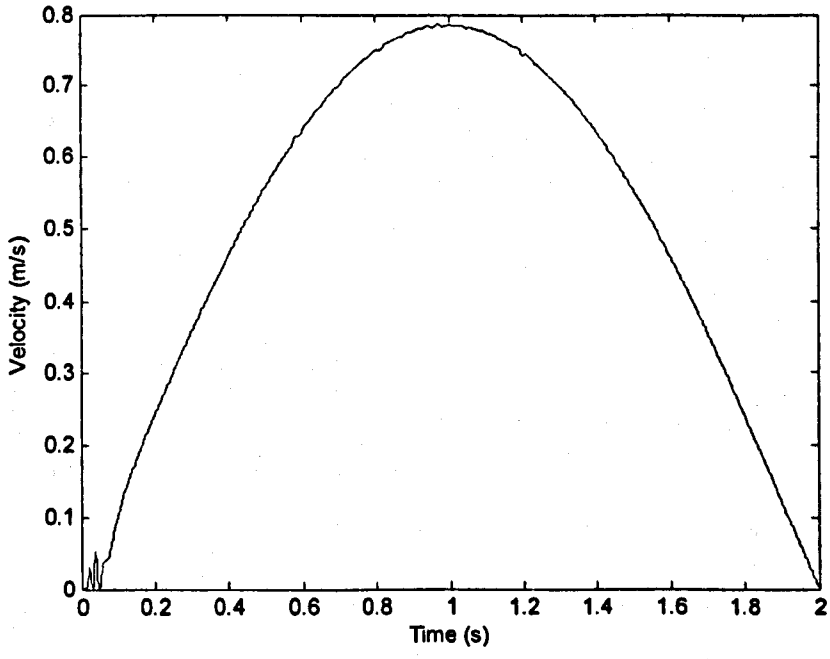

(c) Velocity

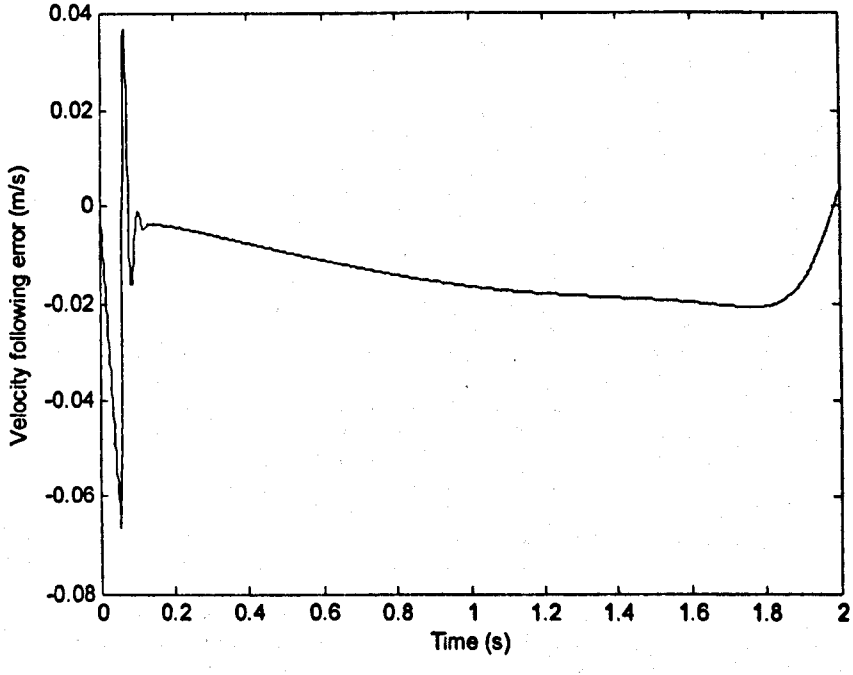

(d) Velocity following error

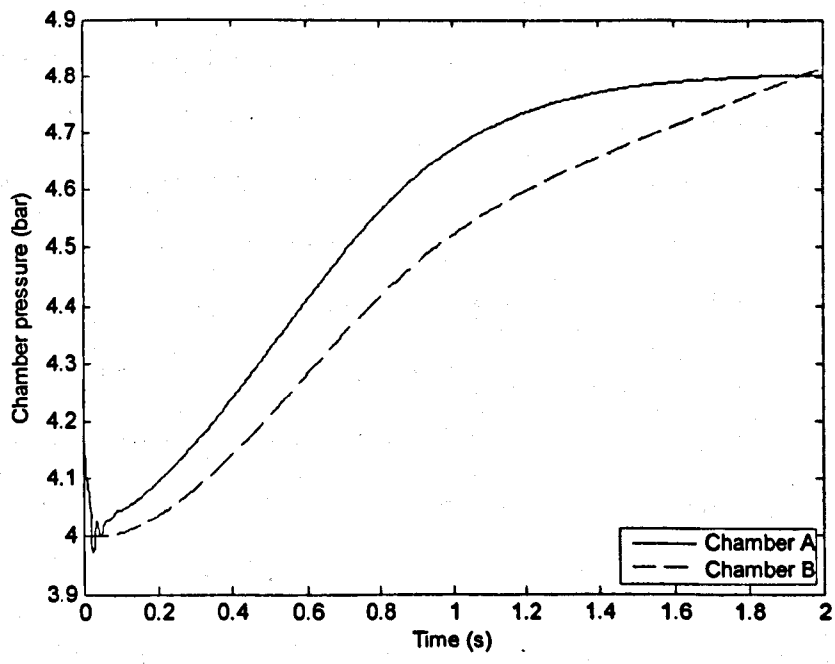

(e) Chamber pressures

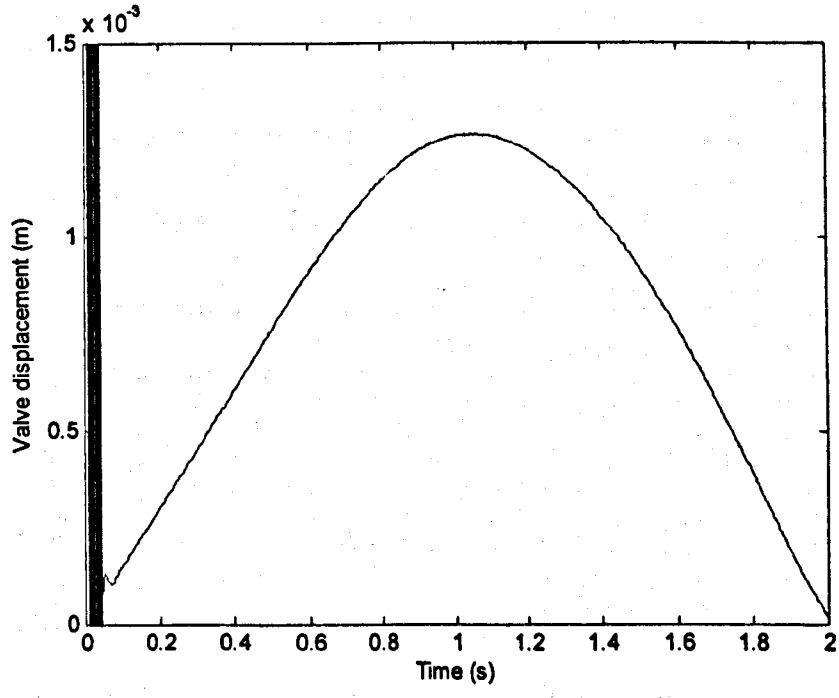

(f) Valve displacement (control input)

Figure 5.2 Simulation results using the simplified feedback tracking control described in Equation (5-11)

Both controllers described in (5-8) and (5-11) use full state feedback, which indicates that it requires measuring the position, velocity and two chamber pressures. To get all those measured information, three sensors are needed at least: position/velocity, Chamber A pressure and Chamber B pressure sensors. Generally, using three sensors in a system is not cost effective for many industrial applications. Therefore, it is necessary to simplify the controller structure further not to include the chamber pressures in state feedback. A test has been conducted to replace the chamber pressure variables by constants. In this rest, the pressures x_3 and x_4 are replaced by μP_s and ηP_s, and also, the feedback parameter $K_3 = 0$, then

$$\begin{aligned} u = {} & \tilde{C}x_2\left[A_a\mu P_s(l/2+\Delta-x_1)+A_b\eta P_s(l/2+\Delta+x_1)\right] \\ & -\tilde{C}Kem\left[(l/2+\Delta)^2-x_1^2\right]/k \end{aligned} \tag{5-14}$$

From previous simulation results, μ is chosen to be 0.78, η is chosen to be 0.75. As the test is using a rodless cylinder, $A_a = A_b = A$, then

$$u = \tilde{C}x_2A\left[(\mu+\eta)(l/2+\Delta)-(\mu-\eta)x_1\right]-\tilde{C}Kem\left[(l/2+\Delta)^2-x_1^2\right]/k \quad (5\text{-}15)$$

Generally, $(\mu-\eta)x_1$ is much smaller than $(\mu+\eta)(l/2+\Delta)$, therefore, (5-15) may be further simplified to

$$u = \tilde{C}x_2A(\mu+\eta)(l/2+\Delta)-\tilde{C}Kem\,(l/2+\Delta)^2/k+\tilde{C}Kemx_1^2/k \quad (5\text{-}16)$$

If using $\hat{K}_i$ to replace the coefficients in (5-16), the feedback tracking control law can be rewritten in this format: $u = \hat{K}_1x_2 - \hat{K}_2Ke + \hat{K}_3x_1^2Ke$ (5-17)

where $\hat{K}_1 = \tilde{C}x_2A(\mu+\eta)(l/2+\Delta)$, $\hat{K}_2 = \tilde{C}m[(l/2+\Delta)^2]/k$ and $\hat{K}_3 = \tilde{C}m/k$. The controller shown in (5-16) is simple enough to be implemented in real-time control. The simulation results are shown in Figure 5.3.

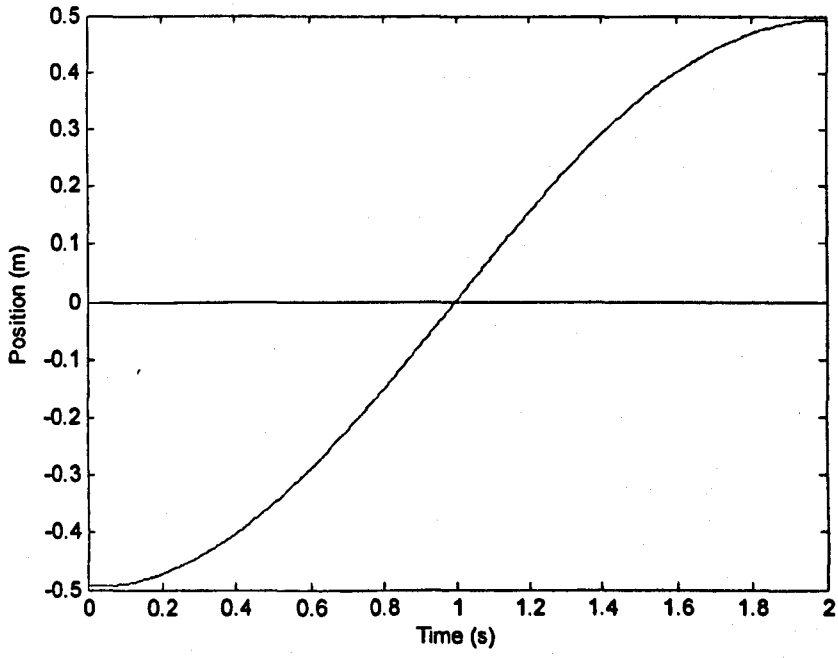

(a) Position

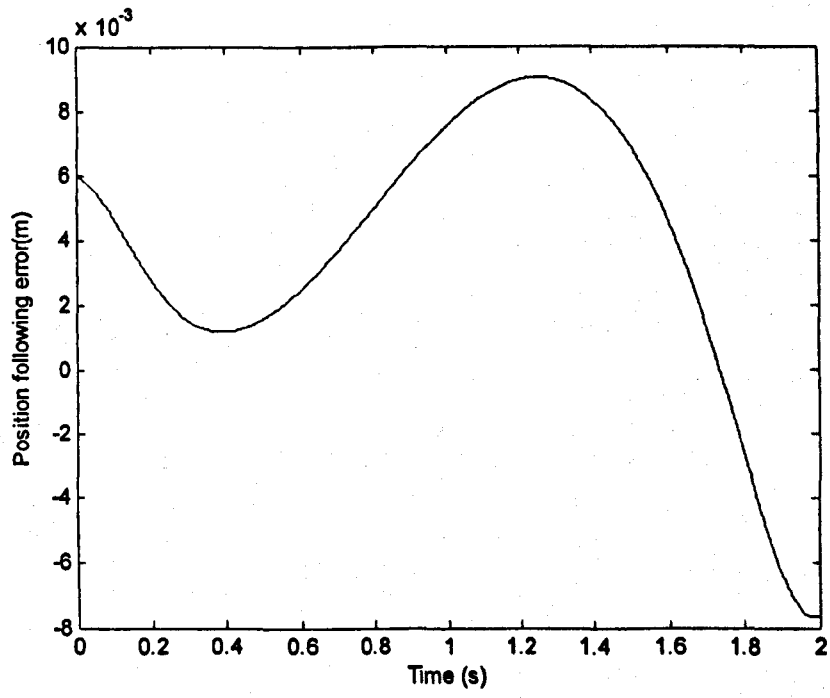

(b) Position following error

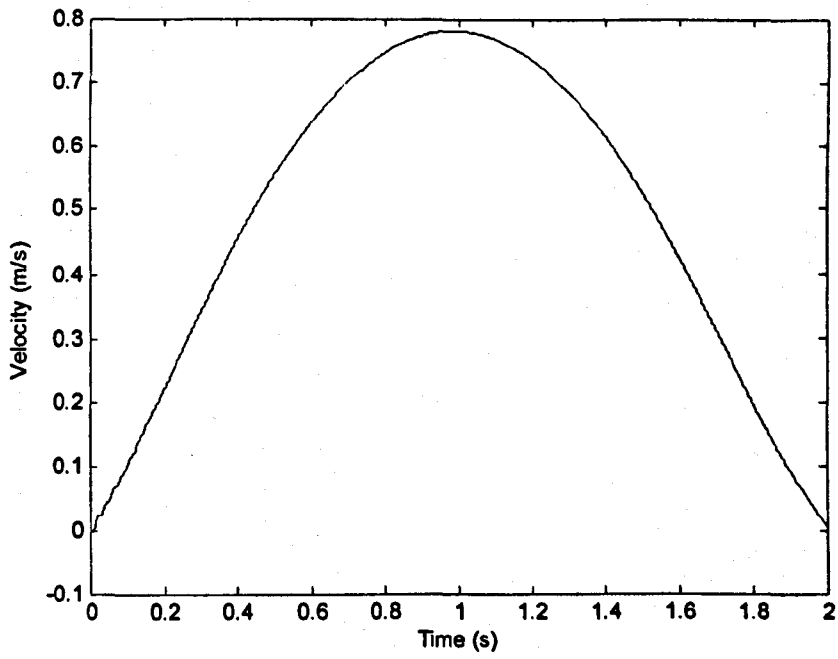

(c) Velocity

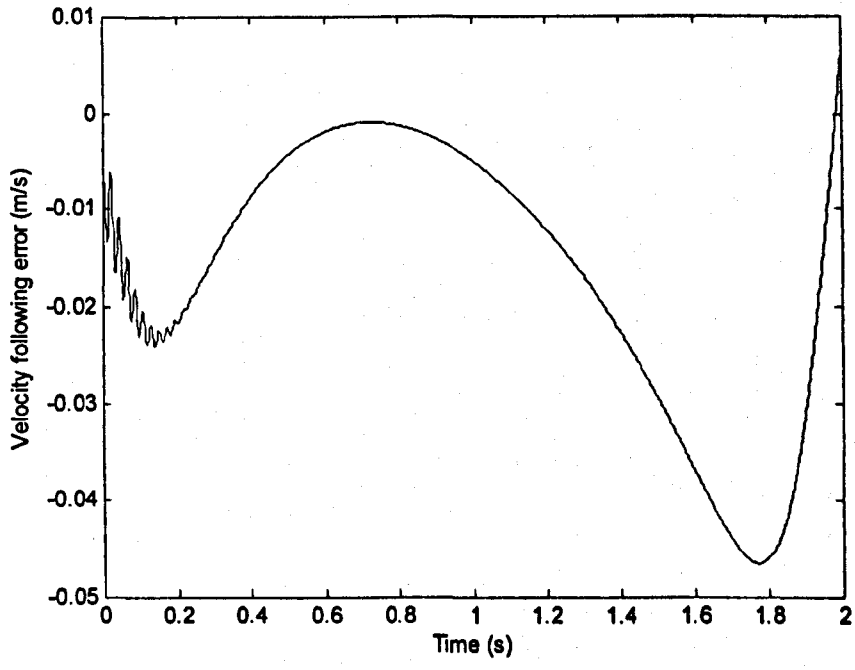

(d) Velocity following error

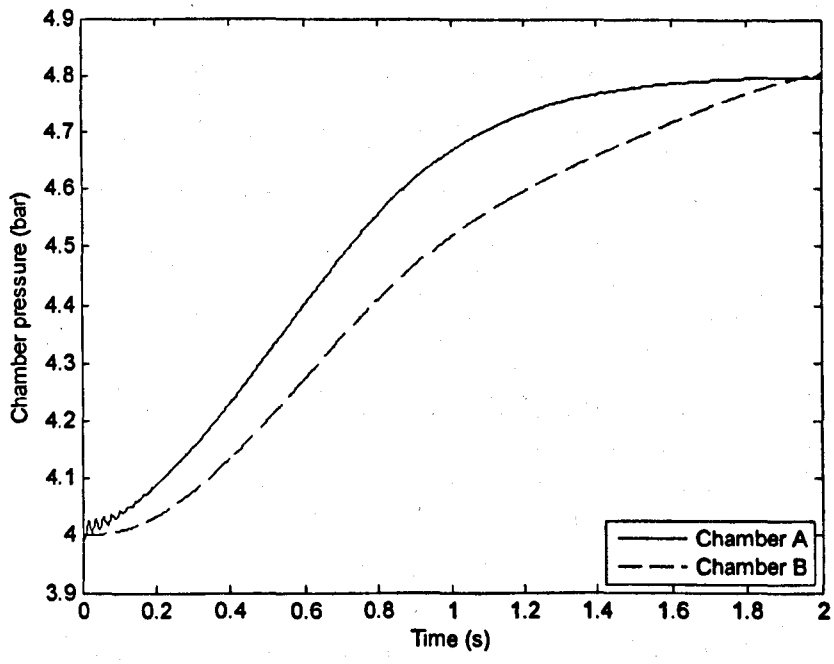

(e) Chamber pressures

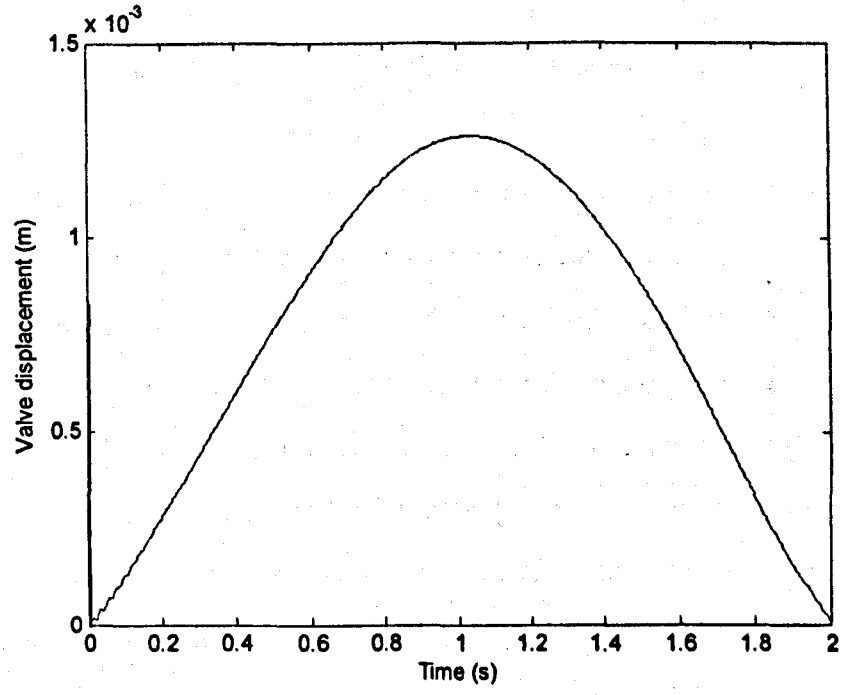

(f) Valve displacement (control input)

Figure 5.3 Simulation results using further simplified feedback tracking control described in Equation (5-16)

From the simulation results in Figure 5.3, the tracking accuracy is within ±9mm, which is acceptable comparing with the results obtained using the nonlinear feedback in (5-8). Although the starting stage of the dynamic responses is more volatile, this further approximate feedback control has the advantage of the much simpler controller structure. It is competent to be used in practice.

5.5 Feedback Control Design with Unknown Frictions

In Sections 5.3 and 5.4, the combined friction force $K_{S\text{-}C}S(x_2,x_3,x_4)$ and the load variation effects have been neglected for the convenience of analysis. When the system includes the combined static and dynamic frictions, simulation was conducted using the feedback controller (5-8) with static friction $F_S = 30\text{N}$, and Coulomb friction $F_C = 15\text{N}$. The simulation results are shown in Figure 5.4.

From Figure 5.4, it can be seen that the tracking error is over 2.2% and there is obvious time delay in velocity responses while the influence of friction forces are considered. In practice, the static friction of a cylinder has an uneven distribution along the cylinder and varies with the environment changes (Wang *et al*, 2001). Therefore, it is necessary to develop a control strategy to address the uncertain frictions and the load effects. From the practical point of view, an efficient way to overcome the static friction to lead the pneumatic system having a fast starting response is to fully open the control valve and give the maximum compressed air flow rate at the initial stage of the piston movement. From the previous simulation and experiment study (Wang *et al.*, 1999a), this method is simple but effective. A similar method is used in this chapter, which is combined with the tracking control strategy described in Section 5.4.

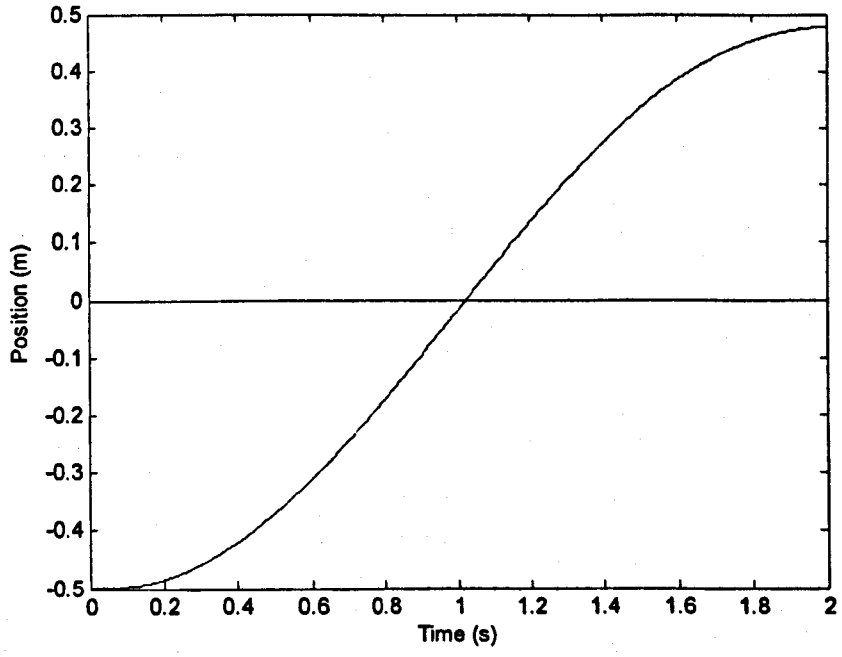

(a) Position

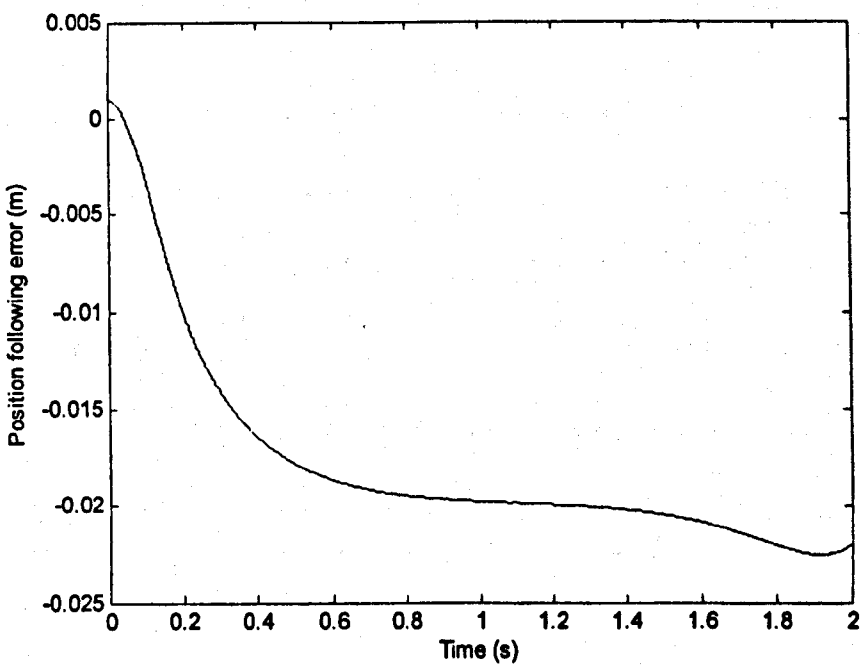

(b) Position following error

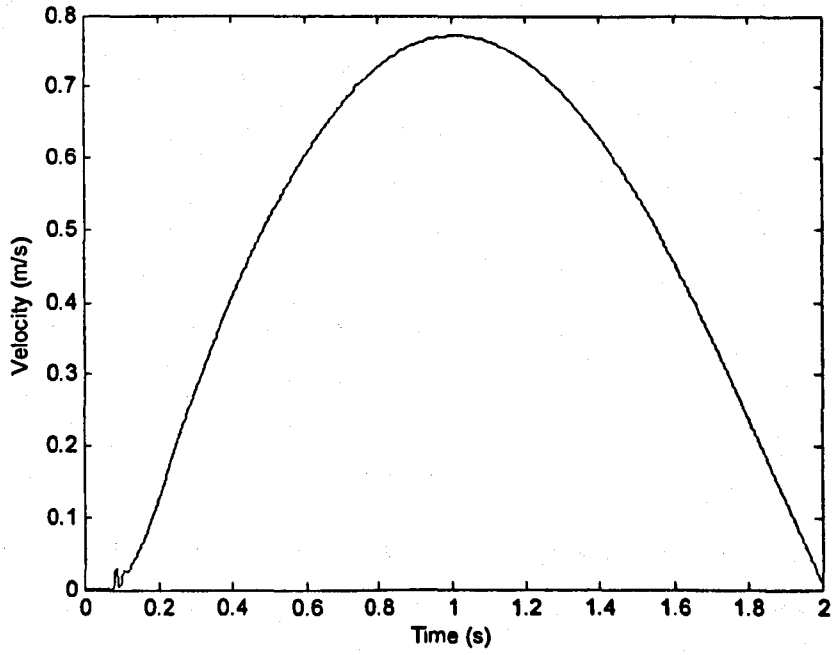

(c) Velocity

Figure 5.4 Simulation results for the system with the effects of friction force

From system equation (2-38.b), $\dot{x}_2 = \frac{1}{m}[-K_f x_2 - K_{S-C} S(x_2, x_3, x_4) + A_a x_3 - A_b x_4]$, when the piston starts moving, the static friction force is zero and only the F_C term is left in $K_{S-C} S(x_2, x_3, x_4)$. The equation (2-38.b) becomes $\dot{x}_2 = \frac{1}{m}[-K_f x_2 - F_c + A_a x_3 - A_b x_4]$, in which $\dot{x}_2$ represents the acceleration of the piston. Due to the effect of F_C, the resulted acceleration by the force $A_a x_3 - A_b x_4$ will be reduced. If the decrease in acceleration can be estimated, then the friction force F_C can be roughly obtained. Based on this idea, a friction compensation control strategy is proposed.

There are two key aspects to the control strategy:

1. To reduce time-delay caused by static friction: When the piston velocity is

zero and $A_a x_3 - A_b x_4$ is less than F_S, the piston stands still. During this period, the valve is set to open fully, that is, u is set to have the maximum positive/negative valve displacement, which will replace the tracking control described in Section 5.3 or 5.4.

2. To reduce the tracking errors caused by the friction term or variable load that is proportional to Coulomb friction F_C: Suppose that the friction force $F_C = 0$. Then the estimated acceleration would be $\hat{a} = \frac{1}{m}[-K_f x_2 + A_a x_3 - A_b x_4]$. In fact, the measured acceleration of the piston is assuming to be represented by $\tilde{a}$. The relative difference of acceleration between the measured and estimated values can be expressed by $a_{er} = (\tilde{a} - \hat{a})/\hat{a}$. This difference will be used to amend the tracking control law. The amendment of tracking control law should also use the information of position tracking error, that is, the difference of the desired and measured positions, e_1. The proposed update tracking control law is $u^* = u(1 + \kappa a_{er} e_1 / x_{1max})$, where u is the tracking control law obtained in Section 5.3 or 5.4, x_{1max} is the absolute value of the maximum piston position, and κ is a parameter of updating rate, which will be determined through simulation or experiment test.

Using the same pneumatic cylinder system described in Section 5.4, adopting the tracking control strategy proposed above, with the tracking control law described in (5-8), the simulation results are shown in Figure 5.5, in which x_{1max}=0.5m, κ is chosen to be 100. In Figure 5.5, the static friction and Coulomb friction are considered, which are $F_S = 60\text{N}$, $F_C = 30\text{N}$.

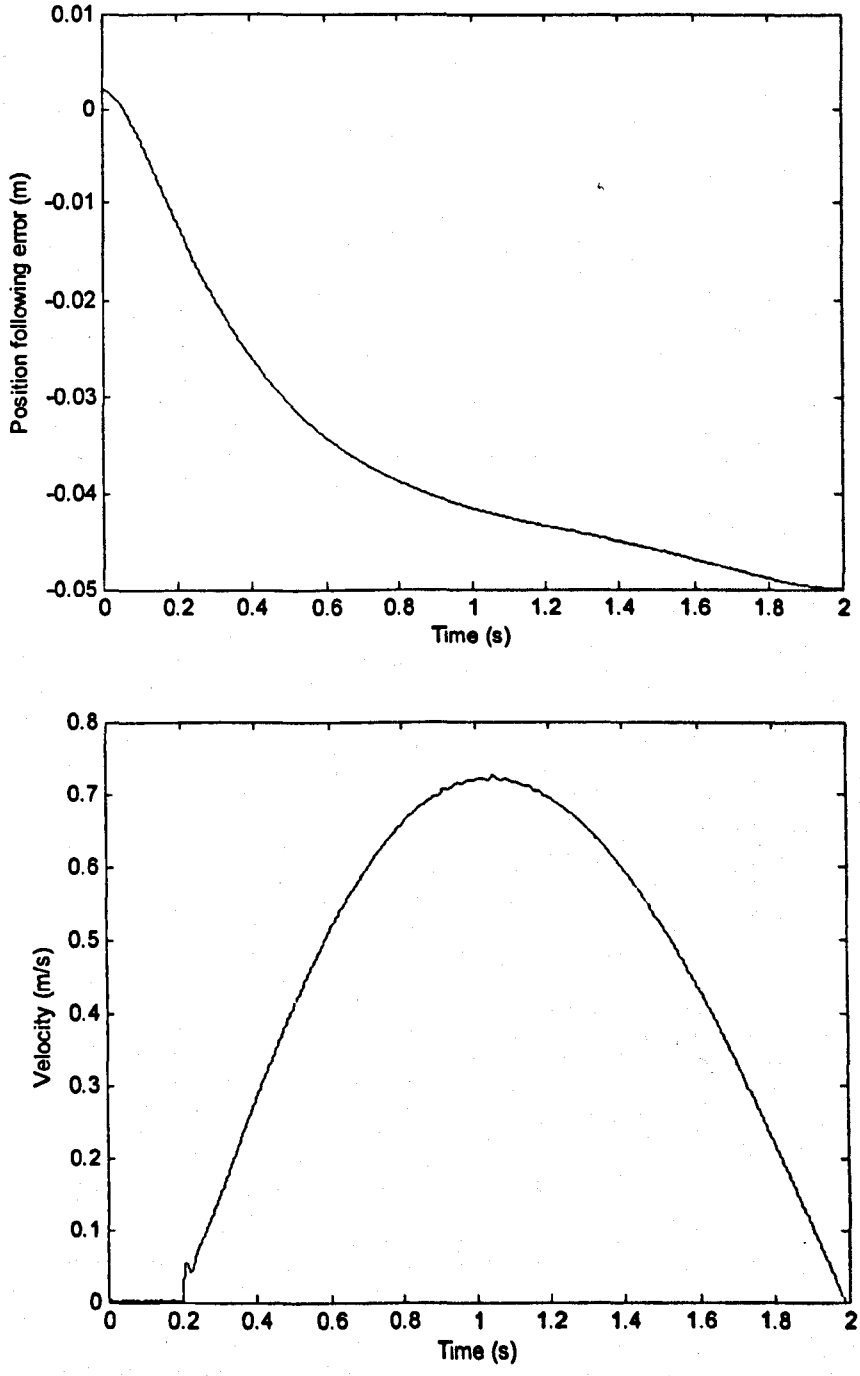

(a) Simulation results using the control strategy described by (5-8)

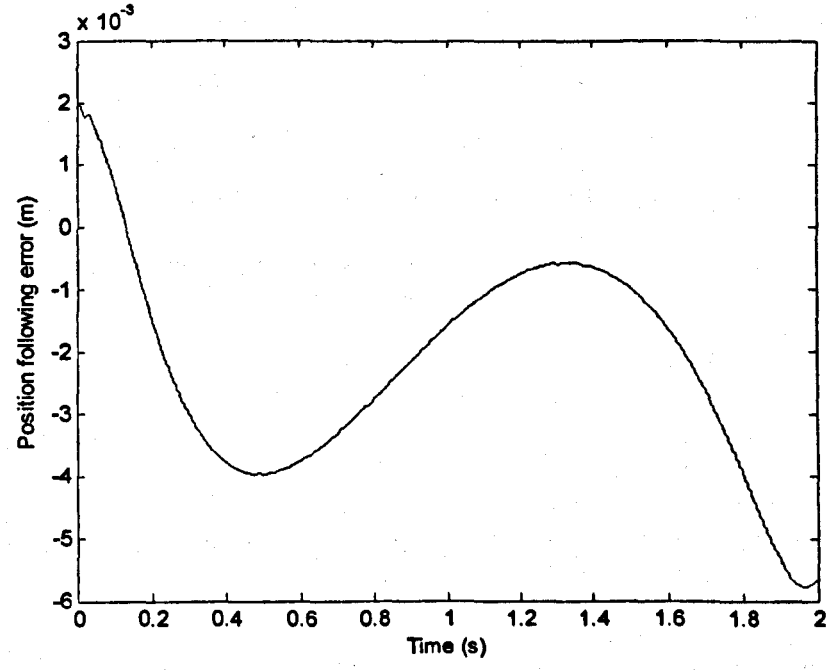

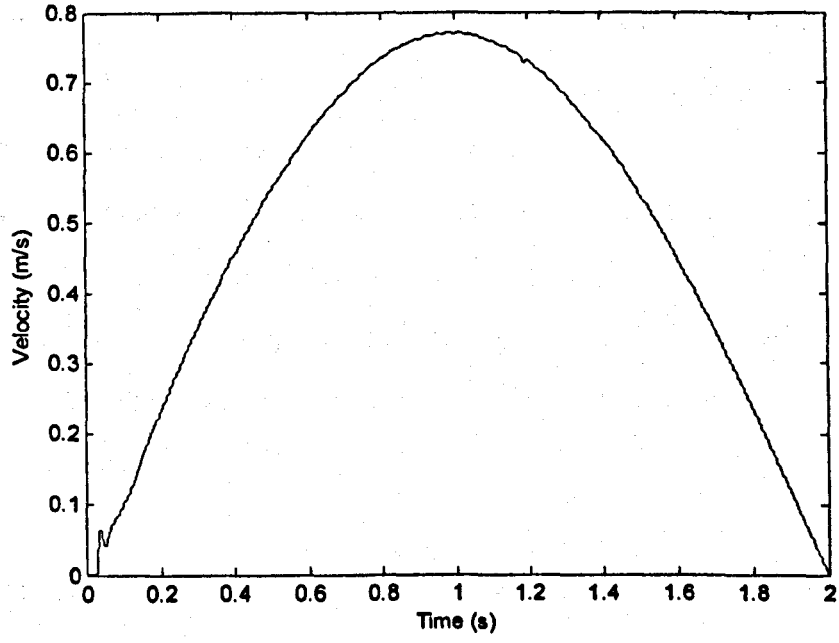

(b) Simulation results using enhanced control strategy to address the static frictions

Figure 5.5 Simulation results for the system with the friction forces $F_s = 60\text{N}$ and $F_c = 30\text{N}$

From Figure 5.5, the time-delay in the velocity responses and the position tracking errors are reduced dramatically when the enhanced control strategy is applied to address the problems caused by the friction forces. These results indicate that the control strategy described in this section is competent to overcome the influence of friction forces.

5.6 Summary

In this chapter, the nonlinear pneumatic cylinder actuating system is initially linearised via input/output feedback linearisation. Two cases are discussed respectively: the system using a single five-port valve and two three-port valves. Based on the linearised model, a feedback tracking control is proposed using well developed linear control theory. Then the feedback control is transformed back to the nonlinear state space. For the convenience of analysis, the static friction is ignored initially and treated as an uncertainty in the Section 5.5. However, the resulting nonlinear feedback control is too complicated for the purpose of real-time implementation, so simplification has been done. Simulation results have shown that the simplified control satisfies the desired tracking accuracy.

When the static friction and Coulomb friction are added into the system, two problems emerge: large tracking error and time delay in dynamic response. To address the problems caused by the friction forces, an enhanced tracking control strategy is proposed, which is based on a simple idea, that is, to compare the measured acceleration with the estimated acceleration under the condition without friction's influence. The estimated value is then used to amend the

control strategy proposed under the condition that the friction forces are ignored. The main advantage of the method proposed is that it has a clear theoretic guidance at the initial stage of controller design and leads to a tracking control strategy with a simple structure.

Since the optimal energy efficient profiles have been found (refer to Chapter 4) and the practical tracking control strategy has been designed, users of pneumatic cylinders can simply use tracking control technology to follow the optimal profiles to improve the energy efficiency of the pneumatic cylinder systems. However, to improve the energy efficiency of pneumatic cylinder systems, an idea to innovate the geometrical structure of the pneumatic cylinder has been emerged and Chapter 6 will present this idea.

Chapter 6

An Energy Efficient Pneumatic Cylinder

6.1 Introduction

The work described in the previous chapters is to improve system energy efficiency through better control and optimisation of velocity profiles. They are limited only to servo-pneumatic systems. For general positioning applications, an effort has been made in this chapter to identify if it is possible to improve the energy efficiency of pneumatic actuators with modification of its mechanical structure. A new cylinder mechanical structure is proposed in this chapter with the hope of improving energy efficiency of pneumatic actuator systems.

This chapter starts from the description of the mechanical structure of the new cylinder and explains why the cylinder with the new structure can provide high energy efficiency compared with conventional cylinders. A mathematical model of the new cylinder is developed in this chapter and a number of design restrictions were derived which can be used as useful design guidance for manufactures. Simulation studies were carried out for the cylinder with different sets of design parameters. The simulation results reveal that the new cylinder uses much less compressed air compared with conventional cylinders for doing

the same job, and energy efficiency can be improved significantly. Also, the simulation study shows that the cylinder has faster responses because it requires less time to charge the smaller chamber volume. Therefore, the new cylinder has an advantage of higher timing efficiency as well.

6.2. Description of the New Pneumatic Cylinder

The new design of the pneumatic cylinder applies for both rodded and rodless cylinders. To simplify the analysis, the rodless cylinder is used as an example. A conventional rodless cylinder has the structure shown in Figure 6.1.

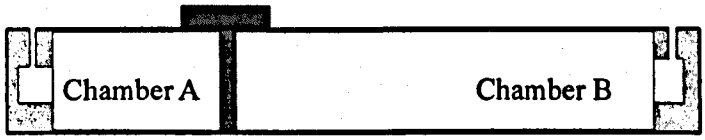

Figure 6.1 Structure of a rodless conventional cylinder

For a pneumatic cylinder, the force acting on the piston can be calculated by

$F = P_a A_a - P_b A_b$, when Chamber A is the driving chamber, or

$F = P_b A_b - P_a A_a$, when Chamber B is the driving chamber,

where F represents the acting force, P_a, P_b represent the pressures in Chambers A and B, respectively, and A_a, A_b are the effective piston areas for Chambers A and B. Therefore, the acting force can be strengthened by either increasing the driving chamber pressure or driving chamber piston area. When the piston area increases, the chamber volumes will be increased accordingly. However, the increased chamber volumes need more compressed air to achieve the required

chamber pressures. So it will accumulate more compressed air in the downstream chamber which will be exhausted and wasted, and then this will result in low energy efficiency.

The proposed new pneumatic actuator has a flexible, stretchable corrugated conduit inside each cylinder chamber as shown in Figure 6.2. The conduits could be manufactured from rubber or a synthetic elastomer. Certainly, the choice of suitable materials is still a challenging topic for implementation of the idea. The main feature of the design is that the chamber volumes are smaller compared to those of conventional actuators with the same piston area. This means less compressed air is needed to build up the required chamber pressure, yet it can provide the same acting force. Furthermore, the pleats of the conduit close together as the piston approaches either end of the cylinder, providing a natural shock absorber.

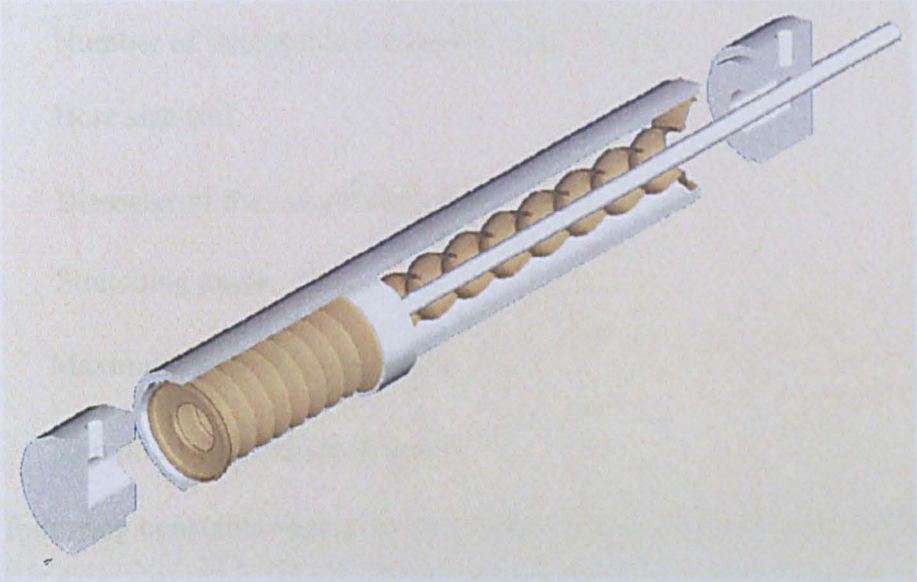

Figure 6.2 Cross section schematic of the new design cylinder

6.3 Mathematical Model of the Novel Pneumatic Cylinder

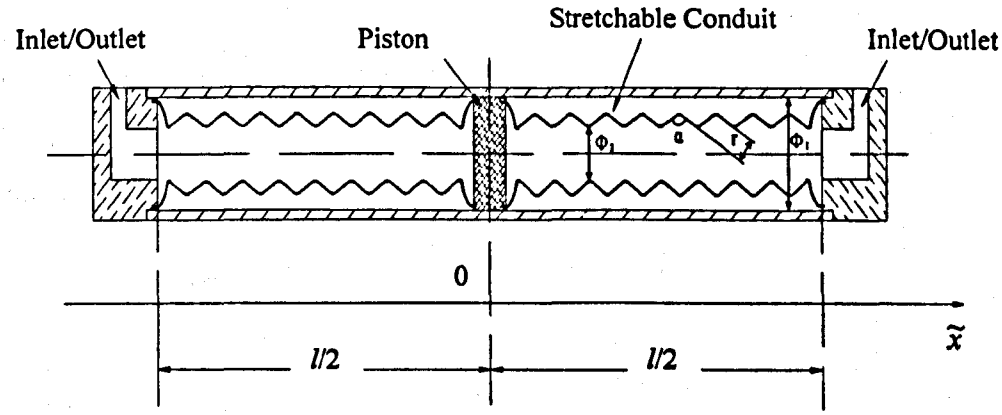

Figure 6.3 Structure of the new design for a rodless cylinder

As mentioned in Section 6.2, the rodless cylinder is chosen as an example for analysis with the coordinate system as shown in Figure 6.3. Universal symbols used throughout the thesis can be found in Nomenclature at the very beginning of the thesis and the specific symbols used through this chapter are listed below:

N Number of stretchable triangles for half a stroke

$\hat{\phi}_1$ Bore size (m)

$\hat{\phi}_2$ Diameter of the inner tube (m)

α Stretching angle (°)

α_{max} Maximum s tretching angle (°)

γ Length of the triangle side (m)

The following constants appear in the system model, which are same as those in Chapter 2:

$k=1.4$, $T_s=293\text{K}$, $C_d=0.8$, $P_s=6\times10^5\text{N/m}^2$, $P_e=1\times10^5\text{N/m}^2$,

$$C_r = \left(\frac{2}{k+1}\right)^{\frac{k}{k-1}} = 0.528, R = 287\frac{\mathrm{J}}{\mathrm{K}\cdot\mathrm{kg}} \text{ and } C_k = \sqrt{\frac{2}{k-1}\left(\frac{k+1}{2}\right)^{\frac{k+1}{k-1}}} = 3.864.$$

Figure 6.4 (a) shows the particular connection of the inner tube to the piston and Figure 6.4 (b) shows the schematic of a typical stretchable triangle taking out the inner tube.

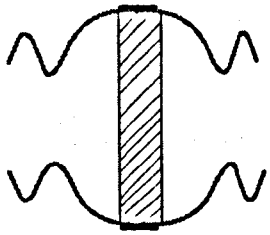

(a) Connection of the inner tube to the piston

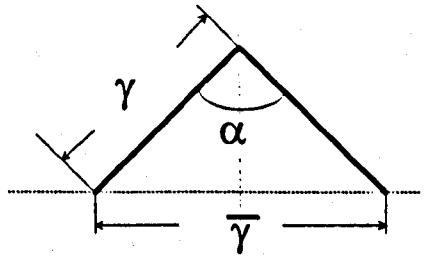

(b) A typical stretc hable triangle

Figure 6.4 Typical structure part of the new cylinder

From Figure 6.4(b) and the principle of trigonometry,

$$\sin(\alpha_{max}/2) = \frac{\bar{\gamma}/2}{2} = \frac{\bar{\gamma}_{max}}{2\gamma}$$

thus $\bar{\gamma} = 2\gamma\sin(\alpha_{max}/2)$ and $\bar{\gamma}_{max} = 2\gamma\sin(\alpha_{max}/2)$

Since the maximum stretchable length must not be longer than the stroke length,

$$l = N\cdot\gamma_{max} = 2N\gamma\sin(\alpha_{max}/2)$$

Therefore, the minimum number of stretchable triangles can be found as

$$N_{min} \geq \frac{l}{2\gamma\sin(\alpha_{max}/2)} \qquad (6\text{-}1)$$

From the geometry of the cylinder, the relationship between the bore size and inner corrugated conduit size must satisfy

$$\hat{\phi}_1 \geq 2\gamma + \hat{\phi}_2 \tag{6-2}$$

Then, $\gamma \leq \dfrac{\hat{\phi}_1 - \hat{\phi}_2}{2}$

The volume of Chamber A can be calculated by

$$\begin{aligned} V_a = {} & \frac{\pi(l/2+x)^3}{12N^2}\tan^2\left[\cos^{-1}\left(\frac{l/2+x}{2N\gamma}\right)\right] + \frac{\pi(l/2+x)^2\hat{\phi}_2}{4N} \\ & \times\tan\left[\cos^{-1}\left(\frac{l/2+x}{2N\gamma}\right)\right] + \frac{\pi}{4}\hat{\phi}_2^2(l/2+x) \end{aligned} \tag{6-3}$$

And the volume of Chamber B can be calculated by

$$\begin{aligned} V_b = {} & \frac{\pi(l/2-x)^3}{12N^2}\tan^2\left[\cos^{-1}\left(\frac{l/2-x}{2N\gamma}\right)\right] + \frac{\pi(l/2-x)^2\hat{\phi}_2}{4N} \\ & \times\tan\left[\cos^{-1}\left(\frac{l/2-x}{2N\gamma}\right)\right] + \frac{\pi}{4}\hat{\phi}_2^2(l/2-x) \end{aligned} \tag{6-4}$$

With the chamber volume described by Equations (6-3) and (6-4), the complete system model from the proportional flow control valve to the cylinder payload can be derived (Wang *et al.*, 1998 and 2001). The system model of the new design of the cylinder is

$$\begin{cases} \dot{x}_1 = x_2 \\ \dot{x}_2 = \dfrac{1}{m}[-K_f x_2 - K_{S\text{-}C}S(x_2,x_3,x_4) + A_a x_3 - A_b x_4] \\ \dot{x}_3 = -\dfrac{k\dot{V}_a x_3}{V_a+\Delta} + \dfrac{kRT_s C_d C_0 w_a f_n(x_3,P_s,P_e)u_1}{V_a+\Delta} \\ \dot{x}_4 = -\dfrac{k\dot{V}_b x_4}{V_b+\Delta} + \dfrac{kRT_s C_d C_0 w_b f_n(x_4,P_s,P_e)u_2}{V_b+\Delta} \end{cases} \tag{6-5}$$

where x_1 denotes the piston position, x_2 denotes the piston velocity, x_3 and x_4 represent the pressures of Chamber A and Chamber B, while u_1 and u_2

are the spool displacements of the two control valves. The functions $f_n(x_3,P_s,P_e)$, $f_n(x_4,P_s,P_e)$ and $K_{S-C}S(x_2,x_3,x_4)$ in system (6-5) are defined as Equation (2-33), (2-34) and (2-39) in Chapter 2, respectively.

In the system (6-5), the derivatives of chamber volumes can be calculated as (6-10) and (6-11).

$$\dot{V}_a = x_2 \cdot \left\{ \frac{\pi}{12N^3\gamma} \cdot \frac{\left(\frac{l}{2}+x_1\right)^3}{\sqrt{1-\left(\frac{l/2+x_1}{2N\gamma}\right)^2}} \cdot \tan\left[\cos^{-1}\left(\frac{\frac{l}{2}+x_1}{2N\gamma}\right)\right] \cdot \left\{1+\tan^2\left[\cos^{-1}\left(\frac{\frac{l}{2}+x_1}{2N\gamma}\right)\right]\right\} \right.$$
$$+\frac{\pi}{4N^2}\cdot\left(\frac{l}{2}+x_1\right)^2 \cdot \tan^2\left[\cos^{-1}\left(\frac{\frac{l}{2}+x_1}{2N\gamma}\right)\right] \frac{\pi}{8N^2\gamma}\cdot\hat{\phi}_2 \cdot \frac{\left(\frac{l}{2}+x_1\right)^2}{\sqrt{1-(\frac{l/2+x_1}{2N\gamma})^2}} \qquad (6\text{-}10)$$
$$\left. \cdot\left\{1+\tan^2\left[\cos^{-1}\left(\frac{\frac{l}{2}+x_1}{2N\gamma}\right)\right]\right\} + \frac{\pi}{2N}\cdot\hat{\phi}_2\cdot\left(\frac{l}{2}+x_1\right)\cdot\tan\left[\cos^{-1}\left(\frac{\frac{l}{2}+x_1}{2N\gamma}\right)\right] + \frac{\pi}{4}\cdot\hat{\phi}_2^2 \right\}$$

$$\dot{V}_b = x_2 \cdot \left\{ \frac{\pi}{12N^3\gamma} \cdot \frac{\left(\frac{l}{2}-x_1\right)^3}{\sqrt{1-\left(\frac{l/2-x_1}{2N\gamma}\right)^2}} \cdot \tan\left[\cos^{-1}\left(\frac{\frac{l}{2}-x_1}{2N\gamma}\right)\right] \cdot \left\{1+\tan^2\left[\cos^{-1}\left(\frac{\frac{l}{2}-x_1}{2N\gamma}\right)\right]\right\} \right.$$
$$\frac{\pi}{4N^2}\cdot\left(\frac{l}{2}-x_1\right)^2 \cdot \tan^2\left[\cos^{-1}\left(\frac{\frac{l}{2}-x_1}{2N\gamma}\right)\right] + \frac{\pi}{8N^2\gamma}\cdot\hat{\phi}_2 \cdot \frac{\left(\frac{l}{2}-x_1\right)^2}{\sqrt{1-\left(\frac{l/2-x_1}{2N\gamma}\right)^2}} \qquad (6\text{-}11)$$
$$\left. \cdot\left\{1+\tan^2\left[\cos^{-1}\left(\frac{\frac{l}{2}-x_1}{2N\gamma}\right)\right]\right\} - \frac{\pi}{2N}\cdot\hat{\phi}_2\cdot\left(\frac{l}{2}-x_1\right)\cdot\tan\left[\cos^{-1}\left(\frac{\frac{l}{2}-x_1}{2N\gamma}\right)\right] - \frac{\pi}{4}\cdot\hat{\phi}_2^2 \right\}$$

6.4 Dynamic Characteristics of the New Cylinder

To investigate the dynamic characteristics of the new cylinder, simulation studies are conducted and the results are presented in this section. The conditions specified for the simulations are:

- Cylinder: Rodless cylinder
- Stroke length: 0.6m
- Bore size: 0.06m
- Diameter of the inner tube: 0.025m
- Length of the triangle side: 0.016m
- Number of stretchable triangles for half a stroke: 22
- Supply air pressure: 6 bars
- Exhaust pressure: 1 bar
- Temperature: 293K
- Payload mass: 1kg
- Static friction forces: ignored
- Viscous frictional coefficient: 15Ns/m
- Initial piston position: -0.3m
- Initial piston velocity: 0m/s
- Initial chamber pressures: 3.5 bars for both chambers
- Simulation time: 1s

The control inputs are selected as $u_1 = 0.00055\text{m}, u_2 = -0.00055\text{m}$, which are about one tenth of the full opening valve displacement. The simulation results of step input responses are shown in Figure 6.5.

From Figure 6.5, it can be seen that the stabilised velocity increases when the piston is close to the end of the stroke. This is because the equivalent diameter

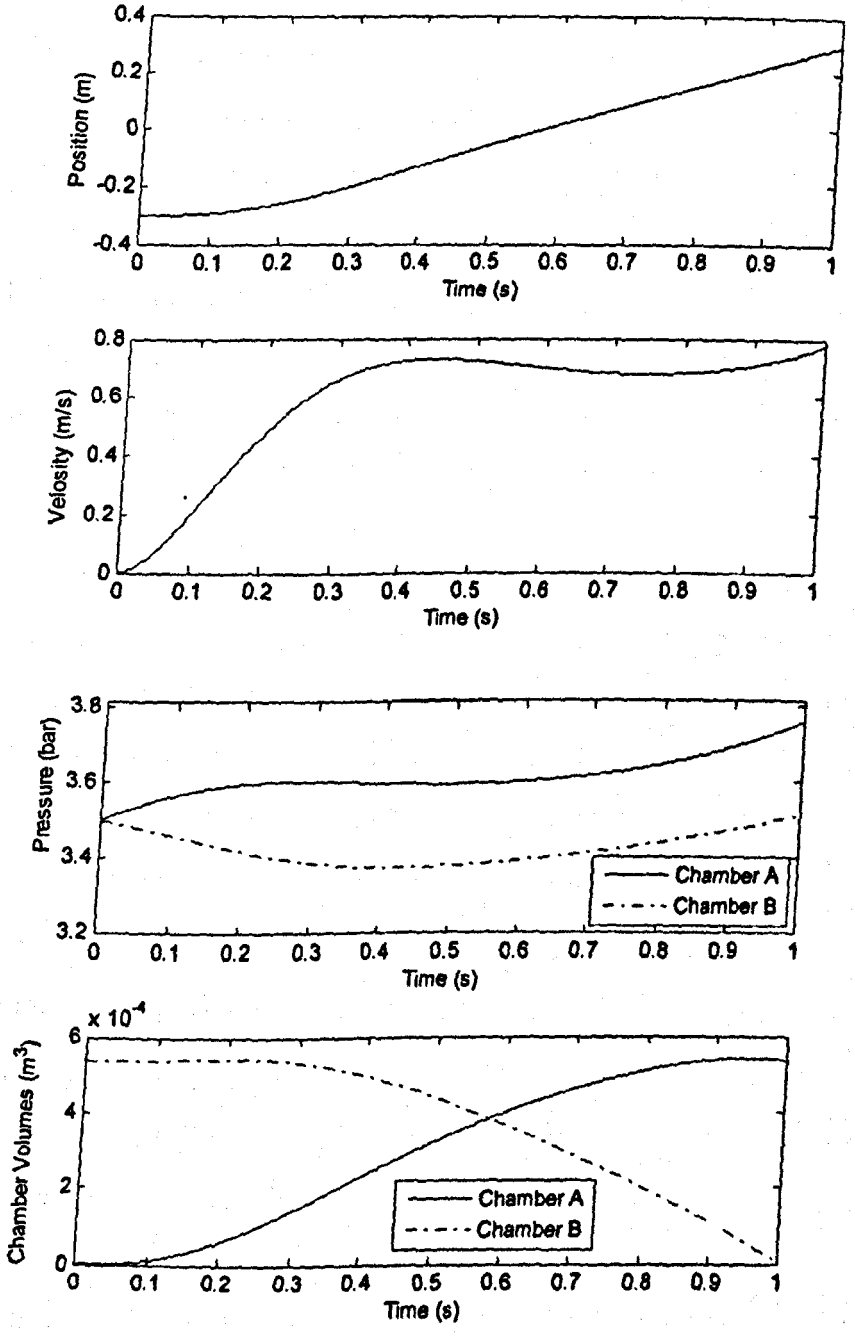

Figure 6.5 Dynamic responses of the new cylinder with a step input

of the driving chamber is getting smaller and smaller as the flexible stretchable corrugated conduit becomes thinner with movement of the piston. The

variations of chamber volumes with respect to the piston position are shown in the bottom of Figure 6.5. It is clearly seen that the volume changes is not linear, which indicates that the new cylinder is more difficult to be controlled to have a stable response. Even for open-loop control of the new cylinder, valve opening characteristics need to be designed carefully to achieve a "soft-landing" at the end of piston movement. Although the new cylinder may be more difficult to control for a stable velocity response, the new cylinder has a fast response as it requires less compressed air to build up the chamber pressures demanded by the acting forces compared with conventional cylinders.

Simulation work also has been done to investigate the effect of different parameters to the dynamic responses of the new cylinder with open-loop control. In Figures 6.6 to 6.8, the dynamic responses are shown with different initial chamber pressures P_{0a}, P_{0b}, different air supply pressure P_s, and different numbers of stretchable triangles in half stroke N, respectively. There are three groups of dynamic responses in Figure 6.6 with different initial chamber pressures, 2.0, 3.5 and 5 bars, where both chambers have the same initial pressures, $P_{0a} = P_{0b}$. From Figure 6.6, it can be seen that when the cylinder has smaller initial chamber pressures, the piston can go faster, and then the terminal piston velocity is bigger, which is not easy to control. This phenomenon not only exists in the novel cylinder, but also exists in conventional pneumatic cylinder systems, because the compressed air supply has more potential power when it flows into a chamber with lower pressure. Furthermore, when the initial chamber pressures are fixed, different air supply pressures are applied on the cylinder, results show in Figure 6.7 with P_s=6, 8, 10 bars, respectively. From Figure 6.7, it can be easily seen that the higher the air supply pressure, the faster the piston velocity, which is consistent with the industrial common sense.

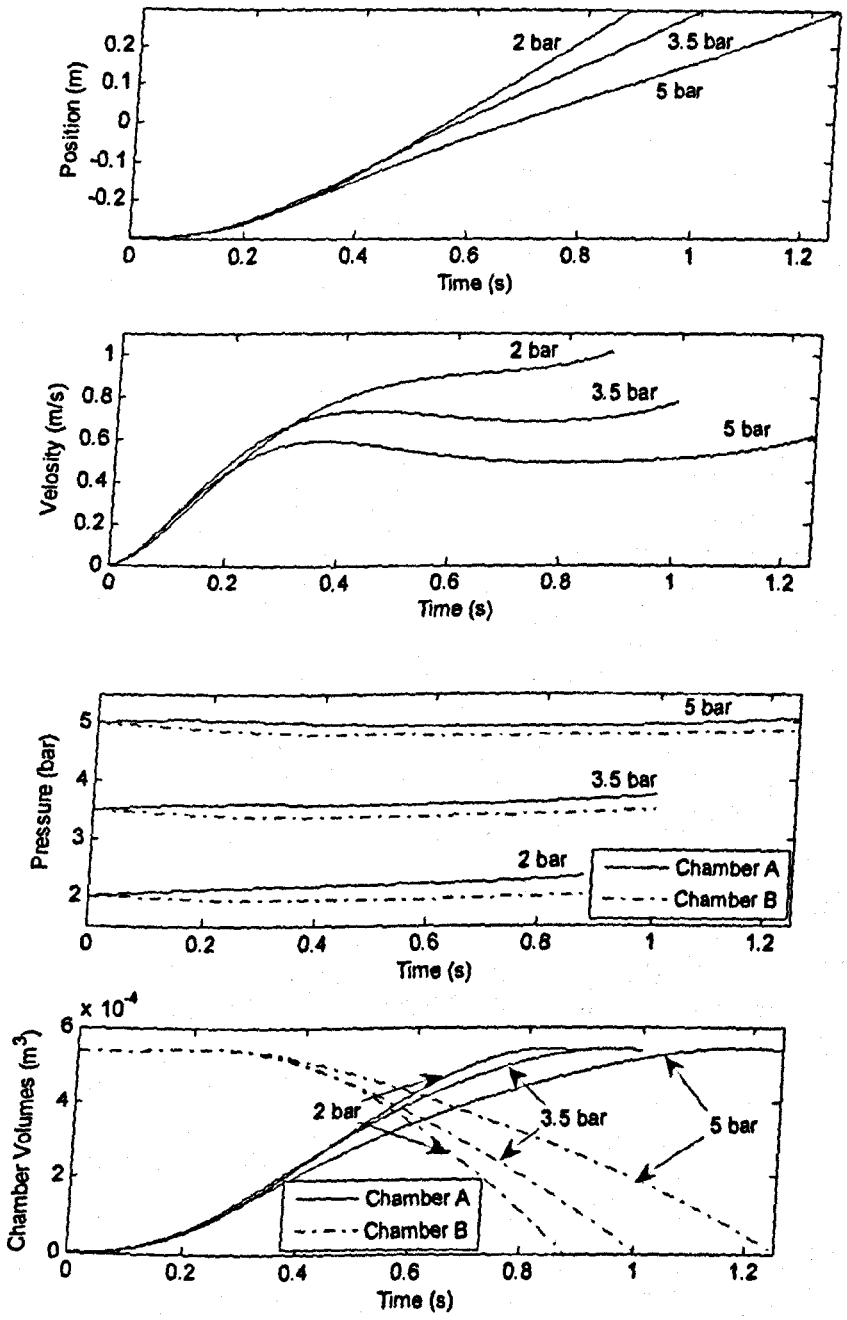

Figure 6.6 Dynamic responses of the new cylinder with different initial chamber pressures

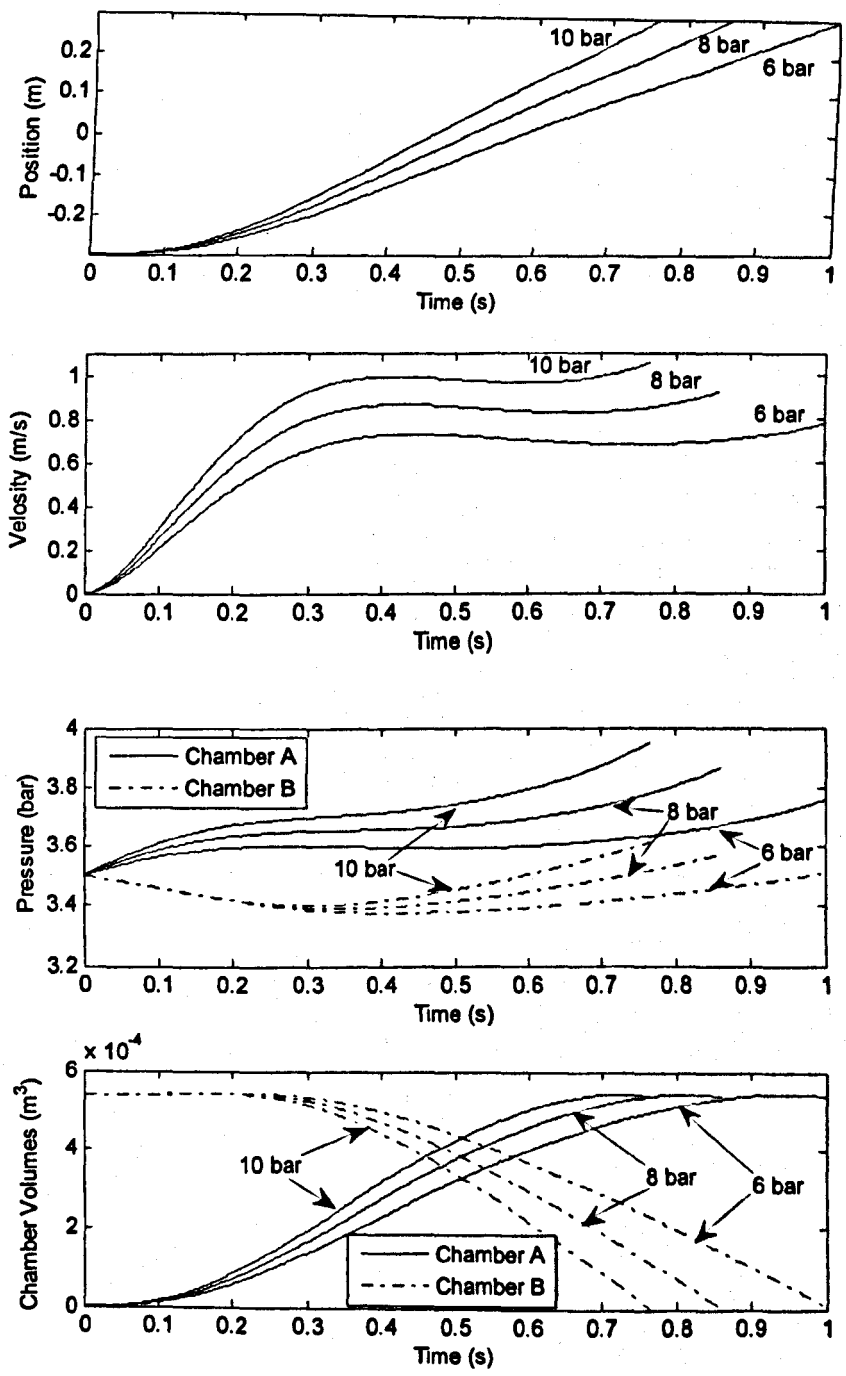

Figure 6.7 Dynamic responses of the new cylinder with different air supply pressures

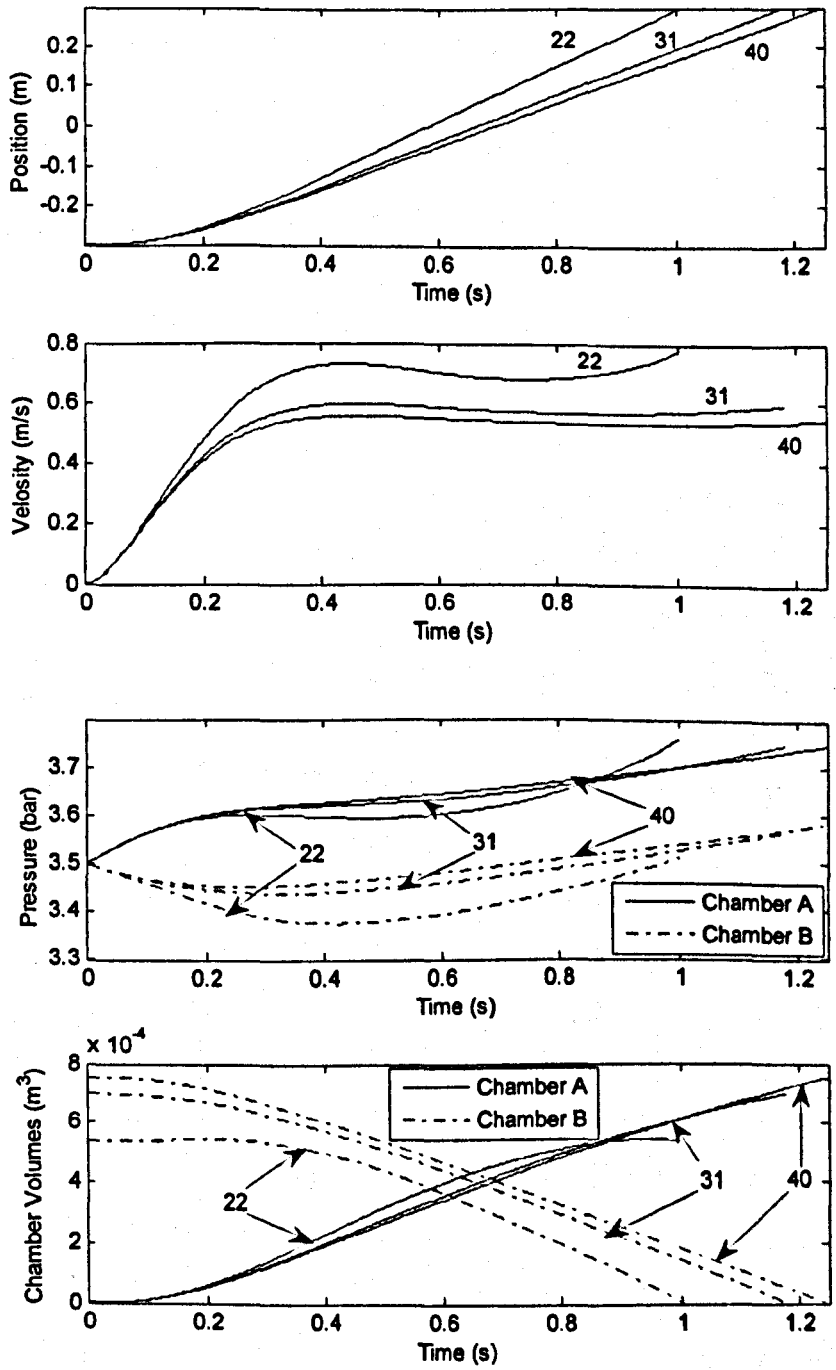

Figure 6.8 Dynamic responses of the new cylinder with different quantity of stretchable triangles in half stroke N

The effect of different numbers of stretchable triangles in half stroke N has been investigated as well. Figure 6.8 shows the dynamic responses with $N=22$, $N=31$ and $N=40$. It can be seen from Figure 6.8 that the piston can move faster with smaller numbers of triangles, but with the larger numbers of triangles, the terminal piston velocity can level down. When the numbers of triangles are decreased to enhance the piston speed, one should bear in mind that the minimum numbers of stretchable triangles are limited by the expression (6-1).

6.5 Energy Efficiency Analysis of the New Cylinder

To gain a quantified figure of energy saving, a simulation study for energy efficiency has been carried out using the same parameters as described in the above section. Comparison has been made between a conventional rodless cylinder with a bore size 60mm and the new cylinder with a bore size 60mm and inner tube diameter 25mm. Both cylinders are working under the same conditions for the compressed air supply pressure, initial chamber pressures, initial velocity, payload and friction characteristics. Both cylinders move the load from the initial position of -0.3m to the end position of 0.25m. The mass of compressed air consumed by both cylinders is presented in Figure 6.9. From the results, it is obvious that the new cylinder can save over 50% compressed air which indicates the energy efficiency can be improved dramatically.

However, the analysis in this chapter is purely based on the possible structure of the new cylinder. Further analysis based on the energy balance is still required. The energy consumed must be balanced by the potential energy contained in the compressed air.

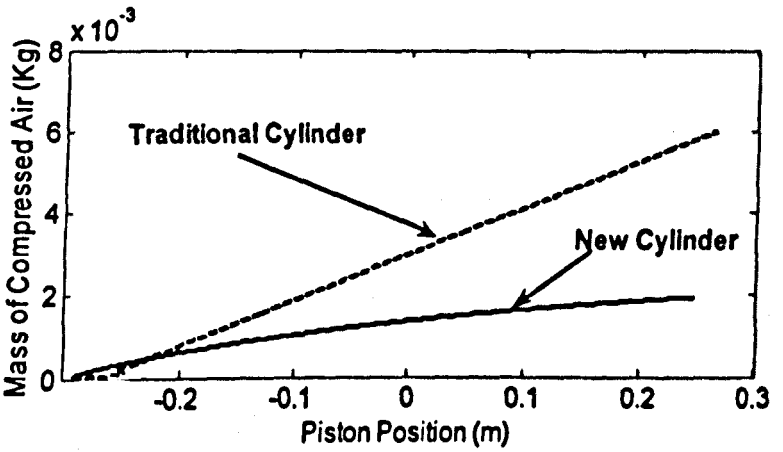

Figure 6.9 Compressed air consumptions for both conventional and new cylinders under the same working conditions

The effects of different parameters on the consumption of compressed air are also investigated. From the simulation work, the results are shown below. Figure 6.10, Figure 6.11 and Figure 6.12 show the consumed compressed air changes with different initial chamber pressures P_0, different air supply pressures P_s and different quantity of stretchable triangles in half stroke N, respectively. In Figure 6.10, the mass of air consumption is smallest when initial pressures are set as 2 bars. When initial pressures are set as 3.5 bars and 5 bars, the air consumptions are similar. However, air consumption with 5 bars is a bit smaller than that with 3.5 bars. This will help users to choose the suitable initial pressures for energy efficient purposes. From Figure 6.11, it can be seen that the air consumption will be increased when higher air supply pressure is used, which is consistent with industrial common sense. As for Figure 6.12, it shows the quantity of stretchable triangles also impacts the air consumption, but the changing rates of consumed air remain the same.

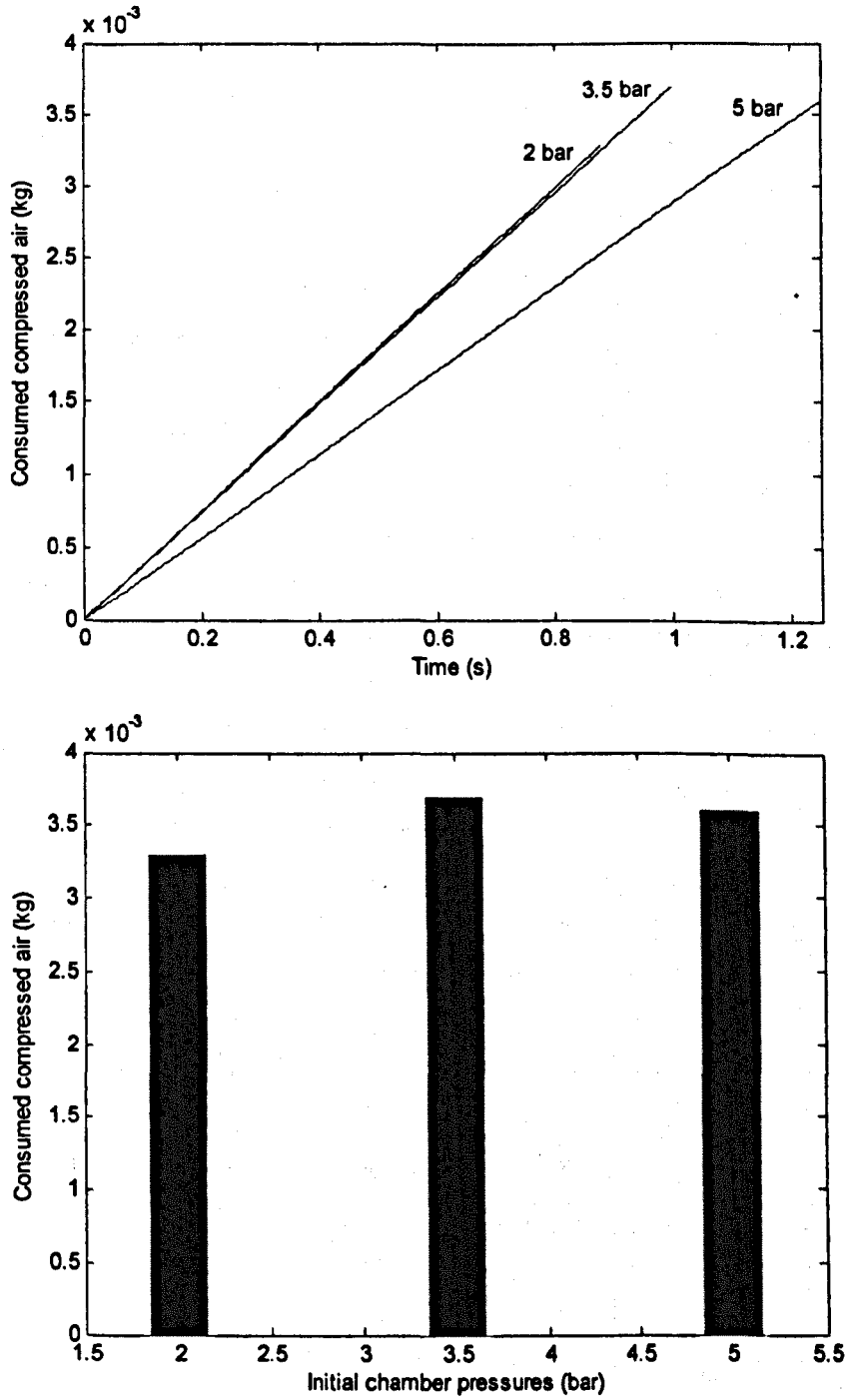

Figure 6.10 Mass of compressed air consumptions with different initial chamber pressures

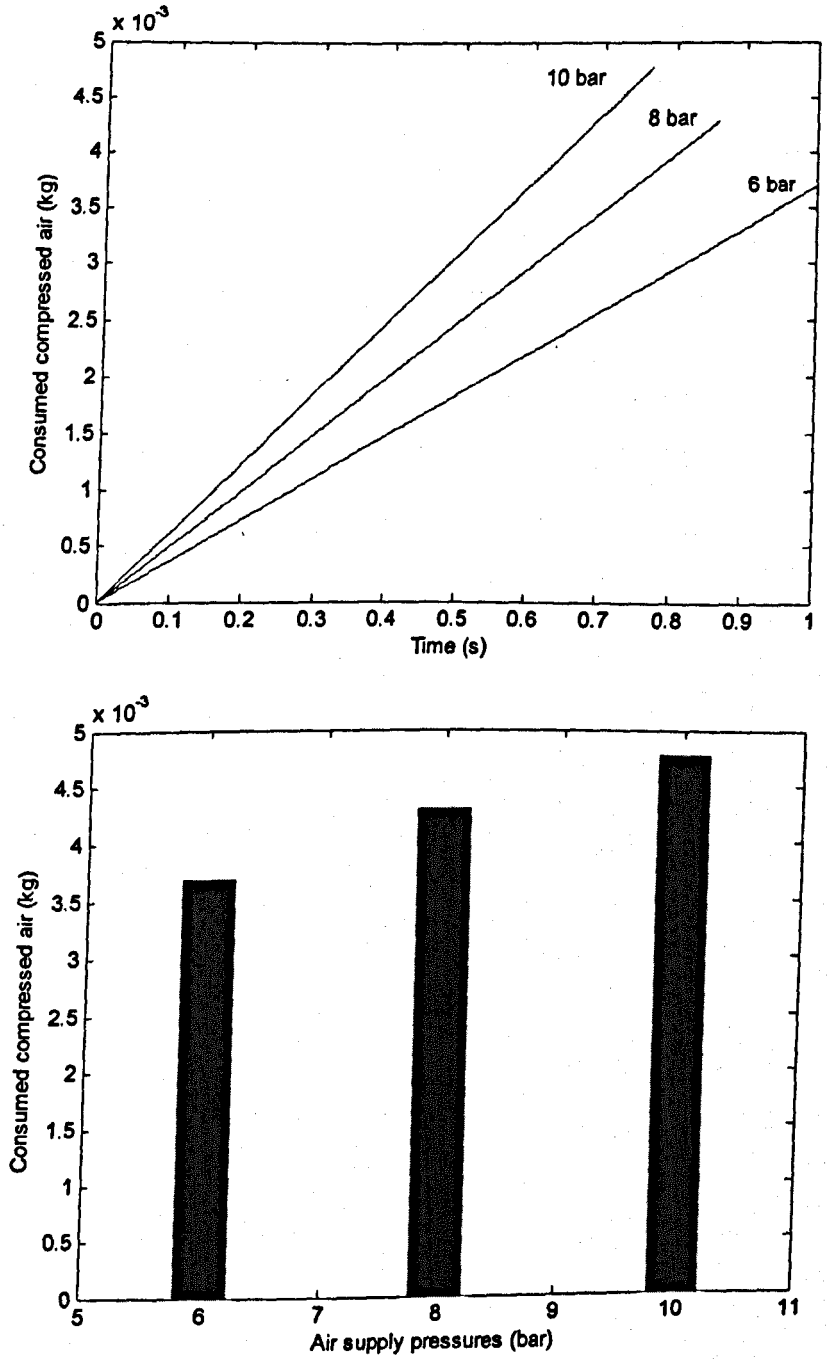

Figure 6.11 Mass of compressed air consumptions with different air supply pressures

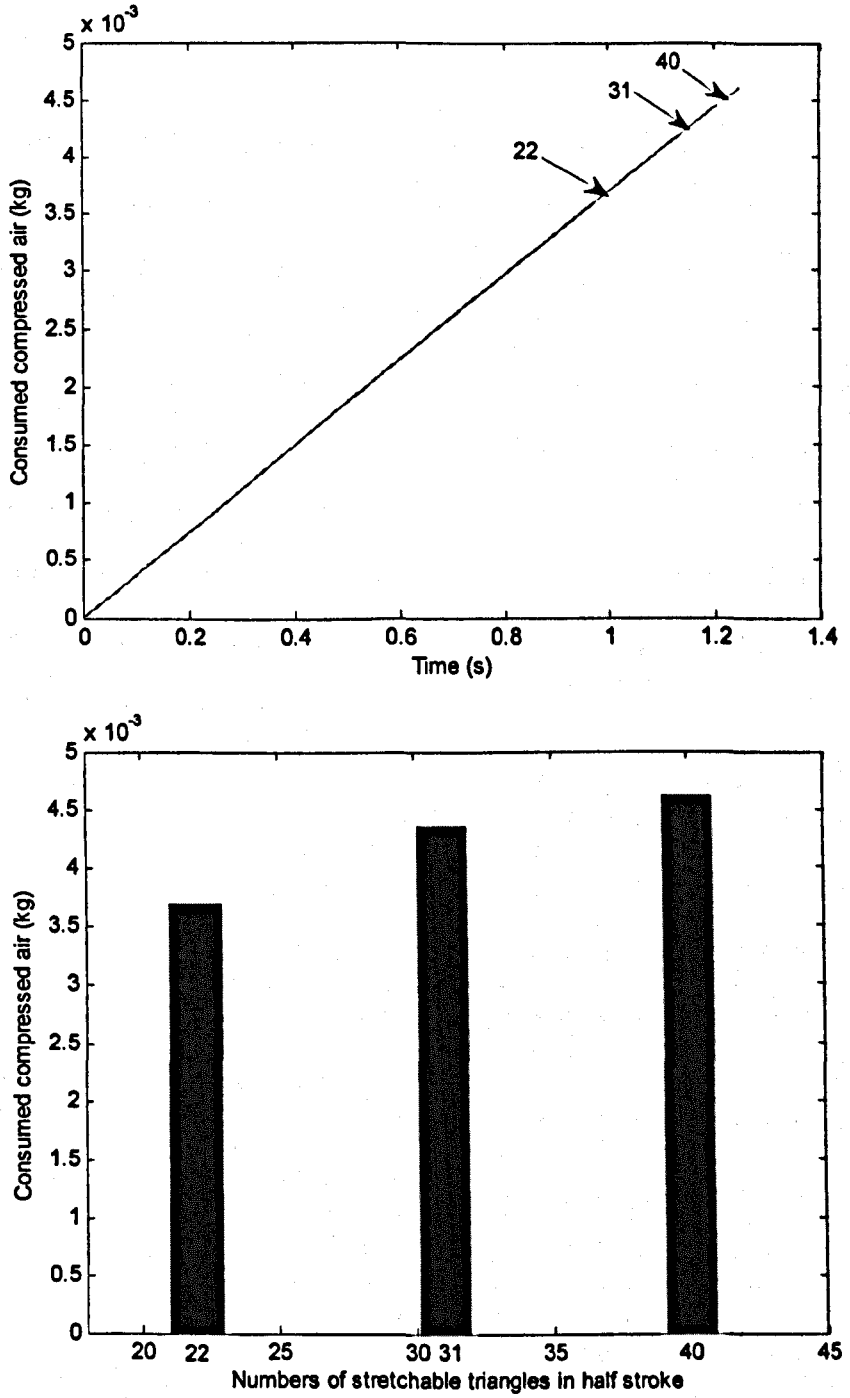

Figure 6.12 Mass of compressed air consumptions with different quantity of stretchable triangles in half stroke

6.6 Summary

In this chapter a new pneumatic cylinder is presented. Starting from the conventional rodless cylinder, the reason why the new design can save energy is explained. The structure of the new design is illustrated. The detailed mathematical model is presented. This chapter also includes the dynamic responses of the new design cylinder with open-loop control input under different design parameters. Then the simulation studies and analysis have shown that the cylinder is fast in responses and energy efficient. The results consistently indicate that the new pneumatic cylinder design would consume up to 50 per cent less compressed air when doing the same job as a conventional pneumatic cylinder, which offers dramatic energy savings. It is also found that the new design has faster responses because it requires less time to charge the smaller chamber volume, which offers higher timing efficiency than the conventional design. Therefore, this new approach holds out hope of significant savings. The new cylinder has a great potential to be manufactured and widely used in industry, which, in turn, will save a great amount of energy consumed by manufacturers and end-users.

Chapter 7

Conclusions and Future Work

7.1 Conclusions

At the beginning of the thesis, project background and objectives are presented. Due to the low energy efficiency of pneumatic cylinder actuator systems, this PhD project has focused on the improvement of energy efficiency of the pneumatic cylinders through finding the optimal energy efficient trajectories and innovation of the mechanical structure of the cylinders.

The pneumatic actuator system has been introduced, including the description of each component and their functions. Then the historical overview of the development and research of pneumatic systems has been given. The mathematical model of each component of the pneumatic system has been discussed, and then the integrated mathematical model of pneumatic cylinder actuating system has been presented. In the integrated system model, the frictions have been investigated in detail. Friction phenomena and simplified friction model for simulation study purpose have been illustrated. To understand the dynamical characteristics of pneumatic cylinder systems, open-loop simulation studies associated with a variety of different parameters have been conducted on rodless and rodded cylinders respectively. However, for simplicity, it was decided that the rodless cylinder be adopted throughout the entire project

due to its symmetric geometrical structure.

It is desired to find the optimal energy efficient profiles, which can be introduced to industry. Without using optimal controllers, the users can track the optimal profiles to save energy. For this purpose, energy efficient optimal control of pneumatic cylinder system has been developed. When optimal control theory is applied on the system model, an extra set of co-state differential equations are generated. A detailed derivation has been shown. These co-state equations and the original system equations compose an eighth-order new system model. However, the derived set of system equations are too complicated to be solved analytically, so numerical solutions must be used. The shooting method and genetic algorithms were chosen to be applied. However, the complexity of the system model and the extreme nonlinear characteristics result in the difficulty to search the unknown co-state initial values. An alternative way to conduct the optimal control on pneumatic cylinder system needs to be found.

To avoid solving this set of complicated nonlinear differential equations with unknown boundary conditions, the pneumatic cylinder system is linearised through input/output state feedback. The feedback linearisation control law and the detailed procedure have been explained. Then the optimal control theory can be applied to the linearised system model. An energy efficient optimal control strategy is developed with respect to the transformed states of the linearised system. The solution of the state trajectory results in a group of energy efficient piston position, velocity, acceleration and chamber pressure trajectories. Through simulation studies, it is found that the optimal energy efficient

trajectories of piston position, velocity and acceleration are not affected by the initial and terminal chamber pressures and compressed air supply pressure; they only depend on the length of the stroke and the preset time period. This finding and the set of optimal energy efficient profiles can be very useful in practice.

After the generalised nonlinear controls are substituted back to the transformed system, the same group of trajectories is obtained through simulation studies, which proves they are truly optimally energy efficient. The simulation study also validates that the energy efficient optimal profile worked out by this method shows the cylinder to use the least quantity of compressed air compared with other three different velocity profiles. In addition, an investigation of the conditions yielding the minimum performance index occurrence has been conducted. It is found that under these conditions, that is, as long as the initial chamber pressures are the same as the terminal chamber pressures, the performance index can attain its minimum value, and this condition is independent of the air supply pressure. However, this condition will be slightly changed, but, is still correlated when a new practical criterion is adopted in the original system. The relations of initial and terminal chamber pressures, air supply pressures and the occurrence of the minimum value of the criterion also depend on the selection of the criterion.

These results suggest that industry may need to reform their traditional trapezoidal velocity profile to the newly developed velocity profile (4-32) and make an effort to make the terminal pressures of the both chambers the same level as the initial chamber pressures. One system may not save big amount of energy consumption but with the huge numbers of pneumatic actuators in use,

optimal control could deliver significant savings in the total amount of electricity used.

Based on the linearised model via state feedback, a feedback tracking control of pneumatic cylinder system has been proposed. With practical and more precise tracking control, undoubtedly the pneumatic actuator system can save more energy. Two cases are discussed respectively: the system using a single five-port valve and two three-port valves. The feedback control is transformed back into the nonlinear state space. Since the obtained nonlinear feedback controller is too complicated for real-time implementation, some simplification has been done. Simulation results have shown that the simplified control yields the satisfied tracking accuracy.

For the convenience of analysis, the static and Coulomb frictions are ignored initially. When these frictions are counted in the system, two problems emerge: a large tracking error and time delay in the dynamic response. To address the problems caused by the friction forces, an enhanced tracking control strategy is proposed, which is based on a simple idea, that is, to compare the measured acceleration with the estimated acceleration under the condition without frictions' influence. The estimated value is then used to amend the control strategy proposed under the condition of that the friction forces are ignored. The main advantage of the method proposed is that it has a clear theoretic guidance at the initial stage of controller design and leads to a tracking control strategy with a simple structure.

Additionally, to improve the energy efficiency of pneumatic cylinder, a novel

design of pneumatic cylinder is presented. Starting from the conventional *rodless cylinder,* the theoretical reasons why the new design can save energy is explained. The geometrical structure of the new design is illustrated and the mathematical model is developed. To understand the dynamic response of this new design, open-loop simulation results and analysis with a variety of different design parameters are also shown.

The simulation studies and energy efficiency analysis have shown that the cylinder is fast in dynamic response and is energy efficient. The results consistently indicate that the new pneumatic cylinder design would save up to 50% compressed air when doing the same job as a conventional pneumatic cylinder. It is also found that the new design has faster responses because it requires less time to charge the smaller chamber volume. Therefore, this new cylinder has a great potential to be manufactured and widely used in industry, which, in turn, will save a great amount of energy consumed by manufacturers and end-users.

7.2 Recommended Future Work

Based on the current research of energy efficiency improvement of pneumatic cylinder actuating system, some work could be carried out in the future, which is listed as follows:

- For the eighth-order system model generalised for optimal control purposes in Chapter 3, further research work could be focused on finding out the possible initial ranges of the four co-states, lambdas. Knowing these ranges,

genetic algorithms or shooting method can be applied to find out the accurate initial conditions of the co-states. Then the optimal control law and profiles can be obtained to verify the optimal profiles obtained from the linearisation method.

- It would be of interest to investigate the practical control strategies for the new design of cylinder, especially for addressing the soft-landing problem at each end of stroke. PWM associated on/off control valve application would be one interesting technique.

Bibliography

Al-Dakkan, K.A., Goldfarb, M. and Barth, E.J., 2003, Energy saving control for pneumatic servo systems, *Proceedings of the 2003 IEEE/ASME International Conference on Advanced Intelligent Mechatronics (AIM 2003)*, Kobe, Japen, July 2003.

Al-Dakkan, K.A., Barth. E.J., and Goldfarb, M., 2006, Dynamic constraint based energy saving control of pneumatic servo systems. ASME Journal of Dynamic Systems, Measurement, and Control, vol. 128, no. 3, pp. 655-662.

Andersen, B. W., 1976, The analysis and design of pneumatic system, *Robert E. Krieger Publishing Company*, New York.

Andrew, P., 1998, Hydraulics and Pneumatics A Technician's and Engineer's Guide, *Butterworth Heinemann*, Oxford, UK.

Armstrong-Helouvry, B., Dupont, P., and De wit, C.C., 1994, A survey of models analysis tools and compensation methods for the control of machines with friction. *Automatica*, vol. 30, No.7, pp. 1083-1183.

Backe, W., 1986, The application of servo pneumatic drives for flexible mechanical handling techniques, *Robotics*, vol. 2 pp. 45-56.

Backe, W. 1993, The present and future of fluid power, *Proceeding Institute Mechanism Engineers, Part I, Journal of System and Control Engineering*, vol. 207, No. 4, pp. 193-212.

Belforte, G., 2000, New developments and new trends in pneumatics, keynote lecture of *FLUCOME 2000, the Sixth International Symposium on Flow Control, Measurements and Flow Visualization*, Sherbrooke, Québec, Canada, 13th-17th August 2000.

Blackburn, J.F., Reethof, G., Shearer, J. L., 1960, Fluid Power Control, *The Technology Press of MIT/John Wiley & Sons*, New York.

Ben-Dov, D. and Salcudean, S.E., 1995, A force-controlled pneumatic actuator, *IEEE Transactions on Robotics and Automation*, vol. 11, pp. 906-911.

BOSCH Automation, 1998, Pneumatics. Theory and applications, *Omega Fachliteratur*, Ditzingen, Germany.

Botting, L.R., Eynon, G.T. and Foster, K., 1970, The response of a high-pressure pneumatic servomechanism to step and sine wave inputs, *Proceedings Institute. Mechanism Engineers*, 184(1), pp. 993-1012.

Bowden, F.P. and Tabor, D., 1974, Friction: an introduction to tribology, *Heinemann Educational*, London.

Bryson, A. and Ho, Y., 1975, Applied optimal control, *Emisphere Publ. Co.* Washington DC.

Burrows, C.R. and Webb C. R., 1966, Use of root locus in the design of *pneumatic servomotors, Control*, pp. 423.

Burrows, C.R. and Webb C. R., 1967-1968, Simulation of an on-off pneumatic servomechanism, *Proceedings Institute Mechanism Engineers*, 182(1), pp. 631-641.

Burrows, C.R., 1969, Effect of position on the stability of pneumatic servo mechanisms, *Research Notes in Mechanical Engineering Science*, II(6), pp. 615-616.

Burrows, C.R. and Webb C. R., 1969-1970, Further study of a low pressure on-off pneumatic servomechanism, *Proceedings Institute Mechanism engineers*, 184(1), No. 45, pp. 849-858.

Cai, M., Kagawa, T. and Kawashima, K., 2002, Energy conversion machines

and power evaluation of compressible fluid in pneumatic actuator systems, *37th Intersociety Energy Conversion Engineering Conference (IECEC)*, Washington DC, USA, July 2002.

Davis, L., 1987, Genetic Algorithms and Simulated Annealing, *Morgan Kaufmann Publishers, Inc.*, Los Altos, California.

Drakunov, S., Hanchin, G.D., Su, W.C., and Ozguner, U., 1997, Nonlinear control of a rodless pneumatic servoactuator, or sliding modes versus Coulomb friction. *Automatica*, vol. 33, pp. 1401-1408.

Drives and Control, 1999, Switched reluctance motor drives energy-saving compressor, *Drives and Control*, pp. 43.

Engineeringtalk, 2006, Screw compressors cut energy costs by half, available at: http://www.engineeringtalk.com/news/bog/bog135.html, March, 2006.

Fok, S.C., Wang, Z. And Dransfield, P.D., 1995, A digital simulation study of an adaptive controller for a pneumatic cylinder system. *International journal of computer applications in technology*, vol. 8, No. 3-4, pp. 163-171.

Forsyth, A.R., 1927, Calculus of variations, *Cambridge University Press*, Cambridge.

Franklin, G.F., Powell, J.D. and Emami-Naeini, A., 1994, Feedback control of dynamic systems, *Wokingham: Addison-Wesley Pub. Co.*, England.

Horner, M., 1998, Compressor control, *Engineering & Technology*, Vol. 1, No.1, pp. 24-25.

Hsiung, S., Matthews, J., 31st Mar. 2000, An introduction to genetic algorithm, http://www.generation5.org/.

Isidori, A. 1995, Nonlinear Control Systems, Third Edition, *Springer-Verlag London Limited.*

Johnson, O. A., 1975, Comparison of Pneumatic and Hydraulic Systems. *Fluid Power: Pneumatics, American technical society*, Chicago.

Kagawa, T., M L Cai, T Fujita, and M Takeuchi, 2000, Energy consideration of pneumatic cylinder actuating system, *Proceedings of Sixth Triennial International Symposium on Fluid Control, Measurement and Visualization*, 13-17, August, Sherbrooke, Canada.

Kalman, R.E., 1960, Contributions to the theory of optimal control, *Bol. Soc. Mat. Mexicana*, vol. 5, pp. 102-119.

Kane, J.W. and Sternheim, M., 1980, Physics SI Version, *Lawrenceville*, PA, U.S.A.

Karnopp, D., 1985, Computer simulation of stick-slip friction in mechanical dynamical systems, *ASME J. of Dynamic Systems, Measurement and Control*, vol. 107, pp. 100-103.

Kawakami, Y., Akao, J. and Kawai, S., 1988, Some considerations on the dynamic characteristics of pneumatic cylinders, *The Journal of Fluid Control*, vol. 19, No.2, pp. 22-36, Sep. 1988.

Kawakami, Y., Masuda, S. and Kawai, S., 1993, Some considerations on the position control of pneumatic cylinders, *Proc. of the Second JHPS International Symposium on Fluid Power (Tokyo)*, pp. 563-568.

Ke, J., Thanapalan, K., Wang, J. and Wu, Q.H., 2004, Development of energy efficient optimal control of servo pneumatic systems, *The Proceedings of IEE Control Conference 2004*, September 6-9, Bath, UK.

Ke, J., Wang, J., Jia, N., Yang, L. and Wu, Q.H., 2005, Energy efficiency analysis and optimal control of servo pneumatic cylinders, *The Proceedings of IEEE Conference on Control Applications 2005*, August 29-31, Toronto, Canada.

Ke, J. and Wang. J., 2006, Improvement of energy efficiency of servo pneumatic cylinders by optimising velocity profiles, *International Journal of Modelling, Identification and Control*, 6(1), pp. 301-307.

Ke, J., Wang, J. and Yang, L., 2006, A fast response energy efficient pneumatic cylinder, *Proceedings of the 12th Chinese Automation & Computing Society Conference in the UK, CACSK06*, September 16, Loughborough, UK.

Kim, Y.H. and Lewis, F.L., 2000, Reinforcement adaptive learning neural-net based friction compensation control for high speed and precision, *IEEE Transactions on Control Systems Technology*, 8(1), pp. 118-126.

Klein, A. and Backe, W., 1992, An intelligent optimisation of a state loop controller with fuzzy-set-logic. *Bath Int. Workshop on Circuit, Component and System Design*, Research Studies Press, pp. 381-399.

Lewis F.L., and Syrmos V.L., 1995, Optimal Control, Second Edition, *John Wiley & Sons, Inc.* New York.

Lin-Chen, Y., 2001, Software Development for Pneumatic Actuator System Design and Simulation Using Component-based Methods, *MPhil. Thesis of Department of Electrical Engineering and Electronics*, The University of Liverpool.

Liu, S. and Bobrow, J.E., 1988, An analysis of a pneumatic servo system and its application to a computer-controlled robot, *ASME journal of Dynamics Systems, Measurement and Control*, vol. 110, pp. 228-235.

Mannetje, J.J., 1981, Pneumatic servo design method improves system bandwidth twenty fold. *Journal of control engineering*, 28(6), pp. 79-83.

McCord, B.E., 1983, Designing Pneumatic Control Circuits - Efficient Techniques For Practical Application, *Marcel Dekker, Inc.*, New York and Basel.

Mera, N.S., Elliott, L., Ingham, D.B., 2004, Numerical solution of a boundary

detection problem using genetic algorithms, *Engineering Analysis with Boundary Elements*, vol. 28, No. 4, pp. 405-411.

Moore, P.R., Weston, R.H. and Thatcher, T.W., 1985, Compensation in pneumatic actuated servo-mechanisms, *Transaction of the Institution of Measurement and Control*, 7(5), pp. 238-244.

Moore, P.R., Pu, J., Harrison, R. and Weston, R.H., 1992, A general purpose digital motion controller for fluid power systems, *Modelling and Control, Edge and Burrows Ceds*, London, Research Studies Press, pp. 276-290.

Moore, P.R., Pu, J. and Harrison, R., 1993, Progression of servo pneumatics towards advanced applications, in *Fluid Power Circuit, Component and System Design*, Edited by K. Edge C. Burrows, Published by Research Studies Press, pp. 347-365.

Morgan, G., 1985, Programming position of pneumatic actuators, *Applied pneumatics*, May, pp. 16-20.

Naidu D.S., 2003, Optimal Control Systems, *CRC Press LLC*, London.

Norgren, 2003, Energy saving in compressed air systems – how Norgren is helping to improve energy efficiency, available at: http://www.usa.com/products/pdfs/techtips/energysaving. pdf.

Pontryagin, L.S., Boltayanskii, V.G., Gamkrelidze, R.V. and Mishchenko, E.F., 1962, The mathematical theory of optimal processes, *Wiley*, New York (Translated from Russian).

Pearce, M., April/May 2005, Is there an alternative to fluid power? , *IEE Computer & Control Engineering*, pp. 8-11.

Pu, J. and Weston, R.H., 1988, Motion control of pneumatic drives, *Microprocessors and Microsystems*, vol. 12, No. 7, pp. 373-382.

Pu, J. and Weston, R.H., 1989, A new generation of pneumatic servos for

industrial robots, *Robotica*, vol. 7, Jan, pp. 17-23.

Pu, J. and Weston, R.H., 1990, Steady state analysis of pneumatic servo drives, *Proceedings Institute mechanism Engineers*, Part C: *Journal of mechanical Engineering Science*, vol. 204, pp. 377-387.

Pu, J., Harrison, R. and Weston, R.H., 1993, Application and design trends of intelligent servo pneumatics, *Proceedings of the 12th World Congress International Federation of Automatic Control*, Sydney, Australia, 6, pp. 487-492.

Pu, J. Wang, C.B. and Moore, P.R., 1995a, Commissioning of a servo-pneumatic system for timing and profile control in a high speed food packaging application, *International Journal of Production Research*, vol. 33, No. 10, pp. 2907-2922.

Pu, J. Wang, C.B. and Moore, P.R., 1995b, Acceleration characteristics of servocontrolled pneumatic cylinders, *Fluid power systems technology symposia, ASME winter annual meeting*, Nov, pp. 12-17.

Quaglia, G and L Gastaldi, 1995, Model and dynamic of energy saving pneumatic actuator, *The Proceedings of the Fourth Scandinavian International Conference*, vol.1, pp. 481-492, Sept. 26-29, Tempere, Finland.

Shearer, J.L., 1954, Continuous control of motion with compressed air, *Sc.D thesis*, Massachusetts Institute of Technology, Cambridge, MA, USA.

Shearer, J.L., 1957, Nonlinear analogue study of a high pressure servomechanism, *ASME Transaction*, April, pp. 465.

Static Friction Phenomena, 2006, available at: http://www.20sim.com/webhelp4/library/iconic_diagrams/Mechanical/Friction/Static_Friction_Models.htm.

Turner, I.C., 1996, Engineering applications of pneumatics and hydraulics,

Arnold, Butterworth-Heinemann.

Uebing, M. and Vaughan, N.D., 1997, On linear dynamic modelling of a pneumatic servo system. *The Fifth Scandinavian International Conference on Fluid Power (SICFP'97)*, Linköping, Sweden, vol. 1, pp. 363-378.

Vaughan, D.R., 1965, Hot-gas actuators: some limits on the response of speed, *ASME Journal of Basic Engineering*, March, pp. 113-119.

Wang, J., Pu, J. Moore, P.R. and Zhang, Z.M., 1998, Modelling study and servo-control of air motor systems, *International Journal of Control*, vol. 71, No. 3, pp. 459-476.

Wang, J., Pu, J. Moore, P.R., 1999a, A practical control strategy for servo-pneumatic actuator systems, *Control Engineering Practice*, 7, pp. 1483-1488.

Wang, J., Pu, J. Moore, P.R., 1999b, Accurate position control of servo pneumatic actuator systems: an application to food packaging, *Control Engineering Practice*, 7, pp. 699-706.

Wang, J., Lin-Chen, Y., Wang, J.D., Moore, P.R. and Pu. J., 2000a, Modelling study, validation and robust tracking control of pneumatic cylinder actuator systems, *IEE Control Conference 2000*, Sep. 4-7, Cambridge, UK.

Wang, J., Wang, J.D. and Liau V.K., 2000b, Energy efficient optimal control for pneumatic actuator systems, *International Journal of Systems Science*, vol. 26, No. 3, pp. 109-123.

Wang, J., Wang, D.J.D., Moore, P.R. and Pu, J., 2001, Modelling study, analysis and robust servo control of pneumatic cylinder actuator systems. *IEE Proceedings on Control Theory and Applications*, vol. 148, pp. 35-42.

Wang, J., Wang, J.D., Daw, N. and Wu, Q.H., 2004, Identification of pneumatic cylinder friction parameters using genetic algorithms, *IEEE/ASME Transactions*

on mechatronics, vol. 9, No. 1, pp. 100-107.

Wang, J., Ke, J. and Wei, J.L., A high speed energy efficient pneumatic cylinder, *Mechatronics 2006 The 10th Mechatronics Forum Biennial International Conference*, June 19-21, Penn State, USA.

Wang, J., Kotta, U. and Ke, J., 2007, Tracking control of nonlinear pneumatic actuator systems using static state feedback linearization of the input-output map, *Proceedings of the Estonian Academy of Sciences (Physics Mathematics)*, 56(1), pp. 47-66.

Weston R.H., Moore, P.R., Thatcher, T.W. and Morgan, G., *1984, Computer* Controlled Pneumatic Servo Drives, *I Mech*, PartB, 198B, pp. 175-281.

Winnick, J., 1997, Chemical engineering thermodynamics, *John Wiley & Sons, Inc.*, New York.

Zhou, H., 1995, Intelligence in pneumatic servo positioning axis. *The Fourth Scandinavian International Conference on Fluid Power*, Tampere, Finland, vol. 1, pp. 556-568.

Appendix

Simulation Program

A. Pneumatic Cylinder Model

```
%-------------------------------------------------------------------------------
% This function represents the rodless pneumatic cylinder model, which are described by four
% ordinary differential equations. Copyright 2007 Jia Ke
%-------------------------------------------------------------------------------

% Parameter setting
A = pi*(0.032/2)^2; Aa = A; Ab = A; w = 0.006; Co = 0.0404; Cd = 0.8; Ck = 3.8639;
Cr = 0.5283; k = 1.4; l = 1; R = 287; delta = 0.0615; M = 1; Fc = 10; Fs = 60; Kf = 15;

% Restriction of the max and min positions in the stroke
if x(1) >= 0.5
      u1 = 0;
      u2 = 0;
      x(1) = 0.5;
elseif x(1) <= 0.5
      u1 = 0;
      u2 = 0;
      x(1) = -0.5;
end

% Restriction of the max and min pressures in Chamber A and B
if x(3) <= Pe
    x(3) = Pe;
elseif x(3) >= Ps
    x(3) = Ps;
end

if x(4) <= Pe
    x(4) = Pe;
```

```
elseif x(4) >= Ps
    x(4) = Ps;
end

% Calculation of the fn functions
% u1 > 0 means Chamber A is the driving chamber
if u1 >= 0
    if (x(3)/Ps) <= Cr
        Fa_fun = Ps/sqrt(Ts);
    else
        Fa_fun = Ps*Ck*sqrt(power(x(3)/Ps,2/k)-power(x(3)/Ps,(k+1)/k))/sqrt(Ts);
    end

    if (Pe/x(4)) <= Cr
        Fb_fun = x(4)/sqrt(Tb);
    else
        Fb_fun = x(4)*Ck*sqrt(power(Pe/x(4),2/k)-power(Pe/x(4),(k+1)/k))/sqrt(Tb);
    end

% u1 < 0 means Chamber B is the driving chamber
else
    if (Pe/x(3)) <= Cr
        Fa_fun = x(3)/sqrt(Ta);
    else
        Fa_fun = x(3)*Ck*sqrt(power(Pe/x(3),2/k)-power(Pe/x(3),(k+1)/k))/sqrt(Ta);
    end

    if (x(4)/Ps)<=Cr
        Fb_fun = Ps/sqrt(Ts);
    else
        Fb_fun = Ps*Ck*sqrt(power(x(4)/Ps,2/k)-power(x(4)/Ps,(k+1)/k))/sqrt(Ts);
    end
end

% Description of static friction
if (x(2) <= 0) & (abs(Aa*x(3)-Ab*x(4)) <= Fs)
    FscS_fun = Aa*x(3)-Ab*x(4)-Kf*x(2);
else
    FscS_fun = Fc*sign(x(2));
end
```

```
% Description of the pneumatic cylinder model
xdot(1) = x(2);
xdot(2) = (-Kf*x(2)-FscS_fun+Aa*x(3)-Ab*x(4) +F )/M;
xdot(3) = -k*x(2)*x(3)/(1/2+x(1)+delta)+(k*R*Ts*Cd*Co*w*Fa_fun*u1)/
          (Aa*(1/2+x(1)+delta));
xdot(4) = k*x(2)*x(4)/(1/2-x(1)+delta)+ (k*R*Ts*Cd*Co*w*Fb_fun*(u2))/
          (Ab*(1/2-x(1)+delta));

% Description of mass flow rates
madot = (x(3)*A*x(2)+xdot(3)*A*(0.5+x(1)+delta)/k)/(R*Ts);
mbdot = (-x(4)*A*x(2)+xdot(4)*A*(0.5-x(1)+delta)/k)/(R*Ts);
```

B. Adjoint System of Pneumatic Cylinder Model with Optimal Control

```
% ------------------------------------------------------------------------
% This function represents the adjoint system consisting of original state equations and co-state
% equations generated by using Pontryagin's principle, and the optimal controller.
% Copyright 2007 Jia Ke
% ------------------------------------------------------------------------
% y(1) = x(1), which is the piston's position
% y(2) = x(2), which is the piston's velocity
% y(3) = x(3), which is the pressure in chamber A
% y(4) = x(4), which is the pressure in chamber B
% y(5) = lamda(1)
% y(6) = lamda(2)
% y(7) = lamda(3)
% y(8) = lamda(4)

% Parameters setting
A = pi*(0.032/2)^2; Aa = A; Ab = A; Tb = 293; Ts = 293; w = 0.006; Wa = w; Wb = w;
Co = 0.0404; Cd = 0.8; Ck = 3.8639; Cr = 0.5283; k = 1.4; l = 1; Ts = 293; M = 1;
Pe = 1e5; Ps = 6e5; R = 287; Ta = 293; Tb = 293; Kf = 15; delta = 0.0615;

% Restriction of the max and min positions in the stroke
if x(1) >= 0.5
    u1 = 0;
```

```
    u2 = 0;
    x(1) = 0.5;
elseif x(1) <- 0.5
    u1 = 0;
    u2 = 0;
    x(1) = -0.5;
end

% Restriction of the max and min pressures in Chamber A and B
if x(3) <= Pe
   x(3) = Pe;
elseif x(3) >= Ps
   x(3) = Ps;
end

if x(4) <= Pe
   x(4) = Pe;
elseif x(4) >= Ps
   x(4) = Ps;
end

% Calculation of the fn functions
% u1 > u2 means Chamber A is the driving chamber
t1 = y(3)/Ps;
t2 = y(4)/Pe;
t3 = y(3)/Pe;
t4 = y(4)/Ps;

if (u1 >= u2)
   if (y(3)/Ps) <= Cr
      Fa_fun = Ps/sqrt(Ts);
      Fc_fun = 0;
   else
      Fa_fun = Ps*Ck*sqrt(power(y(3)/Ps,2/k)-power(y(3)/Ps,(k+1)/k))/sqrt(Ts);
      Fc_fun = Ps*Ck*(2*power(t1,2/k)-(k+1)*power(t1,(k+1)/k))/(2*k*sqrt(Ts)*y(3)
               *sqrt(power(t1,2/k)-power(t1,(k+1)/k)));
   end

   if (Pe/y(4)) <= Cr
      Fb_fun = y(4)/sqrt(Tb);
```

```
        Fd_fun = 1/sqrt(Tb);
    else
        Fb_fun = y(4)*Ck*sqrt(power(Pe/y(4),2/k)-power(Pe/y(4),(k+1)/k))/sqrt(Tb);
        Fd_fun = Ck/sqrt(Tb)*sqrt(power(t2,-2/k)-power(t2,-(k+1)/k))*
                 (1-(2*power(t2,-2/k)-(k+1)*power(t2,-(k+1)/k)))/(2*k*
                 (power(t2,-2/k)-power(t2,-(k+1)/k)));
    end

% u2>u1 means Chamber B is the driving chamber
else
    if (Pe/y(3)) <= Cr
        Fa_fun = y(3)/sqrt(Ta);
        Fc_fun = 1/sqrt(Ta);
    else
        Fa_fun = y(3)*Ck*sqrt(power(Pe/y(3),2/k)-power(Pe/y(3),(k+1)/k))/sqrt(Ta);
        Fc_fun = Ck/sqrt(Ta)*sqrt(power(t3,-2/k)-power(t3,-(k+1)/k)) *
                 (1-(2*power(t3,-2/k)-(k+1)*power(t3,-(k+1)/k)))/(2*k*
                 (power(t3,-2/k)-power(t3,-(k+1)/k)));
    end

    if (y(4)/Ps) <= Cr
        Fb_fun = Ps/sqrt(Ts);
        Fd_fun = 0;
    else
        Fb_fun = Ps*Ck*sqrt(power(y(4)/Ps,2/k)-power(y(4)/Ps,(k+1)/k))/sqrt(Ts);
        Fd_fun = Ps*Ck*(2*power(t4,2/k)-(k+1)*power(t4,(k+1)/k))
                 /(2*k*sqrt(Ts)*y(4)*sqrt(power(t4,2/k)-power(t4,(k+1)/k)));
    end
end

% Description of optimal controls
u1 = -k*R*Ts*Cd*Co*Wa*Fa_fun*y(7)/(Aa*(l/2+y(1)+delta));
u2 = -k*R*Ts*Cd*Co*Wb*Fb_fun*y(8)/(Ab*(l/2-y(1)+delta));

% Restriction of the control inputs
if u1>=0.004
    u1=0.004;
elseif u1<=-0.004
    u1=-0.004;
end
```

```
if u2>0.004
    u2=0.004;
elseif u2<-0.004
    u2=-0.004;
end

% Description of the adjoint system of pneumatic cylinder model
ydot(1) = y(2);
ydot(2) = (-Kf*y(2)+Aa*y(3)-Ab*y(4))/M;
ydot(3) = -(k*y(3)*y(2)-k*R*Ts*Cd*Co*Wa*Fa_fun*u1/Aa)/(1/2+y(1)+delta);
ydot(4) = (k*y(4)*y(2)+k*R*Ts*Cd*Co*Wb*Fb_fun*u2/Ab)/(1/2-y(1)+delta);

sum=(k*R*Ts*Cd*Co*Wa*Fa_fun*u1*y(7))/((1/2+y(1)+delta)^2*Aa)-(k*R*Ts*Cd*Co*Wb*F
b_fun*u2*y(8))/((1/2-y(1)+delta)^2*Ab);

ydot(5) = -k*y(3)*y(2)*y(7)/(1/2+y(1)+delta)^2-k*y(4)*y(2)*y(8)/(1/2-y(1)+delta)^2+sum;
ydot(6) = -y(5) + Kf*y(6)/M + k*y(3)*y(7)/(1/2+y(1)+delta) - k*y(4)*y(8)/(1/2-y(1)+delta);
ydot(7) = -Aa*y(6)/M + k*y(2)*y(7)/(1/2+y(1)+delta) -
          (k*R*Ts*Cd*Co*Wa*Fc_fun*u1*y(7))/(Aa*(1/2+y(1)+delta));
ydot(8) = Ab*y(6)/M - k*y(2)*y(8)/(1/2-y(1)+delta) -
          (k*R*Ts*Cd*Co*Wb*Fd_fun*u2*y(8))/(Ab*(1/2-y(1)+delta));
```